

# Development of a Biocompatible Hydrogel Platform for Wound Healing and Skin Regeneration

**Ranya Ibrahim**

A thesis submitted to the Faculty of Health Sciences, University of the Witwatersrand, in fulfilment of the requirements for the degree of

Doctor of Philosophy



UNIVERSITY OF THE  
WITWATERSRAND,  
JOHANNESBURG

**Supervisor:** Prof. Yahya E. Choonara

**Co-supervisors:** Dr Hillary Mndlovu and Prof. Pradeep Kumar

Wits Advanced Drug Delivery Platform, Department of Pharmacy and Pharmacology, School of Therapeutic Sciences, Faculty of Health Sciences, University of the Witwatersrand, Johannesburg, South Africa

**August 2024**

## DECLARATION

---

I, Ranya Ibrahim (2399287), am a student registered for the Doctor of Philosophy in the Faculty of Health Sciences at the University of the Witwatersrand, Johannesburg, South Africa in the academic year 2024.

I declare that this thesis is my work. It has been submitted for the degree of Doctor of Philosophy in the Faculty of Health Sciences at the University of the Witwatersrand, Johannesburg. It has not been submitted before for any degree or examination at this or any other university.

Signature:



Date: 1<sup>st</sup> of August 2024

## ANIMAL ETHICS DECLARATION

---

I, Ranya Ibrahim, hereby confirm that the study entitled "Development of a Biocompatible hydrogel Platform for Wound Healing Treatment in the Sprag Dawley rat Model" was approved by the Animal Ethics Screening Committee (AESC) of the University of the Witwatersrand with Ethics Clearance Number 20202/11/03/D.

Appendix A

## RESEARCH OUTPUTS

---

### PUBLICATIONS

Ranya Ibrahim, Hillary Mndlovu, Pradeep Kumar, Samson A. Adeyemi and Yahya E. Choonara (2022). Cell Secretome Strategies for Controlled Drug Delivery and Wound-Healing Applications. *Polymers*, 14142929

Ranya Ibrahim, Hillary Mndlovu, Pradeep Kumar, and Yahya E. Choonara (2024). Secretome-loaded Alginate-Lecithin Hydrogel for wound healing application (To be submitted to Journal).

Ranya Ibrahim, Hillary Mndlovu, Pradeep Kumar, and Yahya E. Choonara (2024). Rat skin fibroblast cells-derived secretome-enriched alginate soy lecithin scaffold accelerates wound healing in vitro (To be submitted to Journal).

## RESEARCH PRESENTATIONS

---

Ranya Ibrahim, Hillary Mndlovu, Pradeep Kumar, and Yahya E. Choonara (2023). Regenerative Effects of Fibroblast Cells Secretome-Based Alginate Gel on Skin Wounds. **(Oral presentation)**. Towards 100 years of excellence, Faculty of Health Sciences, Research Day and Postgraduate Expo, 6 September 2023. University of the Witwatersrand, Johannesburg, South Africa.

## ACKNOWLEDGEMENTS

---

First and foremost, let gratitude be expressed to Allah, through whose grace virtuous deeds are achieved.

Finishing a PhD is a significant accomplishment, and it's still challenging for me to grasp that I've successfully reached this noteworthy milestone. I want to extend my heartfelt thanks to those individuals who played crucial roles in guiding me through my PhD journey.

I wish to convey my profound appreciation to my husband. Your unwavering support has been a constant during the peaks and valleys of this academic journey. Thank you for being my rock. I also extend my deepest gratitude to my family and friends for their belief in my capabilities and steadfast support. Your encouragement has played a vital role in my achievements.

I express my gratitude to my supervisor, Prof. Yahya Choonara for his continuous support, direction, and motivation throughout the entire PhD journey. His unwavering presence and wealth of wisdom have played a pivotal role in moulding my academic progress. I deeply appreciate the invaluable contributions he has made to my development.

I express sincere gratitude to Dr Hillary Mndlovu, my co-supervisor, for generously imparting his vast academic knowledge and playing a pivotal role in assisting me in establishing my presence within the academic community. I am genuinely thankful for his firm yet compassionate guidance, which not only facilitated substantial contributions to publications during my PhD but also opened doors I never thought possible.

I express my gratitude to my co-supervisor, Prof. Pradeep Kumar, for his invaluable guidance, unwavering support, and remarkable patience throughout the duration of the PhD program.

I want to express special appreciation to my colleagues and the WADDP staff. Engaging in intellectually stimulating academic exchanges with all of you while also maintaining a personal connection has been genuinely enriching. I would like to acknowledge Sarjan Patel for his help and support.

I would also like to thank Dr Abu Bakr Abu Median at the De Montfort University for his assistance, guidance, and support in this research.

I would also like to thank the team at the Wits Animal Research Facility (WARF) of the University of Witwatersrand for their assistance and help in carrying out the *in vivo* component of this research.

## DEDICATION

---

To the soul of my father, to my beloved mother, to my husband and children, and my sister and brothers – my pillars of support and encouragement – I dedicate this thesis to you.

## ABSTRACT

---

The skin wound healing process is a meticulously coordinated event involving the reconstruction of various cell types within the epidermal and dermal layers. In severe conditions like severe cutaneous wounds, the normal wound healing process is either delayed or fails to restore the injured tissue's normal structure and function adequately, leading to skin ulceration or other alterations. This has prompted the exploration of advanced therapeutic options such as gene therapy, growth factor therapy, platelet-rich plasma (PRP) therapy, stem cell-based therapy, and tissue engineering. Stem cell-based therapy has recently gained attention for its potential in treating cutaneous wounds due to the therapeutic capabilities of these cells. Despite encouraging results, certain limitations need consideration.

A significant challenge in stem cell-based replacement therapy is the low survival rate post-transplantation. Additionally, tumour-initiating cells share many characteristics with normal stem cells, posing concerns. Moreover, recent research has indicated that the mutation of normal stem cells within tissues may contribute to the emergence of cancer-initiating cells. The diverse array of secreted molecules from stem cells, encompassing growth factors and cytokines, is collectively termed the stem cell secretome. The application of the stem cell secretome for severe cutaneous wounds holds promise as a potential approach to address the limitations associated with the viable transplantation of replacement cells.

The therapeutic efficacy of mesenchymal stem cells (MSCs) secretome in wound healing has been demonstrated. However, there remains a need for a more advanced biomaterial-based carrier system capable of holding a larger quantity of secretome and delivering them more efficiently to enhance wound regeneration. The secretome plays a crucial role in the wound-healing process by stimulating and coordinating key cells, including keratinocytes, fibroblasts, and endothelial cells.

The current study explored the potential of the secretome derived from Rat dermal fibroblast cells incorporated in alginate – soy lecithin hydrogel to expedite the healing of cutaneous wounds both *in vitro* and *in vivo*. To aid the biocompatibility of the hydrogels, natural polymers such as alginate (Alg) were used. Alginate hydrogel dressing provides essential functions, including maintaining a moist environment, absorbing wound exudate, and facilitating swelling. Natural agents such as

Soy lecithin (SL) which has good biocompatibility, were used to modify the internal structure of the hydrogel during the preparation process.

Before incorporating the secretome, the alginate-soy lecithin hydrogel underwent evaluation for its physicochemical and physicommechanical attributes, exhibiting favourable structural characteristics. Subsequently, the harvested secretome underwent qualitative and quantitative analysis, focusing on factors like vascular endothelial growth factor (VEGF). Notably, after 72 hours, the secretome exhibited a heightened concentration of VEGF, reaching 2400 pg./ml, which holds a crucial role in angiogenesis. This study observed various properties, including fluid absorption (897.89% for secretome hydrogel (S. gel) and 4959.22% for Lyophilized secretome hydrogel (LS. gel) within 24 hours), degradation (43% for LS.gel and 94.57% for S.gel within 7 days), and mechanical characteristics (storage modulus of 2890 Pa and loss modulus of 773.4 Pa). Additionally, the *in vitro* bioactive release profile demonstrated an initial burst of protein release (56.6%) within 8 hours, leading to a total release of 60.5% within 3 days.

After incorporating secretome into the alginate-soy lecithin hydrogel, it showed excellent biocompatibility with cell viability exceeding 100%. This resulted in promising performance, indicating non-toxic behavior (cell viability > 100%) when exposed to NIH 3T3 embryonic fibroblast cells and HacaT cells for 3 days. The developed hydrogel demonstrates the potential to accelerate wound closure *in vitro* by effectively stimulating cell migration and proliferation in fibroblasts and keratinocyte cells showing scratch closure (87.4%) within 72 hours on NIH 3T3 cells, while (72.3%) closure on HacaT cells.

In vitro experiments were followed by in vivo assessments, which demonstrated that the secretome-loaded alginate-soy lecithin hydrogel functioned as a protective wound dressing, maintaining moisture and expediting wound healing. This acceleration was attributed to the sustained delivery of growth factors and cytokines from the secretome, enhancing cell-to-cell communication and promoting tissue remodeling. The hydrogel showed superior wound healing capabilities compared to a commercial product (Pharma-plast A) and a control group, with notable scar-less tissue regeneration after 21 days. These findings underscore the potential of fibroblast cell secretome hydrogel as an effective treatment for cutaneous wounds, improving the delivery of therapeutic biomolecules.

## Table of Contents

---

|                           |      |
|---------------------------|------|
| DECLARATION               | ii   |
| ANIMAL ETHICS DECLARATION | iii  |
| RESEARCH OUTPUTS          | iv   |
| RESEARCH PRESENTATIONS    | v    |
| ACKNOWLEDGEMENTS          | vi   |
| DEDICATION                | viii |
| ABSTRACT                  | ix   |
| TABLE OF CONTENTS         | xi   |
| APPENDICES                | xi   |
| LIST OF EQUATIONS         | xi   |
| LIST OF ABBREVIATIONS     | xi   |

## CHAPTER 1

### Introduction and Rationale of the Study

---

|     |   |   |
|-----|---|---|
| 1.1 | Background of the study                 | 1 |
| 1.2 | Rationale and Motivation for this Study | 4 |
| 1.3 | Novelty of the study                    | 6 |
| 1.4 | Hypothesis, aim and objectives          | 6 |
| 1.5 | Overview of the thesis                  | 8 |

### Figures and Tables

|                   |  |   |
|-------------------|--|---|
| <b>Figure 1.1</b> | Schematic representation of the skin layers and their components   | 4 |
| <b>Figure 1.2</b> | Schematic diagram illustrating the methodology of developing a biocompatible hydrogel using a polymeric network loaded with secretome to form an ECM network | 7 |

## CHAPTER 2

### Cell Secretome Strategies for Controlled Drug Delivery and Wound-Healing Applications

---

|     |              |    |
|-----|--------------|----|
| 2.1 | Introduction | 10 |
| 2.2 | Secretome    | 12 |

|       |  |    |
|-------|--|----|
| 2.2.1 | Secretome Composition  | 12 |
| 2.2.2 | Advantage of Secretome over Cell Therapy   | 14 |
| 2.2.3 | The Role of the Secretome in Different Stages of Wound Healing                                     | 15 |
| 2.3   | Secretome Applications in Wound Healing  | 16 |
| 2.4   | Secretome Delivery in Wound Healing  | 23 |
| 2.5   | Structural Formulation Using Biomaterials with Secretome for Wound-Healing Applications            | 26 |
| 2.5.1 | MSC Soluble Secretions and Their Combination with Biomaterials for Application in Different Wounds | 27 |
| 2.5.2 | MSC EVs and Their Combination with Biomaterials for Application in Different Wounds                | 30 |
| 2.5.3 | Secretome in 3D Bioprinting  | 32 |
| 2.6   | Conclusions  | 33 |
| 2.7   | Future Perspectives  | 34 |

### Figures and Tables

|                   |   |    |
|-------------------|---|----|
| <b>Figure 2.1</b> | MSC recruitment to wounded skin and the inflammatory phase and known and potential roles of MSCs in each phase of wound healing   | 14 |
| <b>Figure 2.2</b> | Mechanisms of mesenchymal stem cells secretome on wound healing   | 18 |
| <b>Figure 2.3</b> | Schematic representation of MSC secretome extraction and exosome separation and combination with polymers for in vivo wound application.  | 27 |
| <b>Figure 2.4</b> | Schematic illustration of the hydrogel crosslinking and full-thickness wound excision mouse model used to evaluate the wound healing properties of alginate hydrogel-incorporated exosome (Alg-EXO) | 32 |
| <b>Table 2.1</b>  | The therapeutic outcomes of MSC secretome (MSC-S) in wound healing.   | 18 |
| <b>Table 2.2</b>  | Biomaterials and their application in wound healing   | 24 |

## CHAPTER 3

### Secretome-loaded Alginate-Lecithin Hydrogel for wound healing application

|       |                       |    |
|-------|-----------------------|----|
| 3.1   | Introduction          | 35 |
| 3.2   | Materials and Methods | 37 |
| 3.2.1 | Materials             | 37 |
| 3.2.2 | Methods               | 38 |

|           |   |    |
|-----------|---|----|
| 3.2.2.1   | Secretome collection and quantification using Enzyme-Linked Immunosorbent Assay (ELISA) | 38 |
| 3.2.2.2   | Development of secretome-loaded alginate-lecithin hydrogel                              | 38 |
| 3.2.2.3   | Assessing chemical properties of the alginate bioplatfroms using FTIR                   | 39 |
| 3.2.2.4   | X-ray powder diffraction analysis of the bioplatfroms                                   | 40 |
| 3.2.2.5   | Assessing thermophysical properties of the bioplatfroms using DSC and TGA               | 40 |
| 3.2.2.6   | Zeta potential of the bioplatfroms  | 40 |
| 3.2.2.7   | Determining the degree of crosslinking of the bioplatfroms                              | 41 |
| 3.2.2.8   | Assessing gelling and viscoelastic properties of the bioplatfroms                       | 41 |
| 3.2.2.9   | Hydrogel mechanical evaluation and stability studies                                    | 42 |
| 3.2.2.9.1 | Physical stability of the Hydrogel  | 42 |
| 3.2.2.9.2 | Stability of secretome proteins after loaded into the hydrogel                          | 42 |
| 3.2.2.10  | Swelling and degradation studies of the bioplatfroms                                    | 42 |
| 3.2.2.11  | The release profile of secretome total proteins from the secretome hydrogel             | 43 |
| 3.2.2.12  | Biocompatibility and cytotoxicity assessment of the bioplatfroms                        | 43 |
| 3.2.2.13  | <i>In vitro</i> wound healing test employing the scratch assay.                         | 44 |
| 3.2.2.14  | Cell migration assay using a modified Boyden chamber                                    | 45 |
| 3.2.2.15  | Data Analysis   | 45 |
| 3.3       | Results and Discussion  | 46 |
| 3.3.1     | Secretome collection and quantification using Enzyme-Linked Immunosorbent Assay (ELISA) | 46 |
| 3.3.2     | Development of secretome-loaded alginate-lecithin hydrogel                              | 47 |
| 3.3.3     | Assessing chemical properties of the bioplatfroms using FTIR                            | 48 |
| 3.3.4     | X-ray powder diffraction analysis of the bioplatfroms                                   | 49 |
| 3.3.5     | Assessing thermophysical properties of the bioplatfroms using DSC and TGA               | 50 |
| 3.3.6     | Zeta potential of the bioplatfroms  | 54 |
| 3.3.7     | Determining the degree of crosslinking of the bioplatfroms                              | 54 |
| 3.3.8     | Assessing gelling kinetics and viscoelastic properties of the bioplatfroms              | 54 |
| 3.3.9     | Hydrogel mechanical evaluation and stability studies                                    | 57 |
| 3.3.9.1   | Physical stability of the hydrogel  | 57 |
| 3.3.9.2   | Stability of secretome proteins after loaded into the hydrogel                          | 57 |
| 3.3.10    | Swelling and degradation studies of the bioplatfroms                                    | 60 |
| 3.3.11    | Release profile of total secretome proteins   | 63 |
| 3.3.12    | Biocompatibility and cytotoxicity assessment of the bioplatfroms                        | 65 |

|          |   |    |
|----------|---|----|
| 3.3.12.1 | Cytocompatibility on NIH 3T3 cells                                  | 65 |
| 3.3.12.2 | Cytocompatibility on HacaT cells                                    | 66 |
| 3.3.13   | <i>In vitro</i> wound healing test employing the scratch assay.     | 69 |
| 3.3.13.1 | Wound healing impact of the hydrogel on murine fibroblast (NIH-3T3) | 70 |
| 3.3.13.2 | Wound healing impact of the hydrogel on human keratinocytes (HacaT) | 74 |
| 3.3.14   | Cell migration assay using a modified Boyden chamber                | 78 |
| 3.4      | Conclusion  | 79 |

### Figures and Tables

|                   |  |    |
|-------------------|--|----|
| <b>Figure 3.1</b> | Schematic representation of secretome collection and loading in alginate-soy lecithin hydrogel   | 39 |
| <b>Figure 3.2</b> | Quantitative analysis of Fat's Dermal Fibroblast condition media for VEGF Concentration in secretome collected over different times  | 47 |
| <b>Figure 3.3</b> | The analytical techniques (a) FTIR spectra, (b) X-ray diffractograms, (c) DSC and (d) TGA thermograms of the bioplatfroms used to evaluate chemical composition, functional groups, and phase changes of the bioplatfroms induced by cross-linking | 50 |
| <b>Figure 3.4</b> | The hydrogel formation Kinetics of Alg-SL in water at 37 °C  | 56 |
| <b>Figure 3.5</b> | The hydrogel appearance, mechanical stability over 3 months and the quantitative assessment of VEGF to illustrate the stability characteristics of different formulations  | 59 |
| <b>Figure 3.6</b> | (a) Biodegradation (weight loss) and (b) swelling behaviour of the S.gel and LS.gel in PBS (pH 6.5) solution at 37°C at 50 rpm   | 62 |
| <b>Figure 3.7</b> | Protein release profiles. Protein content released from LS.gel and S.gel into the supernatant was estimated using BCA protein assay kit  | 64 |
| <b>Figure 3.8</b> | Cytotoxicity assessments to evaluate the cell viability of hydrogel formulations and starting materials at six different concentrations on (a) NIH 3T3 and (b) HacaT cells.  | 68 |
| <b>Figure 3.9</b> | Cytotoxicity assessments on NIH 3T3 and HacaT cells using concentrations of 100 µg/ml for both secretome-loaded hydrogels and lyophilized secretome-loaded hydrogel over 24, 48, and 72 hours(n=3)   | 69 |
| <b>Figure3.10</b> | Microscopic scratch closures over time for the three formulations (lyophilized secretome-loaded hydrogel, secretome-loaded hydrogel, secretome collected after 72 hrs at the concentration (2.7% w/v of VEGF) evaluated on the 3T3 cell line.      | 72 |
| <b>Figure3.11</b> | Results of wound healing analysis of NIH 3T3 exposed to different treatments   | 73 |
| <b>Figure3.12</b> | Microscopic scratch closures over time for the three formulations (lyophilized secretome hydrogel, secretome hydrogel, secretome alone) at a concentration (2.7% W/V of VEGF) evaluated on the HacaT cell line.                                    | 76 |
| <b>Figure3.13</b> | Results of wound healing analysis of HacaT exposed to different treatments   | 77 |
| <b>Figure3.14</b> | The result of migration assay of HacaT and NIH 3T3 cells with 4%V/V hydrogel pre-incubation with secretome-loaded hydrogel and normal hydrogel   | 79 |

|                  |  |    |
|------------------|--|----|
| <b>Table 3.1</b> | Summary of the chemical and physical characteristics of bioplatfroms using FTIR, XRD, DSC, and TGA     | 52 |
| <b>Table 3.2</b> | The migration of HacaT and NIH 3T3 cells pre-incubated with secretome-loaded hydrogel versus controls. | 78 |

## CHAPTER 4

### Evaluation of the wound closure rate and histological analysis of Alginate soy lecithin loaded secretome hydrogel in an acute incisional rat model.

|         |  |     |
|---------|--|-----|
| 4.1     | Introduction   | 81  |
| 4.2     | Materials and Methods  | 82  |
| 4.2.1   | Materials  | 82  |
| 4.2.2   | Animal Husbandry   | 83  |
| 4.2.3   | The Surgical Procedure and Experimental Design   | 84  |
| 4.2.4   | Post-surgery care and follow up  | 85  |
| 4.2.5   | Evaluation of wound size   | 86  |
| 4.2.6   | Histological analysis  | 86  |
| 4.2.7   | Scores of wound healings   | 87  |
| 4.2.8   | Statistical analysis   | 87  |
| 4.3     | Results and Discussion   | 88  |
| 4.3.1   | Results  | 88  |
| 4.3.1.1 | Evaluation of Wound Size   | 88  |
| 4.3.1.2 | Histopathological analysis to evaluate the extent and characteristics of wound healing | 91  |
| 4.3.1.3 | Histopathological assessment after the three-day treatment                             | 92  |
| 4.3.1.4 | Histopathological assessment after the 7th-day treatment                               | 95  |
| 4.3.1.5 | Histopathological assessment after the 14th-day treatment                              | 97  |
| 4.3.1.6 | Histopathological assessment after the 21st -day of treatment                          | 99  |
| 4.3.1.7 | Scores of wound healings   | 101 |
| 4.4     | Discussion   | 103 |
| 4.5     | Conclusion   | 108 |

### Figures and Tables

|                   |   |    |
|-------------------|---|----|
| <b>Figure 4.1</b> | The housing conditions provided for the individual rat include regulated temperature and readily available food and water | 83 |
| <b>Figure 4.2</b> | Visual representation illustrating the experimental design, displaying the breakdown of the four experimental groups.     | 85 |

|                   |   |     |
|-------------------|---|-----|
| <b>Figure 4.3</b> | Wound morphology images of Sprague–Dawley rats treated with the bioplatforms and allowed to heal over 21 days   | 90  |
| <b>Figure 4.4</b> | A graphical illustration showing the progression of wound healing in rats subjected to secretome hydrogel and commercial comparative product compared to the control group. | 91  |
| <b>Figure 4.5</b> | Histology of the wound tissues at the early wound healing stage treated with different groups of bioplatforms. (1) After H and E stain while (2) after MT stain             | 94  |
| <b>Figure 4.6</b> | Histology of the wound tissues at the early to mid-wound healing stage treated with different groups of bioplatforms. (1) After H and E stain while (2) after MT stain      | 97  |
| <b>Figure 4.7</b> | Histology of the wound tissues at the early late wound healing stage treated with different groups of bioplatforms. (1) After H and E stain while (2) after MT stain        | 99  |
| <b>Figure 4.8</b> | Histology of the wound tissues at the late wound healing stage treated with different groups of bioplatforms. (1) After H and E stain while (2) after MT stain              | 101 |
| <b>Table 4.1</b>  | Scoring system for histological assessment of wound healing   | 87  |
| <b>Table 4.2</b>  | The percentage of wound closure observed during the 3-day, 7-day, 14-day, and 21-day investigations   | 89  |
| <b>Table 4.3</b>  | Scores of wound healing   | 103 |

## Chapter 5

### Conclusions, Future considerations, and recommendations

|     |                 |     |
|-----|-----------------|-----|
| 5.1 | Conclusion      | 109 |
| 5.2 | Limitations     | 111 |
| 5.3 | Recommendations | 112 |
|     | References      | 114 |

### APPENDICES

|            |                                     |     |
|------------|-------------------------------------|-----|
| Appendix A | Animal Ethics Clearance Certificate | 141 |
| Appendix B | Review Paper                        | 142 |
| Appendix C | Presentation abstract               | 158 |

### List of equations

|              |                              |    |
|--------------|------------------------------|----|
| Equation 3.1 | % <i>Cross-linking index</i> | 41 |
| Equation 3.2 | Swelling (%)                 | 43 |
| Equation 3.3 | Equation 3.3 Degradation (%) | 43 |
| Equation 3.4 | Wound closure (%)            | 45 |
| Equation 4.1 | Wound closure (%)            | 86 |

### List of Abbreviations

---

---

|   |            |
|---|------------|
| Activated phosphatidylinositol 3 kinase/Protein kinase    | PI3K/Akt   |
| Adipose tissue-derived stem cells                         | ADSCs      |
| Alginate  | Alg        |
| Alginate hydrogel-incorporated exosome                    | Alg-EXO    |
| Analysis of Variance                                      | ANOVA      |
| Angiopoietin  | Ang        |
| Basic fibroblast growth factor                            | bFGF       |
| Beta-tricalcium phosphate _                               | TCP        |
| Bone marrow mesenchymal stem cells                        | BM-MSCs    |
| Chemokine   | CXCL5      |
| conditioned medium  | CM         |
| Conditioned medium from human uterine cervical stem cells | CM-hUCESCs |
| Differential Scanning Calorimetry                         | DSC        |
| Dimethyl Sulfoxide  | DMSO       |
| Dulbecco's modified eagle's medium                        | DMEM       |
| Epidermal Growth Factor                                   | EGF        |
| Endothelial growth factor                                 | EGF        |
| Enzyme-Linked Immunosorbent Assay                         | ELISA      |
| Extracellular matrix                                      | ECM        |
| Extracellular signal-regulated kinase 1                   | ERK1       |
| Extracellular vesicles                                    | EV         |
| Fetal Bovine Serum  | FBS        |





|  |         |
|--|---------|
| Fibroblast Growth Factor                   | FGF     |
| Focal adhesion kinase                      | FAK     |
| Fourier Transform Infra-Red                | FTIR    |
| Gelatin methacrylate                       | GeIMA   |
| Good manufacturing practice                | GMP     |
| Granulocyte-colony stimulating factor      | G-CSF   |
| Hematoxylin and Eosin stain                | H&E     |
| Hepatocyte growth factor                   | HGF     |
| Human adipose tissue mesenchymal stem cell | HATMSC  |
| Human bone marrow mesenchymal stem cell    | BMSC    |
| Human microvascular endothelial cells      | HMEC    |
| Human umbilical cord perivascular cells    | HUCPVCs |
| Human umbilical vascular endothelial cells | HUVECs  |
| Human uterine cervical stem cells          | hUCESCs |
| Hyaluronic acid                            | HA      |
| Hyperbaric oxygen therapy                  | HBO2    |
| Interleukins                               | IL      |
| Keratinocyte growth factor                 | KGF     |
| Leukaemia inhibitory factor                | LIF     |
| Lyophilized secretome hydrogel             | LS. gel |
| Masson's trichrome stain                   | MT      |
| Matrix metalloproteinase                   | MMP     |
| Mesenchymal stem-cell-conditioned media    | MSC-CM  |
| Mesenchymal stem cells                     | MSC     |

|  |         |
|--|---------|
| Mesenchymal stromal cell secretome-chitosan hydrogel | MSC-Ch  |
| Monocyte chemoattractant protein                     | MCP     |
| Mouse embryonic fibroblast cells                     | NIH 3T3 |
| Multipotent adult progenitor cell-conditioned medium | MAPC-CM |
| Multipotent mesenchymal stromal cell                 | MMSC    |
| Nanoparticles  | NPs     |
| Phosphate Buffered Saline                            | PBS     |
| Platelet-derived growth factor                       | PDGF    |
| Polyethylene glycol                                  | PEG     |
| Poly isocyanate                                      | PIC     |
| Poly(lactide-co-glycolide)                           | PLGA    |
| Poly-L-lactic acid                                   | PLLA    |
| Rat dermal fibroblast cells                          | FR      |
| Roswell Park Memorial Institute                      | RPMI    |
| Secretome collected after 24 hrs                     | S24 hrs |
| Secretome collected after 48 hrs                     | S48 hrs |
| Secretome collected after 72 hrs                     | S72 hrs |
| Secretome hydrogel                                   | S. gel  |
| Sickle cell disease                                  | SCD     |
| Smooth muscle actin                                  | SMA     |
| Soy lecithin   | SL      |
| Statistical Package for Social Sciences              | SPSS    |
| Synovium mesenchymal stromal cell                    | SMSC    |
| Tissue inhibitors of metalloproteinases              | TIMP    |

|  |           |
|--|-----------|
| Thermogravimetric Analysis                               | TGA       |
| Thiazolyl Blue Tetrazolium Bromide                       | MTT       |
| Transforming growth factor                               | TGF       |
| Tumour necrosis factor-alpha                             | TNF       |
| Umbilical cord mesenchymal stem cells C-derived exosomes | UMSC-Exos |
| Vascular endothelial growth factor                       | VEGF      |
| Wits Research Animal Facility                            | WRAF      |
| Wharton's jelly mesenchymal stem cells                   | WJ-MSCs   |
| X-ray powder diffraction                                 | XRD       |

## CHAPTER 1

### INTRODUCTION AND RATIONALE OF THE STUDY

---

#### 1.1 Background of the study

The skin is characterized by a complex structure that encompasses the epidermis, dermis, and hypodermis layers (Figure 1.1). Severe skin injuries, especially those causing full-thickness damage to the epidermis and dermis, as well as affecting appendages such as sweat glands, sebaceous glands, hair follicles, and subcutaneous tissue, result in the formation of non-functional scars. Wounds are skin defects that occur due to external factors like thermal/chemical/physical injury or due to pathological conditions. Wounds are categorized into acute and chronic based on the repair process involved (Mir et al., 2018). The Body's wound healing process involves inflammation followed by the cellular proliferation process and the remodelling process. These processes take place from two days to two years depending on the wound type (Xiang et al., 2020).

Despite numerous efforts to facilitate effective healing through wound dressings or skin grafts, these attempts have demonstrated therapeutic limitations, highlighting the need for enhancements to achieve more advanced wound regeneration. The emergence of regenerative medicine as an alternative approach provides additional treatment possibilities, with a focus on improving wound healing and restoring the skin's innate structure (Nourian Dehkordi et al., 2019). Mesenchymal stem cells (MSCs) have attracted interest in clinical therapeutic applications, due to their multipotency and capacity for self-renewal, intending to rejuvenate tissues and manage diverse diseases (Han et al., 2019). The research conducted by (Gao et al., 2024; Guillamat-Prats, 2021) on the involvement of MSCs in the inflammatory, proliferative, and remodelling stages of wound healing highlights the potential of MSC therapy in addressing challenging or slow-healing wounds. A recent research study showed that the application of topical MSCs improves wound healing and promotes angiogenesis (Azari et al., 2022). In addition, administering MSC injections has been observed to reduce inflammation and elevate levels of vascular endothelial growth factor (VEGF) (Sears et al., 2021).

Nevertheless, obstacles such as inadequate engraftment efficiency, restricted cell retention, and low cell survival pose challenges to the success of MSC-based therapies (Zhou et al.,

2021). Recent research underscores the pivotal role of the MSC "secretome," encompassing angiogenic factors, hormones, cytokines, growth factors, and extracellular matrix proteases, in reparative processes (Sandona et al., 2021). Studies suggest that MSC-conditioned media contribute to improved wound healing by reducing inflammation, enhancing cellular functions, and promoting the formation of granulation tissue (Xu et al., 2023). Moreover, the enhanced safety profile of MSC-secretome in comparison to direct cell delivery, coupled with an extended shelf life, positions MSC-secretome-based therapy as a more clinically translatable strategy (Bormann et al., 2023).

The secretome comprises a range of chemokines, cytokines, growth factors, and exosomes released by cells. Notably, the secretome of (MSCs) has demonstrated therapeutic effects in wound healing (Ahangar et al., 2020). However, there remains a necessity for more sophisticated biomaterial-based carrier systems capable of effectively retaining larger amounts of secretome to boost wound regeneration. (Kwon et al., 2023). These secretomes serve as crucial mediators in the wound healing process by facilitating and coordinating various contributing cells such as fibroblasts, endothelial cells, and keratinocytes. Key factors such as Vascular Endothelial Growth Factor (VEGF), Hepatocyte Growth Factor (HGF), FGF, and Platelet-Derived Growth Factor (PDGF) play pivotal roles in angiogenesis and the formation of granulation tissue. Additionally, Transforming Growth Factor- $\beta$  (TGF- $\beta$ ), Fibroblast Growth Factor (FGF), Epidermal Growth Factor (EGF), Interleukin-1 (IL-1), Interleukin-6 (IL-6), and Tumor Necrosis Factor- $\alpha$  (TNF- $\alpha$ ) are essential for re-epithelialization. Furthermore, FGF and PDGF are heavily involved in remodelling and matrix formation (Hur et al., 2017).

Alternatively, readily available cells such as skin fibroblasts, which possess a high proliferative potential, may offer an attractive option for wound healing compared to stem cells (Ichim et al., 2018). Fibroblasts, the predominant cells in connective tissues, are well-known for their essential role in building and modifying the extracellular matrix (Plikus et al., 2021). Despite their diverse functions, defining them precisely proves challenging due to the considerable heterogeneity within the stromal cell population (Li et al., 2023). To broaden the therapeutic capacity of the secretome, advanced biomaterial-based hydrogel systems can efficiently be developed to hold larger quantities of secretome for enhanced wound regeneration (Arifka et al., 2022).

Biomedical research has identified the application of hydrogel to fulfil a crucial function in wound healing (Kirsner and Eaglstein, 1993). Wound management aims to facilitate wound healing in the shortest time. Hydrogels could aid the wound healing processes by fulfilling the following requirements (a) providing a moist wound environment, (b) minimal frequency of dressing change, (c) absorption of excess exudates from wound sites, (d) prevention of secondary infection, (e) maintaining adequate gaseous exchange, (f) controlling the release of incorporated bio-actives, and (g) assimilation of extracellular matrix (ECM) physicochemical attributes in terms of elasticity, biocompatibility and biodegradability (Chirani et al., 2015; Mndlovu et al., 2019). To achieve the above requirements, hydrogels have been designed from various biomolecules which range from natural/synthetic polymers, antibiotics, and peptides/proteins (Mayet et al., 2014).

An optimal natural/synthetic polymer-based hydrogel for wound dressing applications should assimilate the physicochemical and physicochemical properties of the skin tissues. Alginate, derived from seaweed, is a natural polymer extensively employed in various industries, including foods, pharmaceuticals, fertilizers, cosmetics, and medicine (Sreya et al., 2023). Recognized for its biocompatibility, hydrophilicity, ease of handling, and durability, alginate has emerged as a compelling material for wound dressing (Aderibigbe and Buyana, 2018). Commercially available alginate hydrogel dressings offer essential features like maintaining a moist environment, absorbing wound exudate, and facilitating swelling (Minsart et al., 2022).

Modifying the properties of hydrogel materials is crucial for their potential use in modern material engineering. One way to alter these properties is by introducing additional components into their internal structure. The use of natural substances, which are biocompatible and biodegradable, is advantageous. In this study, soy lecithin, a naturally occurring substance found in human tissues, was used to modify the internal structure of hydrogels (Heger et al., 2022). Soy lecithin is a phospholipid mixture that exhibits hydrophobic and hydrophilic properties and can increase the bioavailability of concurrently administered drugs. Modulating the proportion of soy lecithin within a multi-component hydrogel system can improve the gel's effectiveness and ease of use. Changes made to the internal structure of materials can significantly influence their mechanical and transport properties (Heger et al., 2022). Hydrogel is a material that has gained considerable attention for its ability to produce a moist microenvironment and absorb wound exudates, which is crucial for facilitating wound healing.

In this investigation, an alginate soy lecithin hydrogel incorporating secretome derived from fibroblast cells was developed. The study posits that secretome-loaded alginate soy lecithin hydrogel can effectively retain and facilitate a prolonged release of the bioactive molecules from the secretome, leading to a significantly enhanced therapeutic impact. The main objective was to fortify the hydrogel with a substantial quantity of secretome, enabling more efficient delivery of these therapeutic biomolecules into skin wounds. To achieve this, the conditioned medium (CM) rich in secretome was prepared through centrifugation, and an alginate-soy lecithin incorporated hydrogel containing this secretome was developed (Figure 1.2).

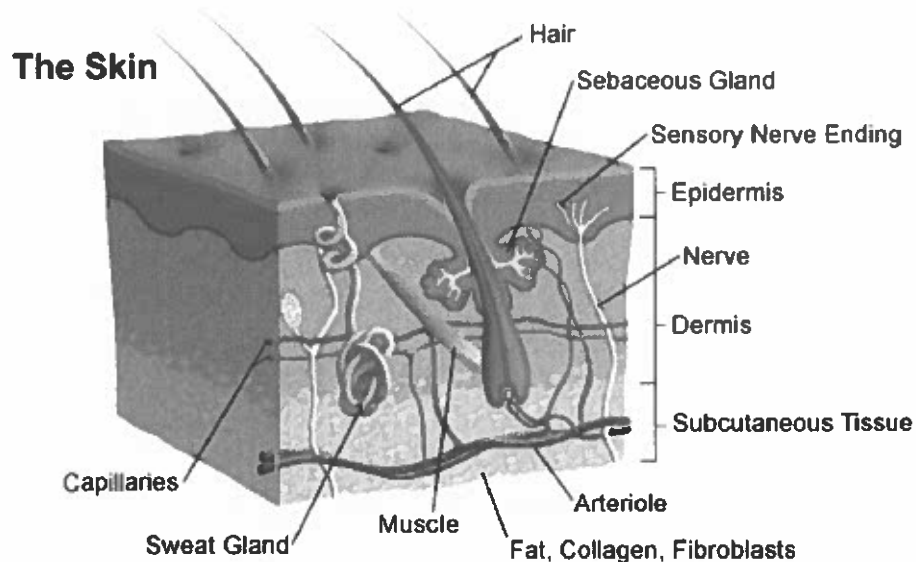


**Figure 1.1** Diagram illustrating the layers of the skin and their constituents (Kolimi et al., 2022)

## 1.2 Rationale and Motivation for this Study

Wounds pose a high financial burden in hospitals, clinics, and individual patients in general. The financial burden ranges from long hospitalization duration due to chronic wounds, expensive treatment of wound injuries and high frequency of dressing changes. Treatment of wounds includes gauze, nano/microparticles, foams, scaffolds, fibres, mats, sprays and gels. Although there are a variety of treatment forms, an ideal wound dressing that fulfils all requirements has yet to be developed. These criteria encompass but are not limited to, ensuring and regulating balanced hydration levels via skin absorption, and managing wound

exudates, The hydrogel enables adequate gaseous exchange at the wound site, thus preventing secondary infections, controlling and localizing the release of embedded bioactive substances, and demonstrating characteristics comparable to the extracellular matrix (ECM), including facilitating cellular communication. The present investigation focuses on the exploration of polymers and the secretome, to develop a biocompatible hydrogel for the treatment of acute wounds. The secretome was chosen for this study to address challenges such as biosafety concerns, tumorigenicity, infections, and high costs associated with cell therapy. Moreover, enhancing the bioavailability and retention time of the secretome requires its combination with biomaterials, thereby amplifying its therapeutic potential.

Natural polymers such as alginate were used to develop hydrogel. Furthermore, soy lecithin, a naturally occurring substance in human tissues known for its biocompatibility and biodegradability, was employed to modify the internal structure of hydrogels. Crosslinkers such as Calcium Chloride could be explored in the study to attain desirable properties of the hydrogel and controlled release of the bioactive molecules of the secretome. The combination of biocompatible polymers, secretome and crosslinkers will improve the hydrogel properties. These properties will include but are not limited to visco-elasticity, exudates absorption, and also biodegradation. Exudate absorption will provide essential nutrients for optimal skin tissue regeneration. Secretome fluid will be used in fabricating the hydrogels. The secretome contains several proteins and biological markers which are crucial for cellular communications. This includes but is not limited to tumour growth factor- $\beta$  (TGF- $\beta$ ), VEGF, keratinocyte growth factor (KGF), FGF2, PDGF, fibronectin and collagen. In the present study, the Vascular Epithelial Growth Factor (VEGF) has been chosen as the target protein for quantification, aiming to assess the presence of this biological marker in the secretome.

The use of secretome in fabricating the hydrogel will aid cellular attachment to the hydrogel and facilitate accelerated tissue regeneration. The presence of secretome will aid the hydrogel's ability to mimic the ECM whilst the polymers will provide structural support for cellular and tissue growth. Success in this study would be the development of a biocompatible hydrogel with controlled secretome release, fluid absorptive properties, cytocompatibility, and demonstrated accelerated *in vivo* wound healing abilities.

### **1.3 Novelty of the study**

The novelty of the study lies within the use of secretome in fabricating hydrogel. Secretome area set of proteins found in the extracellular space which function to communicate with local cells. This cellular communication property of the hydrogel will aid biocompatibility, cellular adhesion and tissue regeneration. The presence of a secretome will aid communication between the cells and the hydrogel to facilitate cell attachment and tissue regeneration. The use of natural polymers is a major development in the design. This hydrogel is designed to mix with wound exudate, which is crucial for presenting an environment conducive to optimum tissue regeneration. Interaction of these biocompatible materials with wound fluid will greatly enhance tissue repair mechanisms. Furthermore, the selection of biodegradable and bioresorbable polymers is of great importance in the sense that there will be no need for biomaterial changes during the skin regeneration process. This will improve patient compliance throughout treatment.

### **1.4 Hypothesis, aim and objectives**

The research hypothesizes that incorporating the secretome into polymeric biomaterials during the hydrogel fabrication process substantially influences the properties and performance of the resulting hydrogel.

This research aims to develop a biocompatible, bio-adhesive, and exudate-absorbing hydrogel, while also possessing controlled release capabilities for secretome bioactive molecules. The ultimate goal is to optimize its potential for tissue regeneration and repair. The above aim will be achieved through the following objectives:

1. Collect secretome from Rat dermal fibroblast cell line (FR, CRL-1213, ATCC, Manassas, or VA), qualitative and quantitative evaluation of VEGF in the secretome.
2. Develop a biocompatible hydrogel following the solution gelation approach and using natural-based polymeric biomaterials and secretome.
3. Determine the physicochemical properties of the materials and the formulated hydrogels via the use of FTIR, Differential Scanning Calorimetry (DSC), Thermogravimetric Analysis (TGA), X-ray powder diffraction (XRD), to confirm the presence of starting biomaterials.
4. Determine the physicommechanical properties of the hydrogels via the use of ElastoSens™ Bio<sup>2</sup> and Rheometer which will give insights into how the compositions

of hydrogels can be adjusted to create a hydrogel with mechanical properties resembling those of the skin. Assess hydrogel-forming kinetics using ElastoSens™ Bio<sup>2</sup>

5. Evaluation of the cytocompatibility of the hydrogel *in vitro* following the cell viability assay employing a mouse embryonic fibroblast NIH 3T3 cell line. This will help prevent using toxic concentrations of biomolecules.
6. Assess the *in vitro* bioactivity of the hydrogel following the scratch assay employing a mouse embryonic fibroblast NIH 3T3 and Human keratinocytes (HacaT) cell lines. This will help reflect *in vitro* wound healing.
7. Assess the cell migration capability of the hydrogel to validate the acceleration efficacy of the hydrogel on 3T3 and HacaT cell lines.
8. Evaluate the wound healing potential of hydrogel on acute wounds using the Sprague Dawley Rat model.

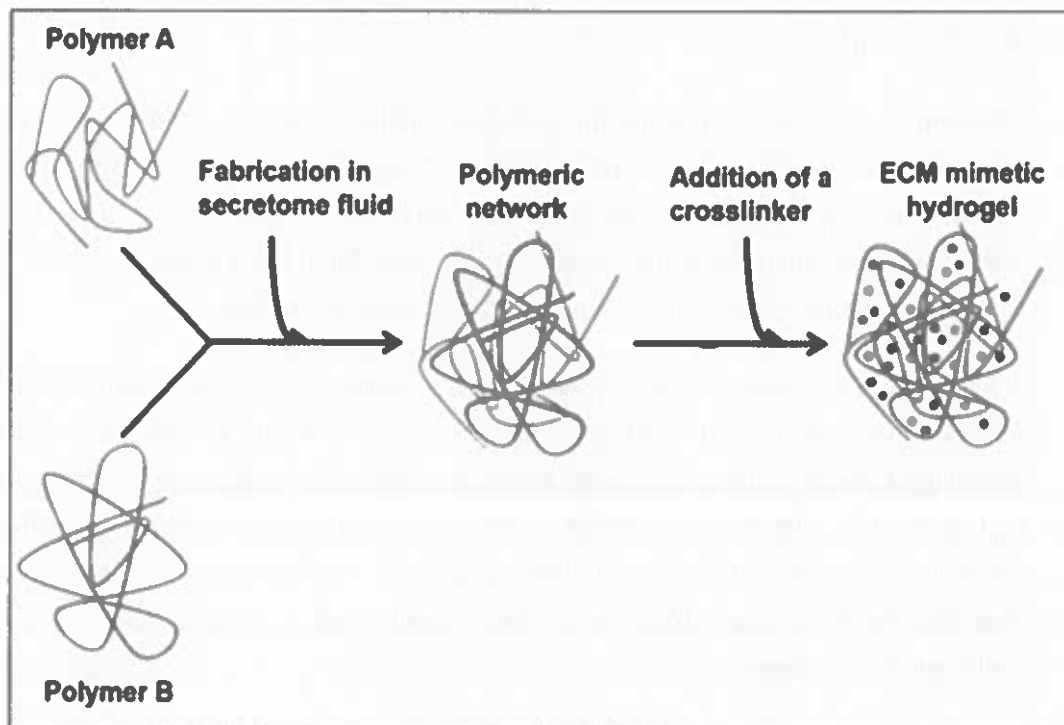


**Figure 1.2** Schematic diagram illustrating the methodology of developing a biocompatible hydrogel using a polymeric network loaded with secretome to form an ECM network.

## 1.5 Overview of the thesis

**Chapter 1:** This section provides an overview of the current state of research in advanced tissue engineering, emphasizing the constraints of cellular therapy and identifying the existing gap in the field. This gap serves as the foundation for the rationale and objectives of the study. Alginate polymer and a natural phospholipid Soy lecithin were chosen for this investigation due to their well-documented favourable biological properties.

**Chapter 2:** This chapter defines the secretome and delves into its prospect as a cell-free therapy for addressing cutaneous wounds, offering an alternative to overcome the limitations of whole-cell transplantation. It highlights the exploration of *in vitro* and *in vivo* applications that integrate biomaterials with the secretome to effectively treat wounds, improve retention, and regulate release, thus maintaining its biological efficacy. Additionally, the chapter emphasizes diverse strategies employed in crafting biomaterials infused with conditioned media or extracellular vesicles, underscoring their promising clinical utility in wound management.

**Chapter 3:** This section reveals the outcomes derived from the initial screening of the secretome for bioactivity. The secretome obtained at distinct time intervals, specifically S24 hrs, S48 hrs, and S72 hrs, underwent an assessment to ascertain their *in vitro* bioactivity. The optimal secretome, selected for formulation, was determined based on the evaluation of *in vitro* cytotoxicity and scratch closure rates of each secretome.

Additionally, this chapter details the development, characterization, and optimization of the instructive hydrogel incorporating the secretome. The selected optimal secretome, identified during the screening phase as S72hrs, was incorporated into an alginate soy lecithin-loaded hydrogel. The resulting formulation underwent characterization to evaluate its physicochemical and physicochemical properties. Furthermore, the formulation was assessed for *in vitro* cytotoxicity and scratch closure rate to ascertain its impact on cell proliferation and migration.

**Chapter 4:** This section explores the *in vivo* assessment of wound closure rate and biocompatibility using a rat model with a secretome-loaded alginate soy lecithin hydrogel. Formulations that demonstrated positive *in vitro* results were advanced to *in vivo* testing through the punch biopsy method in rat models. The evaluation focused on comparing wound closure rates and assessing biocompatibility in this context.

**Chapter 5:** This chapter delineates the characteristics and functionality of the secretome-loaded alginate soy lecithin hydrogel. It furnishes the research findings, along with prospective recommendations, offering insights into future perspectives and suggesting avenues for further studies in the domain of wound healing formulations and skin tissue regeneration.

## CHAPTER 2

### CELL SECRETOME STRATEGIES FOR CONTROLLED DRUG DELIVERY AND WOUND-HEALING APPLICATIONS

---

---

Published in Polymers

Ibrahim, R., Mndlovu, H., Kumar, P., Adeyemi, S.A. and Choonara, Y.E., 2022. Cell Secretome Strategies for Controlled Drug Delivery and Wound-Healing Applications. *Polymers*, 14(14), p.2929.

#### 2.1 Introduction

The skin is considered the largest human organ that protects the outer body against the external environment. This includes physical, chemical, and microbial invasion, which leads to skin injury or trauma upon exposure (Proksch, Brandner et al. 2008; Kim and Dao 2021; Xu, Zhang et al. 2021). Skin wounds and complicated wound-healing processes affect about one billion people worldwide and have an enormous influence on the human healthcare system, leading to an increase in financial cost (Rodrigues, Kosaric et al. 2019; Raziyevea, Kim et al. 2021). Wounds are categorized as acute or chronic; acute wounds can heal quickly in a short period; however, if not treated properly, they can become chronic wounds (Uzun 2018; Okur, Karantas et al. 2020).

Wound healing is an organized and highly regulated process that comprises the following phases: inflammation, proliferation, tissue remodelling, and extracellular matrix ECM deposition (Rittié 2016; Wang 2018; Rezvani Ghomi, Khalili et al. 2019; Rodrigues, Kosaric et al. 2019; Ma, Lam et al. 2021). Acute wounds can be managed generally with a physiological wound-healing process. Chronic wounds can be managed with growth factors and cytokines, skin substitutes composed of polymeric materials and biologically derived substances to act as a structural support at the wound site; hyperbaric oxygen therapy (HBO<sub>2</sub>); and skin grafts (Han and Ceilley 2017; Ma, Lam et al. 2021). Wound-healing management has been extending from traditional dressing to modern advanced types, which to some extent solve the problems associated with the traditional ones. Modern dressings must be biocompatible, biodegradable, and mimic the biological molecules

involved in the body's natural healing stages to provide greater adaptability to the wound bed, which is reflected in accelerated wound healing (Uzun 2018; Xu, Han et al. 2020). However, the approaches mentioned above have practical limitations such as wound treatments (Berwin Singh, Park et al. 2018).

New therapeutic approaches for the treatment of non-healing wounds have now been developed. One of the most promising approaches is using stem-cell-based therapy as an alternative approach for tissue repair and wound healing. Stem cells have a high capacity for self-renewal, interacting with the wound environment, and emitting bioactive secretions that accelerate wound healing. However, this technique has been faced with limitations such as biosafety, immune compatibility, potential tumorigenicity, infection risk, complicated material storage, and higher treatment costs (Kucharzewski, Rojczyk et al. 2019; Nourian Dehkordi, Mirahmadi Babaheydari et al. 2019; González-González, García-Sánchez et al. 2020; Gruca, Zając et al. 2022). Therefore, the development of more effective therapeutic strategies for advanced wound healing with minimized costs should be carried out.

Recent research proposed that it is worthwhile to use the paracrine activity of stem cells, where their secreted molecules yield higher therapeutic impacts than using cells. The secretome or condition media of stem cells play an essential role in regenerative medicine alternatives to living cells (Vizoso, Eiro et al. 2017; González-González, García-Sánchez et al. 2020; Mendes-Pinheiro, Marote et al. 2020; Brembilla, Modarressi et al. 2022). The secretome is defined as a range of bioactive molecules produced by a cell in the extracellular space, which includes but is not limited to proteins, nucleic acids, proteasomes, exosomes, microRNA, and membrane vesicles (Ahangar, Mills et al. 2020; Pinho, Cibrão et al. 2020; Pokrovskaya, Zubareva et al. 2020). Secretome components are classified into the following: (a) a soluble portion comprising cytokines, chemokines, and immunomodulatory molecules and growth factors; and (b) the extracellular vesicle, which is composed of microvesicles and exosomes that play an important role in cell-cell communication due to their involvement in microRNA and protein delivery (Mitchell, Mellows et al. 2019; Casado-Díaz, Quesada-Gómez et al. 2020; González-González, García-Sánchez et al. 2020).

Secretomes gained considerable attention in skin-wound management, as presented in vitro and in vivo studies that show the ability of Secretomes to improve the wound healing process by accelerating angiogenesis, inflammation reduction, and the stimulation of

fibroblast and keratinocyte proliferation (Bartaula-Brevik, Bolstad et al. 2017; Guo, Schaudinn et al. 2022). Secretome can exert the tissue-repair capability through different administration methods such as intravenous, intraperitoneal, or subcutaneous injection, either locally or systemically. However, this delivery method can lead to rapid clearance. Biomaterials have been a promising approach to overcome the decreased retention time of secretome components in regenerative medicine. Enhanced bioavailability is reflected in a combination of secretome and biomaterials, which leads to increased therapeutic potential (Spicer 2020; Li, Zhang et al. 2022).

As an attempt to increase the retention time of secretome bioactive at the wound site, biocompatible biomaterials are used as carriers (Robert, Azevedo Gomes et al. 2019). These biomaterials have the potential for re-epithelization and angiogenesis, decrease the possibility of infection after injury, and increase biocompatibility (Lukomskyj, Rao et al. 2022). Both natural and synthetic polymers are widely used in regenerative medicine to deliver entrapped bioactive to tissues. They act as structural supports and controlled delivery systems (Martins, Ferreira et al. 2016; Robert, Azevedo Gomes et al. 2019). This review provides insight into the combination of secretome with biomaterials for potential wound-healing applications. In addition, it highlights the approaches employed to fabricate biomaterials with condition media or extracellular vesicles to identify their future clinical applications in wound therapy.

## **2.2 Secretome**

### **2.2.1 Secretome Composition**

Secretome can be collected from a variety of human stem cell sources, with the most mentioned being umbilical cord tissue (Miranda, Camões et al. 2019), bone marrow (BM-MSCs) (Mendes-Pinheiro, Anjo et al. 2019), Wharton's jelly mesenchymal stem cells (WJ-MSCs) (Shin, Lee et al. 2021), peripheral blood (Beer, Mildner et al. 2016), adipose tissue (ASCs), placental tissues, and human umbilical cord perivascular cells (HUCPVCs) (Pires, Mendes-Pinheiro et al. 2016). However, human adipose tissue-derived stem cells (ADSCs) gained a prime focus in tissue engineering due to their ease of separation and high harvesting rate (Airuddin, Halim et al. 2021). ADSCs secretome has a great magnitude in regenerative medicine due to the positive effects of bioactive components in the treatment of cutaneous wounds, cardiovascular diseases, and CNS regeneration, amongst others (Pinho, Cibrão et al. 2020). ADSCs secretome can promote wound healing and accelerate

wound closure via secreted growth factors (Foo, Looi et al. 2021; Trzyna and Banaś-Ząbczyk 2021).

An analysis of secretome harvested from human adipose-tissue-derived mesenchymal stem cells confirmed the presence of increased levels of endothelial growth factor (EGF), hepatocyte growth factor (HGF), and basic fibroblast growth factor (bFGF). These proteins integrate with the cellular components of the dermis and facilitate the following processes: EGF promotes fibroblast migration and proliferation, HGF inhibits apoptosis, and bFGF promotes skin regeneration without fibrosis (Park, Kim et al. 2018). The secretome of human gingival fibroblasts revealed high amounts of pro-inflammatory cytokines such as IL-6, Arginase, MCP-1, and IL-8 (Ahangar, Mills et al. 2020). HGF, FGF-2, VEGF, Ang-1, Ang-2, MMP-2, MMP-9, and TIMP-1 (Ahangar, Mills et al. 2020). The cytokines revealed enhanced cutaneous wound healing of rapid re-epithelialization, decreased inflammation, angiogenesis promotion, and collagen deposition elevation, in addition to growth factors and ECM protein expressions (Ahangar, Mills et al. 2020). The components of the MSC secretome play an important role in wound-healing phases, as described in (Figure 2.1) below.

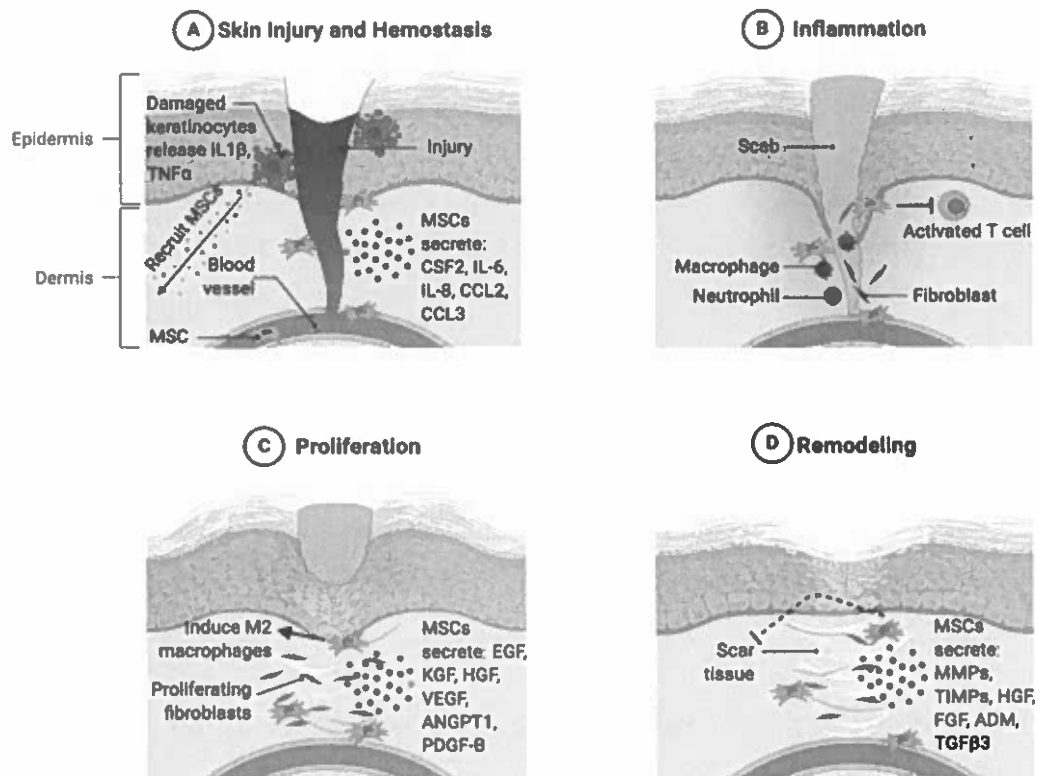


**Figure 2.1** MSC recruitment to wounded skin and the inflammatory phase and known and potential roles of MSCs in each phase of wound healing. (A) Skin injury and hemostasis. (B) Inflammation. (C) Proliferation. (D) Remodeling. Image reproduced with permission from Riedl et al. (Riedl, Popp et al. 2021), Copyright2021, Elsevier B.V. Ltd.

### 2.2.2 Advantage of Secretome over Cell Therapy

Cell-based therapy has been applied for decades in regenerative medicine and tissue repair to treat different pathological conditions. Skin wounds are one of the cases that are treated with cell-based therapy; however, improved ones are required to overcome the wound problem worldwide. Cell-based skin substitutes as an example of cell-based-therapy-exerted positive results in accelerated wound closure with improved re-epithelization and vascularity (Motamed, Taghiabadi et al. 2017; Li, Wang et al. 2020). However, they are very costly, require specific storage conditions, and cause the patient to become susceptible to infection and rejection (Ahangar, Mills et al. 2020). Stem cell secretome has significant advantages over cell-based therapy, which circumvents living-cell-associated problems represented in tumorigenicity, infection transmission, and immune reactions (Foo, Looi et al. 2021). Secretome can be produced according to the GMP-compliant process to be

treated in the same manner as pharmaceutical agents, and this can be viewed as an additional advantage (Daneshmandi, Shah et al. 2020; Foo, Looi et al. 2021).

The use of a conditioned medium from human uterine cervical stem cells (CM-hUCESCs) for eye corneal ulcers in a lyophilized form gives a clear indication that secretome can be stored for an extended period without deterioration or loss of potency (Bermudez, Sendon-Lago et al. 2015). Mesenchymal stem-cell-conditioned media (MSC-CM) was implemented in bone regeneration rather than MSC and showed beneficial effects in avoiding the invasion--collection procedure of cells (Osugi, Katagiri et al. 2012). ADSC secretome produced by the maturation process could be helpful in the mass production of secreted factors and account for a readily available supply of bioactive factors (Foo, Looi et al. 2021). Secretome therapy's cost-effectiveness can overcome the high cost of cellular therapy. The reduction of cell culture and immediate secretome therapies can be applied to manage acute pathological conditions such as military trauma, cerebral ischemia, and myocardial infarction, and modification of the biological product can take place to achieve a cell-specific effect (Vizoso, Eiro et al. 2017; Zhang, Zheng et al. 2022).

Based on the advantages listed above, secretome has the potential to overcome the ethical problems associated with cellular transplantation. In addition to that, complications related to the survival and inaccurate differentiation of cells in the host tissue are reduced. The overall capability of cell therapy can be maintained by paracrine activity. Secretome-based therapies provide advantages such as availability, scalability, and longer shelf life (Driscoll, Yan et al. 2022). In general, both cell-based therapy and secretome have advantages and disadvantages. However, the prolongation of the survival of transplanted cells and knowing how to predict decreased cell viability and biological functions during in vitro culture are the current challenges of cell-based therapies (Foo, Looi et al. 2021). Accordingly, several strategies have been developed to improve the therapeutic efficacy of stem cells and secretome, such as genetic modification, preconditioning, and tissue engineering (Foo, Looi et al. 2021).

### **2.2.3. The Role of the Secretome in Different Stages of Wound Healing**

Skin wound healing is a choreographed and closely regulated process comprised of inflammation, proliferation, matrix formation, and remodelling phases (Gonzalez, Costa et al. 2016). After skin injury, wound healing can be coordinated normally by keratinocytes, dermal fibroblasts, and immune cells (Casado-Díaz, Quesada-Gómez et al. 2020; Riedl,

Popp et al. 2021). However, secretome-based therapy has the potential to contribute to the acceleration of the wound-healing process. This is due to its components that promote anti-inflammatory factors, cell mitogenesis, re-epithelization, proliferation, and tissue remodelling, and induce neovascularization, leading to overall wound healing, particularly wound closure (Park, Kim et al. 2018).

The secretome components relevant to various wound-healing stages include growth factors (PDGF, IGF-1, EGF, FGF, granulocyte-colony stimulating factor (G-CSF), GM-CSF, HGF, PGE2, TGF- $\beta$ s, VEGF, and KGF), inflammatory proteins (IL-1, IL-8, IL-10, IL-6, tumor necrosis factor-alpha (TNF), leukemia inhibitory factor (LIF), IL-11, MCP-1, PGE2, IL-9, and IL-13), ECM proteins (MMP-1, MMP-2, MMP-3, MMP-7, TIMP-1, TIMP-2, ICAM, elastin, collagens, decorin, and laminin), and angiogenic factors (VEGF, ANG-1, ANG-2, PDGF, MCP1, TGF- $\beta$ 1, FGF, EGF, CXCL5, MMPs, and TGF- $\beta$ ). The secretome effect on the inflammatory phase has been assessed by Lotfinia et al.; the report indicated the use of mesenchymal stem-cell-secretome to treat peripheral blood mononuclear cells *in vitro* (Lotfinia, Lak et al. 2017). The study found that pro-inflammatory cytokine production was reduced, while anti-inflammatory cytokine production increased *in vitro* (Lotfinia, Lak et al. 2017). Another study on mice excisional wounds injected with bone marrow-derived stem cell secretome resulted in the promotion of wound healing by reduced inflammation mediated by macrophage polymerization (Ahangar, Mills et al. 2020).

A study by Park et al. indicated that secretome includes bioactive factors such as EGF, bFGF, and HGF, which are known to activate the PI3K/Akt and/or FAK/ERK1/2 signaling pathway (Park, Kim et al. 2018). This pathway is involved in the migration and proliferation of dermal cellular components during tissue repair. The bioactive and the activated pathway are believed to improve the proliferative and migratory capabilities of dermal fibroblasts, keratinocytes, and endothelial cells, among other biological components of the dermis (Park, Kim et al. 2018).

In the proliferation phase of wound healing, soluble substances of the secretome can enhance fibroblast migration and the secretion of ECM components, particularly collagens I and III, resulting in wound-healing acceleration within the wound bed (Park, Kim et al. 2018). During the remodelling phase, the total collagen content increases, leading to wound contraction. This effect has been confirmed in a study that applied a human gingival fibroblast condition medium to treat wounds (Ahangar, Mills et al. 2020). Endothelial cells

treated with human multipotent adult progenitor cell conditioned medium MAPC-CM also formed more vessel-like tube wounds (Ahangar, Mills et al. 2020). The secretome accelerates wound healing by promoting angiogenesis. This has been demonstrated by a study carried out on wounds treated with MAPC-CM. The outcome of the study was an increasing number of endothelial cells and blood vessels in the wound bed due to increased VEGF in the CM, which accounts for a proangiogenic factor stimulating the vessel formation of endothelial cells wounds (Ahangar, Mills et al. 2020). Secretome components can accelerate wound healing by promoting target cell proliferation, differentiation, vascularization, and wound remodeling.

### **2.3 Secretome Applications in Wound Healing**

Stem cell secretome or condition medium shows good outcomes in accelerating wound closure and promoting skin regeneration in wound healing. This evidence has been outlined in many studies due to secreted growth factors and cytokines and their potential for wound healing (Ahangar, Mills et al. 2020). Many physiological processes relevant to wound healing are mediated by stem-cell-mediated paracrine and autocrine cell signalling pathways. Furthermore, the secretome is composed of several constituents with extensive regenerative potential for wound tissue.

An analysis of the human adipose-derived stem cell secretome revealed a high level of various growth factors. These biological factors play a crucial role in wound healing and tissue repair as they can promote skin tissue regeneration and modulate the immune response (Marfia, Navone et al. 2015). These secreted factors can act directly on normal wound-healing stages to promote re-epithelialization and angiogenesis and indirectly by immunomodulatory capacities. These factors can stimulate existing skin cells' proliferative and migratory abilities through PI3K/Akt or FAK-ERK1/2, signaling an acceleration of wound healing (Park, Kim et al. 2018). The mechanisms of mesenchymal stem cell secretome in wound healing are illustrated in (Figure 2.2) Therefore, extensive studies take place in this area to evaluate the different mechanisms for wound repair. Consequently, the focus is on the secretome of stem cells as a novel tool for treating various types of wounds. Current applications of the secretome from the various MSC sources, and their involvement in wound closure acceleration, are summarized in Table 2.1.

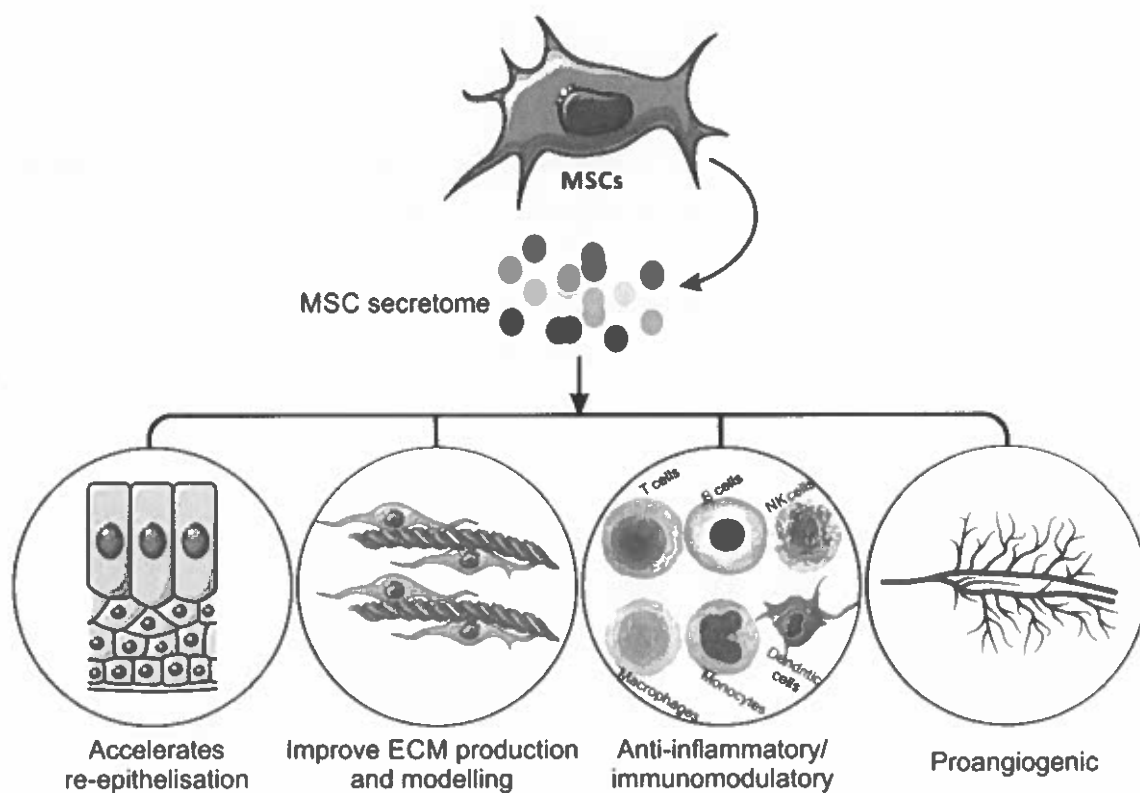


**Figure 2.2** Mechanisms of mesenchymal stem cells secretome on wound healing. Image reproduced under an open access license from Ahangar et al. (Ahangar, Mills et al. 2020), Copyright 2020, © authors.

**Table 2.1** The therapeutic outcomes of MSC secretome (MSC-S) in wound healing.

| Stem cell type                 | Type of wound and model          | Secretome component   | In vitro Outcome                    | In vivo outcome                       | Ref.                            |
|--------------------------------|----------------------------------|-----------------------|-------------------------------------|---------------------------------------|---------------------------------|
| Human (BMSC) from SCD patients | Murine excisional wound/endothel | VEGF, IL8, MCP-1, ANG | Using HUVECs in A dimensional vitro | BMSC media in trophic factors promote | (Ribeiro, Silveira et al. 2019) |

|         |   |                             |   |   |                                     |
|---------|---|-----------------------------|---|---|-------------------------------------|
|         | ial cells in a mouse model                        |                             | demonstrates proliferation and migration in the presence of hypoxic CM that supports angiogenesis.  | angiogenesis and skin regeneration with accelerated wound healing.  |                                     |
| ADMSC   | full-thickness skin excision on SD rats           | VEGF                        | Rat dermal fibroblast cell line treated with secretome revealed viability, proliferation ability, and higher migration capability, which present better wound healing. Macrophages treated with secretome exert reduction of pro-inflammatory cytokines, including IL-6, TNF- $\alpha$ , and MCP-1. | Rapid wound closure enhanced fibroblast proliferation and migration. Moreover, the higher expression of VEGF promotes angiogenesis which accelerates wound healing potential. | (Ma, Lam et al. 2021)               |
| hUCESCs | Corneal epithelial cells/corneal ulcer on SD rats | TIMP-1, TIMP-2, FGF and HGF | Enhanced epithelial wound healing, rapid regeneration, and constitutional of the corneal surface  | Bactericidal effect on corneal contact lenses (CLs) infected with Escherichia coli and Staphylococcus epidermidis.  | (Bermudez, Sendon-Lago et al. 2015) |

|   |  |   |   |   |                                       |
|---|--|---|---|---|---------------------------------------|
| hASC<br>transfect<br>ed with<br><br>miR-<br>146a. | In vitro model<br>using HUVECs   | miR-146a<br>UPA,<br>(DPP IV),<br>HGF,<br>FGF-1<br>and FGF 2 | the<br>secretome<br>promotes<br>proliferation,<br>migration, and<br>tube formation of<br>endothelial cells<br>reflected in<br>enhanced<br>proangiogenic<br>properties. Also,<br>the secretome<br>miR-146ahas<br>immunomodulati<br>on effect can<br>potentially<br>promote wound<br>healing. | <i>In vivo</i> , the outcome<br>was not studied   | (Waters,<br>Subham<br>et al.<br>2019) |
| ADSCs   | 6-mm diameter<br><br>biopsy punch<br>piercing in mice<br>dorsal skin of<br>male balb/c-<br>nude mice | TGF-b1<br>and VEGF  | Increased<br>transdermal<br>delivery of<br>secretome<br>proteins was<br>expressed in an<br>ex vivo porcine<br>skin using<br>iontophoresis as<br>a permeation<br>enhancer.   | Accelerate wound<br>closure with reduced<br>scars represented by<br>rapid re-<br>epithelization,<br>proliferation<br><br>, increased tissue<br>remodeling rate, and<br>high vascularization | (Foo, Looi<br>et al.<br>2021)         |
| HAFS  | the full-<br>thickness<br>cutaneous<br>excisional<br>wound created<br>on the dorsal                  | VEGF  | In vitro effect did<br>not test in this<br>study.   | Speeding up wound<br>closure due to a<br>decrease in<br>myofibroblasts'<br>positive expression<br>of $\alpha$ -SMA-rather than  | (Fukutake<br>, Ochiai et<br>al. 2019) |

skin of BALB/c mice.

contraction enhanced re-epithelialization after

14 days of treatment, and overall fetal-like wound healing without scarring as a result of high expression of type III collagen

accomplished by transformation of dermal fibroblasts into

fetal-like fibroblasts rather than myelo fibroblasts.

HGFs

Dorsal excisional wounds of female BALB/c mice

IL-6, Arginase, MCP-1, and IL-8 are examples of cytokines. Growth factors and ECM proteins such as HGF, FGF-2, VEGF, Ang-1, Ang-2,

Human keratinocytes and foreskin fibroblast cells were used in vitro to evaluate a higher proliferation and migration rate. There was also an increase in capillary density, indicating enhanced angiogenesis. Also, increased collagen deposition is

Wound closure acceleration reduced inflammation, promotion of angiogenesis, and higher collagen deposition. Higher re-epithelization

(Ahangar, Mills et al. 2020)

|                                       |  |  |   |  |   |
|---------------------------------------|--|--|---|--|---|
|                                       |  | MMP-2, reflected in<br>MMP-9, higher wound<br>and TIMP- contraction<br>1 are also without reducing<br>present. fibrosis. |   |  |   |
| human<br>bone<br>marrow<br>MSC        | full-skin<br>thickness<br>incision wound<br>on the dorsal<br>part of diabetic<br>Wistar male rats<br>(chronic<br>diabetic wound) | bFGF and<br>EGF<br>expressio<br>n  | human dermal<br>fibroblasts<br>cultured in a high<br>glucose<br>concentration<br>medium resulted<br>in an in vitro<br>advanced<br>wound closure<br>due to rapid<br>fibroblast<br>migration, higher<br>proliferation, and<br>increased bFGF<br>gene<br>expression. | Acceleration<br>wound<br>healing in terms of<br>reduction of<br>inflammation,<br>increased<br>vascularization,<br>granulation tissue<br>formation enhanced<br>collagen deposition,<br>and some trophic<br>factor gene<br>expression. | (Saheli,<br>Bayat et<br>al. 2020)           |
| (WJ-<br>MSCs)                         | radiation-<br>induced skin<br>injury on<br>Female<br>Sprague-<br>Dawley (SD)<br>rats   | -----  | (HUVECs)growt<br>h rate and<br>proliferation rate<br>are increased.<br>Enhanced<br>number of blood<br>vessels due to<br>increased a-<br>SMA<br>expression.  | Acceleration<br>wound closure<br>enhances the quality<br>of wound healing by<br>promoting cell<br>proliferation,<br>sebaceous gland<br>cell-like<br>regeneration, and<br>angiogenesis.   | (Sun,<br>Zhang et<br>al. 2019)              |
| gamma<br>irradiatio<br>n to<br>induce | Burn wounds of<br>40 cm2 were<br>created on the<br>dorsum of the   | IL-8 and<br>VEGF   | Histology<br>studies carried<br>out by using<br>Wound biopsies,   | improved epidermal<br>regeneration and<br>differentiation,<br>better wound quality   | (Hacker,<br>Mittermay<br>ar et al.<br>2016) |

|  |  |   |   |   |  |
|--|--|---|---|---|--|
| apoptosis<br>PBMCs                     | female<br>Bred pigs  | Dan   |   |   | without a scar, and increased numbers of CD31+ and ASMA+ cells as markers for angiogenesis |
| MSC<br>from fetal<br>umbilical<br>cord | Burn wound on<br>the dorsal area<br>of the Wister rat<br>(Rattus<br>Norvegicus)  | bFGF  | Histological<br>analysis of skin<br>tissues using M<br>and H stains   | Acceleration<br>of wound closure,<br>more significant<br>number of<br>fibroblasts, high<br>density of collagen<br>fibre, and significant<br>number of blood<br>vessels    | (Padeta,<br>Nugroho<br>et al.<br>2017)   |
| Warton<br>Jelly<br>MSC                 | burns on a 47-<br>year-old<br>woman's left<br>hand due to hot<br>water exposure. | _____   | _____   | Three weeks of<br>treatment with 10%<br>secretome gel<br>accelerated wound<br>healing without<br>scarring t   | (Tan,<br>Firmansy<br>ah et al.)  |
| UMSC-<br>Exos                          | Full-thickness<br>skin wound on<br>ICR mice and<br>nude mice.                    | Exosome<br>enriched<br>microRNA<br>represent<br>ed as<br>(miR-21, -<br>23a, -<br>125b, and<br>-145) | fibroblasts<br>treated<br>recombinant<br>TGF-b protein<br>upon exposure<br>to CM, lead to $\alpha$ -<br>SMA<br>suppression. | Wound healing<br>promotion due to<br>suppression of<br>myofibroblast and<br>scar formation<br>through inhibition of<br>transforming Growth<br>factor-b2/SMAD2<br>pathway. | (Fang, Xu<br>et al.<br>2016)   |

## 2.4 Secretome Delivery in Wound Healing

Biomaterials play an important role in tissue regeneration, which comprises delivering bioactives and providing structural support for endogenous cell invasion. For biomaterials

to be applied, they must fulfill the following criteria biocompatibility, degradability, and suitable mechanical properties. Biomaterials are classified into three categories: naturally derived, synthetic, and chemically modified polymers. Natural biomaterials shown in this field comprise alginate, collagen, hyaluronan, and decellularized extracellular matrix (ECM). Biomaterial scaffolds made of synthetic polymers or ceramics such as polylactide-co-glycolide (PLGA) or beta-tricalcium phosphate ( $\beta$ -TCP) are extensively employed, with gelatin methacrylate (GelMA) being the natural material with chemical modifications (Brennan, Layrolle et al. 2020).

Synthetic materials offer multiple advantages, such as cost, supply, and batch-to-batch homogeneity. However, they lack native tissue shape and structure. Hybrid hydrogels combining natural and synthetic materials have also been employed to attain the biological benefits of natural materials while attaining the benefits of tunable synthetic materials (Arifka, Wilar et al. 2022). Biomaterials may be able to overcome the inadequate tissue retention of bolus EV and MSC-CM injections by offering a controlled release platform for healing tissues.

Biomaterials, which include scaffolds, meshes, matrices, hydrogels, and substrates, have completely transformed the way drugs are delivered and used. Some of the most frequently employed scaffolds are collagen-derived matrices, silk-based meshes/matrices, dextran hydrogels, and electrospun nanofiber matrices such as poly-L-lactic acid (PLLA) (Murray, West et al. 2019; Attasgah, Velasco-Rodríguez et al. 2022). However, electrospun nanofiber matrices are recommended in biological applications. These scaffolds provide a three-dimensional (3D) structure that is similar to that of the extracellular matrix (ECM)-like nano-architecture [69]. These matrices have a similar tensile strength to the skin, making them a suitable candidate for skin wound healing.

Biomedical hydrogels, which have a comparable structure to the natural ECM, have been highlighted as promising biomaterials for delivering therapeutics and cell components to wounds. The following characteristics should be present in an ideal wound-healing hydrogel scaffold: suitable mechanical qualities, good water retention, anti-infection capacity, injectable capacity, and excellent cell biocompatibility. Exosome-based administration via hydrogel, on the other hand, is likely to improve angiogenesis and tissue regeneration during wound healing (Deshpande, Kanitkar et al. 2018). Table 2.2 mentions some examples of biomaterials and their application in wound healing.

**Table 2.2** Biomaterials and their application in wound healing

| Polymer   | Secretome source  | Bioactive Molecules     | Type of hydrogel     | Biomedical Apps                                    | References                          |
|---|---|-------------------------|----------------------|--|-------------------------------------|
| Poly isocyanate (PIC)   | human adipose-derived stem cells (hASCs)                | IL-10                   | Gel                  | fibroblast wound healing assay or artificial wound | (Liu, Veenendaa I et al. 2020)      |
| carrageenan / poly (vinyl alcohol)  | SD-MSCs   | VEGF                    | Hydrogel             | full-thickness excisional wounds                   | (Robert, Azevedo Gomes et al. 2019) |
| Polycaprolactone/gelatin  | bone marrow-derived mononuclear cells                   | -----                   | electrospun scaffold | diabetic wounds                                    | (Deshpande, Kanitkar et al. 2018)   |
| hyaluronic acid (HA) and chondroitin sulfate (CS)   | bone marrow-derived Human mesenchymal stem cells (hMSC) |                         | viscoelastic gel     | Corneal wound                                      | (Rogers, Putra et al. 2018)         |
| Methacrylate anhydride, Hyaluronic acid, N-(2-aminoethyl)-4-[4-(hydroxymethyl)-2-methoxy-5- | amniotic-derived conditioned medium (AM-CM)             | VEGF and TGF- $\beta$ 1 | In situ gel          | <i>In vivo</i> Diabetic wound                      | (Zhang, Zheng et al. 2022)          |

|  |   |                          |                                   |   |  |
|--|---|--------------------------|-----------------------------------|---|--|
| nitrophenoxy]-<br>butanamide (NB)  |   |                          |                                   |   |  |
| chitosan/collagen/ $\beta$ -<br>glycerophosphate                                     | human<br>umbilical<br>cord<br>mesenchyma<br>l stem cell                           |                          | Thermosensiti<br>ve hydrogel      | <i>In vivo</i><br>burn<br>wound   | (Zhou, Li et<br>al. 2019;<br>Zhang,<br>Zheng et<br>al. 2022) |
| Pluronic F-127   | human<br>umbilical<br>cord-derived<br>MSC<br><br>(hUCMSC)-<br>derived<br>exosomes | VEGF/(TGF<br>$\beta$ -1) | a<br>thermosensitiv<br>e hydrogel | <i>In vivo</i><br>diabetic<br>wound   | (Yang,<br>Chen et al.<br>2020)                               |
| Pluronic<br>F127 /oxidative<br>hyaluronic acid/( $\epsilon$ -<br>poly-L-lysine, EPL) | adipose<br>mesenchyma<br>l stem cells<br>(AMSCs)-<br>derived<br>exosomes          | -----                    | Hydrogel                          | <i>diabetic</i><br><i>full-</i><br><i>thickness</i><br><i>cutaneou</i><br><i>s wounds</i> | (Wang,<br>Wang et al.<br>2019)                               |

## 2.5. Structural Formulation Using Biomaterials with Secretome for Wound-Healing Applications

Polymer-based biomaterials are widely used in tissue engineering. They can mediate tissue engineering through their *in vitro* structural support to help cell–cell interaction and growth factors. They can aid in the *in vivo* transplantation of the regenerated tissue to integrate structurally and functionally with the system (Khayambashi, Iyer et al. 2021). Hydrogels, which are three-dimensional hydrophilic polymers, have been used as a bioactive scaffold material for drug delivery and cell encapsulation (Khayambashi, Iyer et al. 2021). However, recent studies have identified that biocompatible hydrogels as carriers of MSC CM and MSC exosomes can maintain the bioactive molecules of the CM at the wound site (Xie, Guan et al. 2022). This is an attempt to overcome cell-based therapy-associated risks in terms of lowering processing time and local storage conditions.

MSc-secreted factors, which include extracellular vesicles and soluble factors, contribute mainly to their therapeutic benefit. However, the biomaterials can be combined with those factors, offering a delivery system to enhance the secretome retention rate and accelerate healing efficacy. This review highlights the use of biomaterials with secretome in wound healing, providing insight into different examples applied *in vitro* and *in vivo*. (Figure 2.3) below shows how secretome can be extracted from MSC and the CM and exosome mixed with polymers to develop a biomedical system that can be applied to treat *in vivo* wounds.

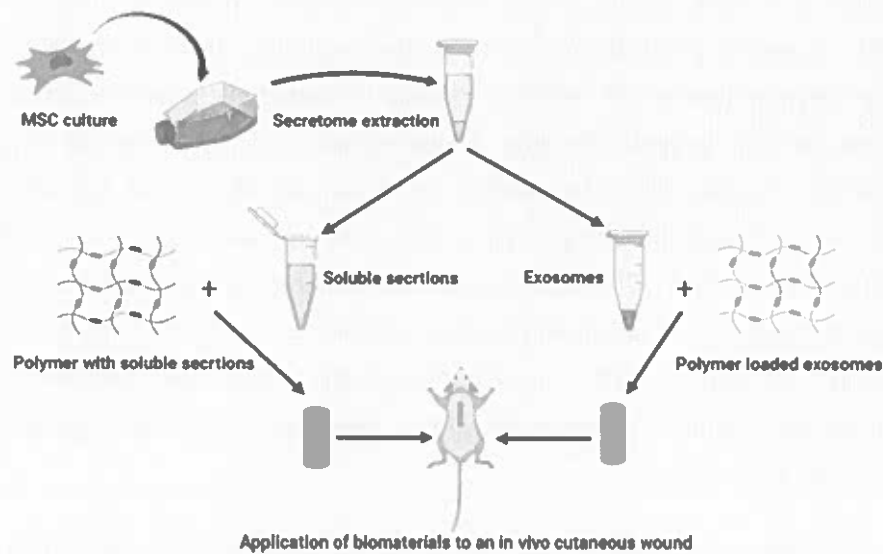


**Figure 2.3** Schematic representation of MSC secretome extraction and exosome separation and combination with polymers for *in vivo* wound application.

### 2.5.1 MSC Soluble Secretions and Their Combination with Biomaterials for Application in Different Wounds

Secretomes collected from *in vitro* culturing of MSC are also known as MSC-conditioned media (MSC-CM). The analysis showed the composition of the soluble factors, which are made up of cytokines, chemokines, growth factors, and hormones, with immunomodulatory, angiogenic, and anti-apoptotic functions (Driscoll and Patel 2019). The second part of secretion is termed extracellular vesicle secretions loaded with specific miRNA involved in both diagnosis and treatment (Eleuteri and Fierabracci 2019). The advantages of the *in vitro*

applications of MSC-CM include cell proliferation and migration enhancement (Chen, Li et al. 2015; Shen, Lie et al. 2015), the promotion of angiogenesis (Shen, Lie et al. 2015; Jin, Yang et al. 2020), and revealing anti-apoptotic and anti-inflammatory effects (Chen, Li et al. 2015; Kwon, Ki et al. 2016; Kay, Long et al. 2017). Furthermore, *in vivo* MSC-CM has demonstrated healing potentials in different wound types, which involve cutaneous wounds (Li, Luan et al. 2017, burn wounds (Zhou, Li et al. 2019), and diabetic chronic wounds (Saheli, Bayat et al. 2020).

MSC CM can be administered by bolus injection, resulting in a shorter half-life and poor tissue retention. A combination of MSC CM with biomaterials presented a controlled release platform for healing tissues to overcome these adverse problems (Brennan, Layrolle et al. 2020). A recent study by Vasily et al. demonstrated the use of placental multipotent mesenchymal stromal cell (MMSC) secretome-loaded in chitosan hydrogel (MSC-Ch-gel) for infected burn wounds (Kudinov, Artyushev et al. 2021). The method used in developing the MSC-CH gel involved the addition of chitosan solution to CM. The study revealed that MSC-Ch-gel had antimicrobial activity along with high anti-inflammatory abilities (Kudinov, Artyushev et al. 2021). The high level of anti-inflammatory mediators was released upon the proteomic analysis of secretome besides proteins crucial for the different stages of wound healing. Furthermore, MSC-CH gel promoted skin tissue repair, which was observed after histological examination regarding higher vascularization and angiogenesis (Kudinov, Artyushev et al. 2021).

Another study conducted by HonorataK et al. evaluated the effect of human adipose tissue mesenchymal stem cell (HATMSC2) secretome-loaded hydrogel on chronic wounds (Kudinov, Artyushev et al. 2021). The collagen hydrogel was prepared by adding the concentrated PBS to the type1 collagen solution and then gently mixed. HATMSC supernatant was added to the collagen mixture before adding the crosslinker. The last step was adding 10K 4-arm Succinimidyl Glutarate PEG crosslinker followed by gentle mixing; then, the formed hydrogel was pipetted into Petri dishes and incubated at 37 °C for 1 h to allow for complete crosslinking (Kudinov, Artyushev et al. 2021). The developed hydrogel was tested in an *in vitro* wound model using different cells, including endothelial, keratinocytes, and fibroblasts, during a 3-day culture. The results showed highly released interleukin-8 and macrophage chemoattractant protein-1proteins from endothelial cells (Kraskiewicz, Hinc et al. 2021). Additionally, pro-angiogenic activity was assessed using an *in vitro* tube formation assay on human skin endothelial cells and confirmed by the

expression of pro-angiogenic miRNAs, especially miR126, which shows the highest expression and antimicrobial activity against *Staphylococcus aureus* MRSA, and *Pseudomonas aeruginosa* was also confirmed (Kraskiewicz, Hinc et al. 2021).

A recent study developed by Victoria et al. focused on developing mesenchymal stem cell (MSC)-conditioned media (CM) loaded in hydrogel and its application in an *in vitro* hyperglycemic human dermal fibroblast to investigate the wound healing potential (Sears, Danaoui et al. 2021). The components of the hydrogel were GelMA-PEGDA, loaded with MSC-CM, which demonstrated higher proliferation of the hyperglycemic fibroblast due to the combined effects of matrix properties together with the prolonged release of MSC-secreted bioactive molecules. Hence, it was potentially beneficial in diabetic chronic wounds (Sears, Danaoui et al. 2021).

A study by Anny et al. investigated the use of biocompatible polymers as transporters to preserve the bioactive molecules of CM at the wound site by combining MSC secretome with carrageenan and polyvinyl alcohol (Robert, Azevedo Gomes et al. 2019). After preparing each hydrogel, the condition media embedded in each of them was polymerized, and then it was derided and tested in *in vitro* human umbilical vein endothelial cells for angiogenic activity. Additionally, in *in vivo* application in mice, the cutaneous wound was carried, which showed the healing potential of both hydrogels' impeded CM based on the proangiogenic properties of the secretome (Robert, Azevedo Gomes et al. 2019).

Another study applied BM-MSC secretome *in vitro* to primary cultured human corneal epithelial cells and an *in vivo* mouse model after both mechanical and alkaline corneal burn, hyaluronic acid (HA), and chondroitin sulfate (CS) gel were used as carriers (they were compared with secretome alone). The secretome was used in a lyophilized form to impart long stability and consistency to the different products. The study revealed secretome HA/CS gel accelerates epithelial wound closure after both injuries and can reduce neovascularization, scar formation, and haemorrhage after chemical injury (Fernandes-Cunha, Na et al. 2019). Yiqing et al developed a photocrosslinking adhesive in situ-formed hyaluronic acid hydrogel grafted with the methacrylic anhydride and N-(2-aminoethyl)-4-[4-(hydroxymethyl)-2-methoxy-5-nitrophenoxy]-butanamide (NB) groups to encapsulate a lyophilized amnion-derived conditioned medium (AM-CM) (Zhang, Zheng et al. 2022). The hydrogel displayed strong tissue adhesion, excellent mechanical properties, high elasticity, favourable biocompatibility, and prolonged AM-CM release. This was reflected in *in vitro*

and *in vivo* accelerated diabetic wound healing resulting from the regulation of macrophage polarization and the promotion of angiogenesis (Zhang, Zheng et al. 2022).

Another study by Gabriella et al. developed a viscoelastic gel composed of hyaluronic acid (HA) and chondroitin sulfate (CS) to deliver lyophilized secretome from human bone marrow-derived mesenchymal stem cells for the treatment of mechanical and chemical corneal injuries (Fernandes-Cunha, Na et al. 2019). The *in vitro* and *in vivo* results accelerated epithelial wound closure and reduced corneal neovascularization, scar formation, and haemorrhage (Fernandes-Cunha, Na et al. 2019). Vasily et al. developed placental multipotent mesenchymal stromal cell (MMSC) secretome-based chitosan hydrogel (MSC-Ch-gel) to treat infected burn wounds in the rats (Kudinov, Artyushev et al. 2021). Accelerated wound healing, tissue regeneration, reduced inflammation, improved re-epithelialization, and the encouragement of the development of well-vascularized granulation tissue were the outcomes (Kudinov, Artyushev et al. 2021). The secretome produced by human fetal mesenchymal stem cells (hfMSC) in diabetic wounds was investigated by Bin Wang et al. (Wang, Pang et al. 2022). The poly lactic-co-glycolic acid (PLGA)-encapsulating lyophilized hfMSC exhibited improved wound healing by encouraging vascularization and reducing inflammation in the cutaneous wound bed (Wang, Pang et al. 2022). Chen et al. developed an adipose-derived stem-cells-conditioned medium loaded in electrospun micro-nano fibres using polylactic acid (PLA), which imparted protection and controlled release properties (Chen, Cheng et al. 2021). The *in vitro* and *in vivo* outcomes of the study were wound-healing acceleration and tissue regeneration (Chen, Cheng et al. 2021).

### **2.5.2 MSC EVs and Their Combination with Biomaterials for Application in Different Wounds**

Extracellular vesicles (EV) are nano or micro-sized vesicles that constitute the insoluble part of the secretome. They play a key role in cell-to-cell communication by transporting cargo directly into the cell or activating specified cell surface receptors. They are important in tissue repair and regeneration, disease detection, and oncology because they can transport membrane and cytosolic proteins, lipids, and RNAs (Shi, Qian et al. 2017; González-González, García-Sánchez et al. 2020). Exosomes, nano-sized vesicles, have become popular for application in cellular regenerative medicine, especially in wound healing. They organize cell-to-cell communication by carrying mRNA, miRNA, and proteins to target cells

(Wang, Wang et al. 2019; Racchetti and Meldolesi 2021). The following studies are examples demonstrating the combination of EV with biomaterials for wound healing.

A study carried out by SHI-CONGTAO et al. describes the use of exosomes from microRNA-126-3p overexpressing synovium MSC mixed with chitosan hydrogel for cutaneous wound healing (Tao, Guo et al. 2017). After the isolation and characterization of SMSC, the miRNA-126-3p lentiviral vector transfected them, and then the exosomes were isolated and identified by specific procedures. After that, chitosan hydrogel-loaded exosome was prepared and tested in vitro and in vivo, which resulted in an in vitro promotion of proliferation and migration in human dermal microvascular endothelial cells (HMEC-1 cells) and human fibroblasts (FBs) (Tao, Guo et al. 2017). However, a faster healing rate was reflected in diabetic wounded rats treated with CS-SMSC-126-Exos, which was reflected by epithelialization, granulation tissue formation, collagen deposition, and vascularization (Tao, Guo et al. 2017).

Another study demonstrated the preparation of chitosan/silk hydrogel sponge loaded with exosome derived from human gingival MSC and application to diabetic rat wounds. After the polymers dissolved, they stirred mechanically for 30 min. The hydrogel was prepared by the freeze-drying method and lyophilized to produce a sponge to which the collected exosomes were added (Shi, Qian et al. 2017). Then, the hydrogel was applied to the wound area of the diabetic rats and accelerated wound healing. This is a noninvasive delivery system compared to the direct injection of exosomes, which can cause infection. The histological results showed enhanced re-epithelization, collagen depositing, neovascularization, and neuronal ingrowth (Shi, Qian et al. 2017).

An adipose-derived MSCs exosome loaded in alginate-based hydrogel has been applied to a full-thickness wound in a rat model. The study was performed by the isolation of ADSCs first, followed by exosome isolation and characterization; after that, the alginate hydrogel was prepared from alginates solution. The exosome was added and finally crosslinked with calcium chloride. The hydrogel was applied to assess its healing potential in a rat model. The exo-loaded hydrogel provided a novel delivery platform that accelerated wound closure by the enhancement of fibroblast migration, collagen synthesis, and vascularization (Shafei, Khanmohammadi et al. 2020). A study done by Qijun Li et al. illustrated the dual-sensitive hydrogel comprised of poloxamer 407, and carboxymethyl chitosan encapsulates exosomes derived from human umbilical cord mesenchymal stem cells (hUCMSCs). The polymers

were crosslinked with genipin, and the exosome suspension was mixed into the solution to form the hydrogel that exhibited sustained release behaviour upon application to the cutaneous wound in a rat model, resulting in an enhancement of wound closure and tissue regeneration. In addition to that, the formation of skin appendages and the inhibition of inflammatory reactions (Li, Gong et al. 2021). occurred.

Wang et al. fabricated self-healing hydrogel from methylcellulose and chitosan via Schiff base reactions (Wang, Liang et al. 2020). The hydrogel was loaded with exosomes extracted from placental mesenchymal stem cells. The hydrogel-loaded exosome exhibited accelerated wound healing, which was reflected in rapid wound contraction, new tissue formation, vascularization, and hair follicle and gland appearance when applied to the full-thickness wound in diabetic mice (Leprdb). Thus, wound healing promotion took advantage of an injectable hydrogel and the biocompatibility of the polymers (Wang, Liang et al. 2020). Liu et al. explored the enhanced retention of adipose stem cell-derived exosome when combined with HA in the acute cutaneous wounds of nude mice (Liu, Chen et al. 2019). The outcomes demonstrated that ASC-Exo+HA could significantly enhanced fibroblast activity, re-epithelialization, and vascularization in wound healing (Liu, Chen et al. 2019). (Figure 2.4) represents the hydrogel formation method using exosome-loaded polymers as one of the examples of the fabrication approach.

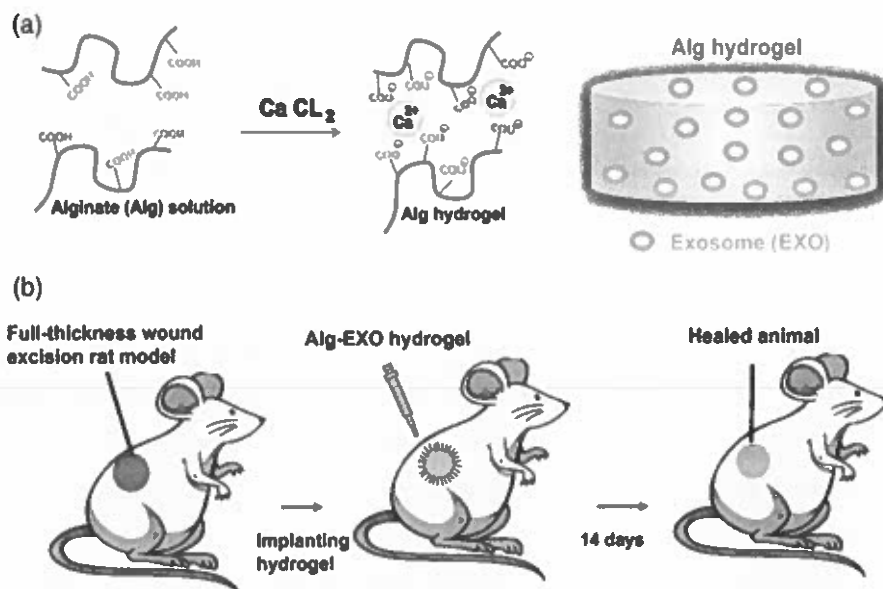


**Figure 2.4** Schematic illustration of the hydrogel crosslinking and full-thickness wound excision mouse model used to evaluate the wound healing properties of alginate hydrogel-incorporated exosome (Alg-EXO). (a) Alginate solution loaded with adipose-derived stem cells (ADSCs)-derived EXOs cross-linked via ionic crosslinking. (b) Creation of a full-thickness wound excision rat model, and the transplantation of hydrogel into the injury area. Image reproduced with permission from Shafei et al. (Shafei et al. 2020). Copyright 2019, John Wiley and Sons.

### 2.5.3 Secretome in Three-dimensional Bioprinting

Three-dimensional printing (3D) technology can be used for wound healing and skin engineering through the application of bioprintable materials known as bioinks. These bioinks must have good printability, mechanical stability, biocompatibility, biodegradability, no toxicity, high availability, and high shape fidelity (Antezana, Municoy et al. 2022). The 3D printing technology, rather than conventional approaches, can generate scaffolds that can resemble the complex ECM structures and provide a microenvironment for cell attachment, proliferation, distribution, and differentiation, with the capability to create functional tissue (Do, Khorsand et al. 2015). 3D technology can be used to carefully distribute cells, biological components, and growth factors into complex 3D bioscaffolds to construct tissue engineering structures that mimic biological ones. Leila et al. developed a collagen/alginate 3D bioprinted gel scaffold loaded with adipose-derived stem cells (ADSCs) for burn-wound healing, which resulted in complete epithelization and accelerated healing (Roshangar, Rad et al. 2021).

A study in bone regeneration used a 3D scaffold constructed from PCL and alginate hydrogel that contains lyo secretome(freeze-dried MSC secretome) for the controlled release of secretome to promote *in vitro* osteogenic differentiation (Bari, Scocozza et al. 2022). Another study on a 3D electrospun fibre scaffold, fabricated with polycaprolactone (PCL) and gelatin, was used as a cell culture medium with harvest(cell-free) MSC secretome, as well as continuous delivery from MSCs. The secretome was harvested and used to evaluate *in vitro* wound healing on corneal fibroblasts and subsequently explored a chemical burn on rabbit corneas employing an organ culture model. The outcome was epithelial layer recovery (Carter, Lee et al. 2019). The effectiveness of 3D scaffold-based exosome treatment for skin regeneration has been examined in several research. Wang et al. verified that a biocompatible 3D porous self-healing methylcellulose-chitosan hydrogel,

supplied with placental MSC-derived exosomes, promoted wound healing by cooperatively promoting angiogenesis and inhibiting apoptosis (Gu, Feng et al. 2021). Therefore, using secretome 3D printing technology for wound healing is a promising area for further research.

## **2.6 Conclusions**

Comprehensive studies have been done on the wound healing capability of MSC. They emphasized that their therapeutic benefit was mediated by paracrine secretions, including soluble factors and extracellular vesicle components collectively named secretome. They explore healing potential through the inhibition of apoptosis and inflammation, fibrosis, and angiogenesis. The secretome components can be delivered to the wound site when combined with biomaterials, which show better retention. Their effects proven *in vitro* and *in vivo* demonstrate valuable results in accelerating wound healing and promoting skin regeneration due to their tissue retention. To translate the experience of secretome to clinical situations, it is necessary to further understand its production procedures, which will pave the way to enhance the production, advancement of isolation, and standardization methods for purification and characterization.

## **2.7 Future Prospectives**

Secretome-based therapeutics have become a potentially effective replacement for cell-based therapies. The secretome is at the vanguard of next-generation tissue and organ regenerative engineering applications due to its capacity to be produced, stored, and used as an off-the-shelf, ready-to-use product with minimal safety issues while maintaining the therapeutic benefits of stem cells. Advancing secretome-based therapeutics and determining their safety and efficacy will require the creation and evolution of methodologies and technology in MSC secretome culture, as well as a comprehensive grasp of secretome components. Biomaterials have also been investigated as a supplement to control secretome production and as delivery systems. To accomplish clinical translation, the expansion of MSCs should be carried out under defined GMP culture conditions that are reproducible, scalable, and well-controlled, intending to limit heterogeneity and enhance the predictability of secretome-derived products in terms of composition and function.

## CHAPTER 3

### SECRETOME-LOADED ALGINATE-LECITHIN HYDROGEL FOR WOUND HEALING APPLICATION

---

#### 3.1 Introduction

Wound healing is a complex process that occurs when the skin is injured by chemicals, physical trauma, or thermal damage. This recovery process involves the interaction of cells, matrix elements, and other biological factors to speed up healing and restore tissue integrity (Negut et al., 2020). Conditions such as burns, infections, and other pathological disorders can all hinder the normal healing process (Negut et al., 2020). The current treatment of skin wounds focuses mostly on providing quick care after an injury to support tissue regeneration while minimizing skin function loss and preventing chronic wound phenomena (Mh Busra et al., 2019). Despite numerous efforts to enhance healing with wound dressings, they have demonstrated therapeutic limitations, highlighting the need for improvements to achieve more advanced wound regeneration (Kolimi et al., 2022)

Cellular treatments using multipotent mesenchymal stromal cells (MMSCs) demonstrate the potential to promote wound healing. This is due to their immunomodulatory and anti-fibrotic properties, as well as their ability to stimulate cell migration and angiogenesis (Capilla-González et al., 2022; Kudinov et al., 2021; Tanaka et al., 2022). Many preclinical studies have shown that different MMSC therapy techniques, including systemic cell delivery, local cell injections, and cell-seeded scaffolds, are effective in treating acute skin burns (Jenssen et al., 2022; Lukomskyj et al., 2022). Nevertheless, the application of MMSCs for therapeutic purposes is constrained by considerations about biosafety, immune compatibility, and cost (Ibrahim et al., 2022).

Recent studies have emphasized the utilization of cell-free therapies based on secretory products obtained from MMSC cultures, such as extracellular vesicles (EVs) or conditioned media. These therapies offer advantages such as long-term preservation and reduced risks associated with cancer, embolism, and pathogen transmission. (Kudinov et al., 2021; Md Fadilah et al., 2022). A secretome refers to a spectrum of bioactive molecules generated by a cell in the extracellular space. This encompasses cytokines, growth factors, extracellular

matrix (ECM) proteins, nucleic acids, proteasomes, exosomes, microRNA, and membrane vesicles, among others (Ding et al., 2023; Ibrahim et al., 2022; Zohora et al., 2023). These elements contribute to enhancing cell viability, proliferation, migration, and immunomodulation (Kim et al., 2022). However, the secretome of Mesenchymal Stem Cells (MSCs) has demonstrated therapeutic efficacy in promoting wound healing and presented a potential alternative to treat wounds (Ma et al., 2023; Merimi et al., 2021).

The secretory proteins present in the secretome are significant in regulating biological processes and facilitating intercellular communication (Ding et al., 2020). The secretome plays a vital role as a key mediator in the wound healing process, by actively stimulating and coordinating the cellular functions involving keratinocytes, fibroblasts, and endothelial cells which is vital in the wound healing process (Ahangar et al., 2020a; Kwon et al., 2023; Md Fadilah et al., 2022).

Alginate, a polysaccharide polymer, has gained attention in pharmaceutical and medical applications due to its unique properties such as biocompatibility, biodegradability, and lack of toxicity (Dattilo et al., 2023; Soleimanpour et al., 2022). It is a naturally occurring anionic biopolymer that can form hydrogels when divalent cations like  $\text{Ca}^{2+}$  are added. Various cross-linking techniques can be employed to develop alginate hydrogels, resulting in a structure that closely resembles the extracellular matrices found in biological tissues (Mndlovu et al., 2022).

In a previous study, lecithin, a naturally occurring substance found in human tissues, was used to modify the internal structure of hydrogels (Heger et al., 2022). Lecithin is a phospholipid mixture that exhibits hydrophobic and hydrophilic properties and can enhance the co-administration of drug therapy's bioavailability. The functionality and effectiveness of a multi-component hydrogel system can be heightened by altering the proportion of lecithin present. Changes in the arrangement of the internal structure of materials can have a significant impact on their transport and mechanical properties (Heger et al., 2022). Hydrogels have gained considerable attention for their ability to create a moist microenvironment and absorb wound exudates, which is essential for wound healing (Norahan et al., 2022).

Various biomedical formulations such as fibre (Tan et al., 2022), membranes (Eskandarinia et al., 2020), polymer and polysaccharide scaffolds (Senthilkumar et al., 2022),

nanoparticles (Wang et al., 2022), and hydrogels (Fan et al., 2021; Giliomee et al., 2021; H. Liu et al., 2018), suitable for use as wound dressings. Hydrogel dressings have garnered significant attention in the wound healing field due to their ability to modify fluid balance and speed up wound repair (Lu et al., 2022; Pan et al., 2021). Some hydrogel dressings have excellent antibacterial activity and accelerate the healing of wounds (Ming et al., 2021; Xiao et al., 2021; Xu et al., 2023). A multifunctional hybrid hydrogel dressing is highly desirable for healing full-thickness wounds (Ding et al., 2022).

This study aimed to explore the potential of combining alginate and secretome fluid to accelerate wound healing. Specifically, focused on developing an alginate–Soy Lecithin hydrogel that incorporated the secretome of rat's dermal fibroblast (FR) cells to maintain the optimal concentration of bioactive molecules and exosomes released by secretome in the wound site. The proposed aim is to protect these exosomes and proteins from proteases and facilitate a continuous release of them along with promoting accelerated wound healing. This approach could lead to a significantly enhanced therapeutic outcome. The method followed for formulating the FR secretome with water-soluble alginate is simple and accessible which is crucial for upscaling. The success of this study has the potential to create new opportunities for researchers to explore the delivery of secretome in various fields related to tissue regeneration. Furthermore, the developed hydrogels could enhance patient compliance and alleviate psychological issues associated with wounds, while simultaneously lowering the financial burden of wound treatment.

## **3.2 Materials and Methods**

### **3.2.1 Materials**

L- $\alpha$ -Lecithin soybean, sodium alginate, Lysozyme powder and calcium chloride were purchased from Sigma-Aldrich (Germany). Rat dermal fibroblast (FR) cells were derived from 18-day gestation Sprague-Dawley rats purchased from AddexBio Catalog NoT0020027. Human keratinocyte (HacaT) and murine fibroblast (NIH-3T3) were purchased from Separation Scientific (South Africa). Dulbecco's modified eagle's medium (DMEM), Roswell Park Memorial Institute medium (RPMI), streptomycin (10,000 units penicillin and 10 mg streptomycin/mL), Fetal Bovine Serum (FBS), penicillin–0.25% (w/v) Trypsin-EDTA solution, Thiazolyl Blue Tetrazolium Bromide (MTT) and Phosphate Buffered Saline (PBS) were purchased from Sigma-Aldrich (Germany).

### **3.2.2 Methods**

#### **3.2.2.1 Utilizing the Enzyme-Linked Immunosorbent Assay (ELISA), secretome collection and quantification**

The FR cells were cultured in (DMEM) supplemented with 10% fetal bovine serum (FBS) and 1% penicillin–streptomycin consisting of 100 Units/mL penicillin G and 100 mg/mL streptomycin. The cells were maintained at standard cell culture conditions, which included being kept at 37°C in a humidified incubator from NuAire, Inc. U.S.A, with 5% CO<sub>2</sub>.

After cells reached 80-90% confluency, the culture medium was replaced with fresh DMEM without supplements. At intervals of 24 hours, 48 hours, and 72 hours, the medium containing products released by FR cells was collected following the procedure described previously (Ahangar et al., 2020b). In brief, the medium was centrifuged for 10 minutes to eliminate cellular debris and apoptotic bodies, then filtered through a sterile 0.22 µm pore diameter filter. The secretome collected from these three-time points was stored at -80°C until needed for subsequent hydrogel fabrication.

The concentration of Vascular Endothelial Cell Growth Factor A (VEGF) secreted by FR cells was quantified using the Elabscience® ELISA kit from Elabscience Biotechnology Inc. following the manufacturer's instructions for each step. Briefly, VEGF standard and secretome samples were introduced into the well plates and incubated for 90 minutes at 37°C. Following this, additional reagents were added, and the process continued with aspiration and washing until the stop solution was introduced. The plate was subsequently analyzed at 450nm using a microplate reader, and the outcomes were computed according to the protocols described by An et al. (2021) and F. Liu et al. (2018). DMEM was used as the negative control, and three samples of secretome collected at 24-hour, 48-hour, and 72-hour intervals were quantified, with each sample being assessed three times.

#### **3.2.2.2 Development of secretome-loaded alginate-lecithin hydrogel**

An 8% w/v solution of sodium alginate was prepared by dissolving sodium alginate in deionized water followed by the addition of soy lecithin in alginate solution to make a 2% w/v soy lecithin concentration and stirred slowly for an hour at 40°C to ensure complete dispersion of the alginate–soy lecithin mixture. The mixture of alginate and soy lecithin was allowed to equilibrate to room temperature (25°C). Subsequently, the conditioned medium of FR secretome (3:1) was added at a predetermined concentration to the mixture, resulting

in a 2% w/v sodium alginate – 0.5% w/v lecithin-Secretome mixture. The resultant mixture was crosslinked with 0.1 M CaCl<sub>2</sub> at room temperature as illustrated in (Figure 3.1) and preserved at 4°C for later usage in cytocompatibility and *in vitro* wound healing tests.

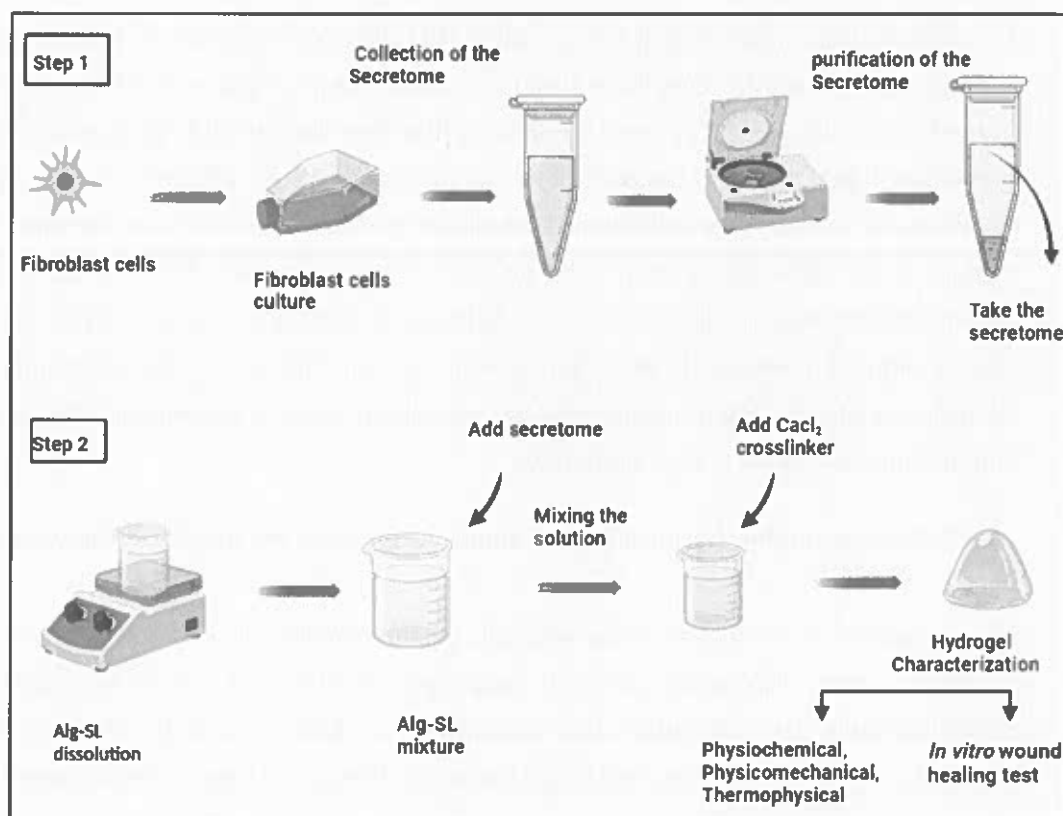


**Figure 3.1** Schematic representation of secretome collection and loading in alginate-soy lecithin hydrogel.

### 3.2.2.3 Evaluating the chemical properties of the alginate bioplatfoms using FTIR analysis

The chemical properties of the starting materials and the developed hydrogel were assessed using Fourier Transform Infra-Red (FTIR) spectroscopy. FTIR spectra of the bioplatfoms were determined to observe the effect of crosslinking on alginates. The analysis was performed utilizing a PerkinElmer Spectrum 2000 ATR-FTIR spectrometer (PerkinElmer 100, Llantrisant, Wales, UK) fitted with a single-reflection diamond MIRTGS detector. The FTIR parameters were set to incorporate 64 scans and cover a wavenumber range of 4000-

650  $\text{cm}^{-1}$ . The purpose of this analysis was to gain a better understanding of the chemical interactions and structural changes that occurred during the crosslinking process.

#### **3.2.2.4 X-ray powder diffraction assessment of the bioplatfoms**

The alginate (Alg) polymer alone, soy lecithin (SL), alginate–soy lecithin mixture (Alg-SL), and alginate-soy lecithin crosslinked with calcium chloride (Alg-SL- $\text{CaCl}_2$ ) solutions were frozen for 24 hours at  $-80^\circ\text{C}$  freezer. Following that, they underwent lyophilization using the Lyophilizer (Free zone 12, Labcono, Kansas City, USA) for an additional 24 hours. After lyophilization, the samples underwent analysis using X-ray diffraction to identify the phases present. X-ray diffraction spectra were acquired using a benchtop MiniFlex 600 (Rigaku, Japan) diffractometer equipped with  $\text{CuK}\alpha$  radiation at 40 kV and 15 mA. The  $2\theta$  scan range was configured between 10-90 degrees with a scan rate of 10 degrees/minute. The diffraction analysis yielded insights into the crystallinity level of the bioplatfoms, enabling further characterization of their properties.

#### **3.2.2.5 Evaluating the thermophysical characteristics of the bioplatfoms using DSC and TGA**

To ascertain the thermophysical characteristics of the bioplatfoms and polymers produced, a Mettler Toledo differential scanning calorimeter (DSC) from the STARe System in Schmelzenbach, ZH, Switzerland was employed. Aluminium crucibles were used to seal hydrogel and polymer samples that ranged from 3 to 10 mg, and these samples were heated under an  $\text{N}_2$  atmosphere within a temperature range of 0 to  $400^\circ\text{C}$  at a heating rate of  $10^\circ\text{C}/\text{min}$ . DSC measures heat flow in a sample to assess its melting point, glass transition temperature, and crystallization during both heating and cooling processes (Iqbal et al., 2023). DSC curves were subsequently generated by associating temperature with heat flow. Additionally, a thermo-gravimetric analyzer (TGA) (PerkinElmer, TGA 4000, Llantrisant, Wales, UK) was used to identify the temperature range of the bioplatfoms degradation. The samples were subjected to heating at a rate of  $10^\circ\text{C}/\text{min}$  from 30 to  $900^\circ\text{C}$  while continuously purged with nitrogen, and thermograms were generated as percentage weight versus temperature.

#### **3.2.2.6 Zeta potential measurement of the bioplatfoms**

For the measurement of the zeta potential of bioplatfoms, a Zetasizer NanoZS instrument from Malvern Instruments (Pty) Ltd. in Worcestershire, UK was utilized. This technique is

based on monitoring the electric potential within the double-layer structure. The point where the diffuse and stern layers intersect offers valuable information about the stability of colloidal dispersions and the extent of repulsion between adjacent charged particles within a dispersion. (Mndlovu et al., 2019). The samples, which included alginate, a mixture of alginate and soy lecithin, and alginate combined with soy lecithin crosslinked with calcium chloride, were subjected to sonication in distilled water, filtration, and subsequent suspension in the cell for zeta potential analysis at 25°C. This analysis yields valuable information regarding the surface charge of the dispersion and its stability within a colloidal system.

### 3.2.2.7 Assessing the extent of crosslinking in the bioplatfoms

The FTIR absorption spectra of alginate and crosslinked alginate regarding the affected carboxylic groups were acquired and employed in Equation 3.1 to determine the degree of crosslinking in alginate bioplatfoms. The optical absorbance of each alginate material corresponds directly to the quantity of free carboxylic groups present before crosslinking ( $C_i$ ) and after crosslinking ( $C_f$ ). Equation 3.1 was applied to calculate the percentage crosslinking index.

$$\% \text{ Cross - linking index} = \frac{C_i - C_f}{C_i} \times 100 \quad \text{Equation 3.1}$$

The degree of COO-/mole in both pristine and crosslinked alginate was obtained by comparing the analyses to the titration analyses, and the results were then substituted in Equation 3.1. Three titrations on average were reported.

### 3.2.2.8 Assessing gelling and viscoelastic properties of the bioplatfoms

The ElastoSens™ Bio<sup>2</sup> (Rheolution Instruments, Canada), was employed in evaluating the formation of hydrogel and network that occurs during interpolymer complexation. The hydrogel formation and gelling kinetics were determined by mixing the polymer solutions with the electrolyte solution and then initiating the complexation process by introducing the mixture into a 3 mL sample holder at a temperature of 37°C. Subsequently, the semi-stiff hydrogel was evaluated for its viscoelastic properties ( $G'$  and  $G''$ ), ionic interaction, and time-dependent gelling. The shear storage ( $G'$ ) and loss ( $G''$ ) moduli of gels can be monitored in real-time, either as a function of temperature or time, using the ElastoSens™ Bio<sup>2</sup> technique

(Ceccaldi et al., 2017). This technique entails gently vibrating a sample within a sample holder while employing a laser to detect its response.

### **3.2.2.9 Hydrogel mechanical evaluation and stability studies**

#### **3.2.2.9.1 Physical Stability of the Hydrogel**

After the successful formulation of alginate-soy lecithin hydrogel, the hydrogels were immediately evaluated for their homogeneity, organoleptic properties, and rheological properties. The hydrogels were then stored at two different temperatures: low temperature ( $8\pm 2$  °C) in the fridge, and room temperature ( $25\pm 2$  °C), for 3 months. The organoleptic properties (Appearance, Odor, Colour) of the hydrogels were checked every week, while the rheological properties were investigated at various intervals on different days, including D0, D3, D7, D15, D21, D28, D60, and D90. Haake Modular Advanced Rheometer System was used for viscosity measurements.

#### **3.2.2.9.2 Stability of secretome proteins after loaded into the hydrogel**

A 3%  $v/v$  of hydrogel formulated at various time intervals was mixed with DMEM to produce solution form. The resultant solution was subsequently diluted with the sample diluent and underwent enzyme-linked immunosorbent assay for analysis of VEGF. The stability of all formulations was assessed over 29 days at  $-20$  °C storage temperature.

#### **3.2.2.10 Swelling and degradation studies of the bioplatfoms**

The bioplatfoms underwent swelling (fluid absorption) and degradation in a simulated *in vitro* exudative environment. The simulated wound fluid comprised 5.8440 g of sodium chloride, 3.3604 g of sodium hydrogen carbonate, 0.2982 g of potassium chloride, 0.2775 g of calcium chloride, 33.00 g of bovine albumin, and 1,000 mL of deionized water. The pH of the resulting solution was adjusted to 6.5. For degradation, 0.2 mg/mL of lysozyme was introduced (Nokoorani et al., 2021). The orbital shaking incubator (LM-530-2, MRC Laboratory Instruments Ltd. Hahistadrut, Holon, Israel) was utilized, maintained at 37 °C and set to a speed of 50 rpm. Pre-weighed samples of the secretome hydrogel (S. gel) and lyophilized secretome hydrogel (LS. gel) were dispersed in 5 mL of simulated wound fluid. Consequently, measurements were conducted for the water uptake analysis over a 24-hour duration. Following the removal of excess fluid from the wet samples, the swelling was determined using Equation 3.2.

$$\text{Swelling (\%)} = (Mh - Md) / Md \times 100 \quad \text{Equation 3.2}$$

The swelling percentage (%) represents the extent of fluid absorbed, with Mh representing the mass of the bioplateforms in their hydrated state and Md representing their mass in the dry states.

The assessment of the degree of degradation was carried out on days 1, 2, 3, 5, 7, 10, and 14. To detect any changes in mass, the dried mass was measured on each of these days. Before weighing the wet samples to determine the eroded mass, they were dried in an oven at (55°C) to ensure complete removal of any remaining moisture. Equation 3.3 was employed to calculate the mass loss of the bioplateforms following degradation at each time point.

$$\text{Degradation (\%)} = (Mo - Md) / Mo \times 100 \quad \text{Equation 3.3}$$

Where Mo represents the initial mass of the sample before immersion in the fluid.

#### **3.2.2.11 The release profile of secretome total proteins from the secretome hydrogel**

Using a BCA protein assay, the release rate and quantity were assessed over a specific duration. Each 50 mg sample was incubated at 37°C in 5 millilitres of Phosphate Buffer Saline PH 6.5 for 168 hours. During this period, fresh PBS (25 µL) was replaced with 25 µL of the supernatant at predetermined intervals (2, 4, 6, 8, 10, 24, 48, 72, 96, 120, 144, and 168 hours) (Selmani et al., 2023). LS. gel and S. gel were each prepared and examined three times at every time point. The assay was conducted according to the manufacturer's instructions, and quantitative analysis was performed using a standard curve.

#### **3.2.2.12 Biocompatibility and cytotoxicity assessment of the bioplateforms**

The NIH 3T3 and HacaT cell lines were used in this study. RPMI supplemented with 10% FBS and 1% penicillin/streptomycin (50 IU/mL) was used to grow NIH 3T3 cells, while DMEM supplemented with 10% FBS and 1% penicillin/streptomycin (50 IU/mL) was used to grow HacaT cells. Both cell lines were incubated at 37 °C with 5% CO<sub>2</sub> in a humidified incubator, and the culture medium was refreshed every 2-3 days.

The viability analysis of the formulated hydrogels was done using the [3-(4,5-dimethylthiazol)-2-yl]-2,5- diphenyltetrazolium bromide (MTT) assay. This assay involves

the transformation of a yellow tetrazolium salt (MTT) into purple formazan crystals by live cells. NIH 3T3 and HacaT cells ( $1 \times 10^4$  cells/ml) were seeded in a 96-well plate and incubated overnight at 37 °C with 5% CO<sub>2</sub>. Following the incubation, the seeded plates were treated with different concentrations of starting materials and hydrogels ranging from 0.03%, 0.06%, 0.125%, 0.25%, 0.5%, and 1%W/V of each. Cells killed with Dimethyl Sulfoxide (DMSO) served as the negative control, while untreated wells acted as the positive control.

To evaluate the metabolic activity of the cells, 10 µl of MTT solution was added into each well plate at specified time intervals (24, 48, and 72 hours) followed by a 4-hour incubation period. Thereafter, to dissolve the formazan crystals, the solubilizing agent was subsequently added to the well plates and further incubated overnight at 37°C. The absorbance of the well plates was measured at 570 nm using a Perkin Elmer® VICTOR 2030 multilabel plate reader to quantify the optical density (OD) according to the colour development followed by the percentage cell viability for each bioplatforms. The experiment was repeated three times, for different types and concentrations of bioplatforms at different time points.

### **3.2.2.13 *In vitro* wound healing test employing the scratch assay**

*In vitro* wound healing analysis was performed using the Scratch assay. NIH3T3 and HacaT cells were used to evaluate the biological effect of the bioplatforms to repair tissue defects. The cells were cultured in 6-well plates at a density of ( $5 \times 10^5$  cells/ml) until they reached confluence after 48 hours of incubation in RPMI and DMEM media supplemented with 10% FBS and 1% penicillin and streptomycin. Thereafter, the cells were starved with their respective unsupplemented media for 12–14 hrs to prevent proliferation. Thereafter, using a sterile 200µl pipette tip, a gap was created by scrapping the cells in a straight line, which allowed the cells to migrate into the scratched areas. This was followed by replacing the medium with various treatments of (23 %  $\nu$ , secretome collected at time intervals (24hrs, 48hrs, and 72hrs) and bioplatforms. To evaluate cell migration, images were captured using Olympus® CKX53 microscope at 0, 24, 48, and 72 hours. These experiments were performed in triplicate (n=3). The area occupied by NIH3T3 and HacaT cells and the empty surface area were quantified in each sample, and the results were standardized to the initial control at time 0, which was regarded as 100% empty space. The ImageJ, a freely available Java-based software developed by the National Institutes of Health (NIH) in Bethesda, MD, USA (Version 1.50c), was utilized to conduct further analysis on the captured images. The

software was employed to measure the width of the wound gaps at different time points. Equation 3.4 outlines the calculation method for determining the wound-healing rate.

$$\% \text{ Wound closure} = (W_i - W_f) / W_i \times 100 \quad \text{Equation 3.4}$$

Where  $W_i$  and  $W_f$  are the initial and final width of the wound, respectively.

#### 3.2.2.14 Cell migration assay using a modified Boyden chamber.

The migration of NIH3T3 and HacaT cells was evaluated using a modified Boyden chamber (Corning Inc., NY, USA). Gelatin-coated polycarbonate filters with a pore size of 8.0  $\mu\text{m}$  and 6.5 mm diameter inserts were utilised. Briefly, the upper chamber was loaded with 200  $\mu\text{L}$  of secretome hydrogel, Normal hydrogel, or a control (untreated cells), along with  $1 \times 10^4$  NIH3T3 and HacaT cells in 200  $\mu\text{L}$  of serum-free medium. A volume of 0.4 mL of medium containing 10% FBS was added to the lower chamber as a chemo-attractant. The cells were then incubated for 12 hours at 37°C. Non-migrating cells on the upper surface of the membrane were subsequently removed using cotton swabs. Thereafter, 80  $\mu\text{L}$  of Alamar Blue reagent was added to the cells that had migrated to the bottom of the membrane and incubated for 4 hours. The quantification was performed using a microplate reader, measuring at maximum emission/excitation wavelengths of 535 nm and 595 nm, respectively. Subsequently, the cells that had migrated to the lower side of the membrane were rinsed twice with PBS and subsequently stained with trypan blue. The stained cells were then examined under an Olympus® CKX53 microscope.

#### 3.2.2.15 Data Analysis

Each experimental procedure was conducted in triplicate. All experimental data is presented as mean  $\pm$  standard deviation (SD). Statistical analyses were performed using Measurements of Analysis of Variance one-way ANOVA in Statistical Package for Social Sciences (SPSS 16.0) software, with the Tukey test used for multiple comparisons. Significance was determined at  $p < 0.05$ . *In vitro*, scratch closure rates were assessed using *Image J* software (version 1.53n). Statistical analysis was carried out for cytotoxicity studies and scratch assays, and the findings were presented as mean  $\pm$  SD along with corresponding p-values. The level of significance is indicated by \* for  $p < 0.05$ .

### **3.3 Results and Discussion**

This study explored the application of hydrogels comprising secretome-loaded alginate-soy lecithin, crosslinked with CaCl<sub>2</sub>, as a potential treatment for acute wounds. Various bioplatfroms, including pristine Alg (P-Alg), pristine SL(P-SL), Alg-SL, Alg - CaCl<sub>2</sub>, and Alg - SL - CaCl<sub>2</sub> bioplatfroms, were investigated for their physicochemical and physicomachanical properties. The hydrogels were prepared to facilitate characterization, providing essential insights into their suitability as wound dressing materials. Biological effect validation of the secretome-loaded hydrogels was carried out using the established *in vitro* scratch assay.

#### **3.3.1 Secretome collection and quantification using Enzyme-Linked Immunosorbent Assay (ELISA)**

When investigating the secretome, it is essential to acknowledge differences in the methods of detection. Identifying secretome protein components typically employs two proteomic approaches: immunological-based or shotgun-based methods (Wechsler et al., 2021). Herein, an immunological-based method was utilized for the FR secretome-specific protein quantification.

To identify the key secreted factors responsible for the impact of the rat skin fibroblast cell secretome on the wound healing process, an ELISA kit was employed to assess the presence of vascular endothelial growth factor (VEGF) in the FR secretome. VEGF, a prominent factor responsible for angiogenesis, plays an important role in the development of granulation tissue and the regeneration of peripheral nerves (Kwon et al., 2023). The VEGF levels in the FR secretome were measured following varying incubation periods (24, 48 and 72 hours). The expression levels of VEGF exhibited an increase with longer incubation times (Figure 3.2). This outcome implies that other proteins related to wound healing could potentially be suspected to serve as the principal components of the FR secretome responsible for speeding up wound healing. In an earlier study, the secretome was collected from ADSC after 48 hours, and the quantification of VEGF revealed a low concentration. However, in this investigation, a concentration of approximately 2000 ng/ml was achieved without the need for supplementary procedures, representing a significant improvement compared to previous findings (An et al., 2021). The factor contributing to elevated VEGFT may be due to a higher cell count of more than 90% cell confluence for secretome collection compared to previous studies that used 70-80% confluent, putting into consideration cell compensation when apoptosis occurs (An et al., 2021). The secretome

collected after 72 hrs incubation time was used for the subsequent tests given its high VEGF concentration.

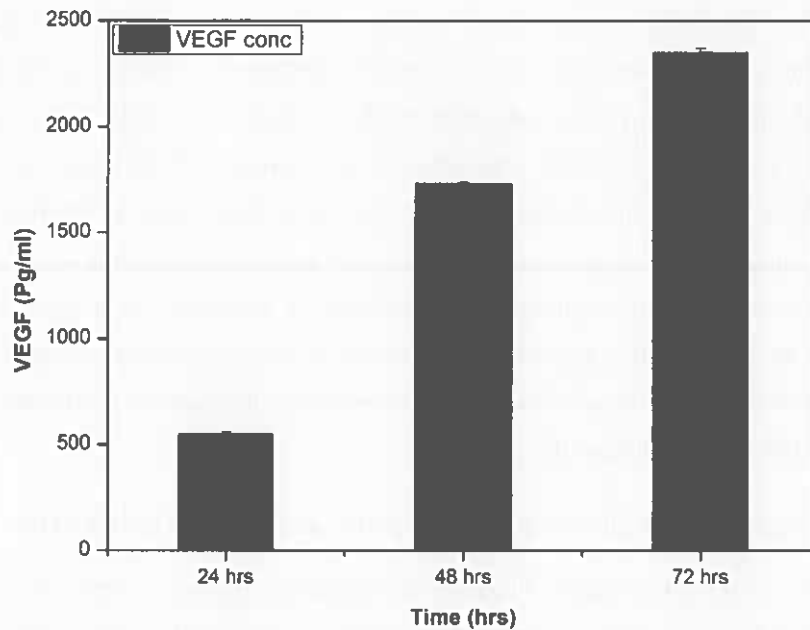


**Figure 3.2** Quantitative analysis of Fat's Dermal Fibroblast condition media for VEGF Concentration in secretome collected over different times.

### 3.3.2 Development of secretome-loaded alginate-lecithin hydrogel

Sodium alginate serves as a representative example of an ionically crosslinked hydrogel matrix. This biocompatible polymer is crosslinked with calcium chloride. The interaction between the negatively charged poly(guluronic) acid units of alginate ( $-\text{COO}^-$ ) and polyvalent ions ( $\text{Ca}^{2+}$ ) results in the formation of ionic bonds. The addition of lecithin also played a role in influencing the final properties of the hydrogel. Lecithin increases the biocompatibility of the hydrogel and modifies the hydrogel network. After calcium ions crosslink alginate, some calcium chloride is still in the system and can bind to the lecithin micelles that have been added because of its dissociated state. A competitive interaction is induced by an increase in lecithin content, which causes lecithin to displace the calcium ions in the crosslinked alginate (Heger et al., 2022). Moreover, additional interactions may take place, as lecithin can bind with alginate via quaternary ammonia or with calcium ions through

negatively charged phosphate residues. These interactions influence the hydrogel structure, enhancing its ability to retain water effectively (Heger et al., 2022).

A study by Sears *et al.* demonstrated that MSC-secretome enhances wound healing by mitigating inflammation, optimizing cellular functions, and facilitating granulation tissue development. Moreover, the MSC-secretome exhibited a superior safety profile compared to direct cell delivery, and its extended shelf life (Sears et al., 2021). To this end, the highly enriched secretome collected from FR cells as previously stated, was mixed with alginate-soy lecithin solution and subsequently crosslinked with  $\text{CaCl}_2$  to produce the secretome-loaded alginate-soy lecithin hydrogel. Through incorporation of the secretome, the primary research objective of augmenting the hydrogel's capability to encapsulate a significant amount of secretome is achieved, seeking to enhance the efficient delivery of therapeutic biomolecules into skin wounds. On the other hand, this simply produced hydrogel can be easily applied to skin wounds.

### 3.3.3 Assessing chemical properties of the bioplatfroms using FTIR

FTIR was used in this study to identify the functional groups in alginate responsible for the binding of divalent calcium cation. The analysis comprised (P-Alg), (Alg-SL), (Alg- $\text{CaCl}_2$ ), and (Alg-SL- $\text{CaCl}_2$ ) and the results are depicted in (Figure 3.3a).

The characteristic peaks observed in (Alg- $\text{CaCl}_2$ ) and (Alg -  $\text{CaCl}_2$  - SL) were as follows;  $3262\text{ cm}^{-1}$  to (O-H stretch), in  $2925\text{ cm}^{-1}$  and  $2854\text{ cm}^{-1}$  to (C-H stretch), in  $1736\text{ cm}^{-1}$  to (-CO- stretch) of carbonyl group due to soy lecithin,  $1596\text{ cm}^{-1}$  to (asymmetric stretching of carboxylated salt group  $\text{COO}^- - \text{Ca}^{+2}$ ) and are specific to ionic binding, the finding correlate with the results on literature (Singh et al., 2016). The peaks at  $1412\text{ cm}^{-1}$  to (symmetric - $\text{CO}_2$ -stretching), in  $1297\text{ cm}^{-1}$ ,  $1248\text{ cm}^{-1}$ ,  $1244\text{ cm}^{-1}$  to C-O stretching), in  $1082\text{ cm}^{-1}$ ,  $1024\text{ cm}^{-1}$ ,  $1025\text{ cm}^{-1}$ ,  $1028\text{ cm}^{-1}$  to (C-O-C stretching) which considerably strengthens in the spectrum of Alg with  $\text{Ca}^{2+}$  ions, can also be attributed to the presence of crosslinking. The C-C stretching peak (around  $1025\text{ cm}^{-1}$ ) shows a higher intensity, suggesting either a stronger O-H binding vibration or a stronger binding of the  $\text{Ca}^{2+}$  to the guluronic acids of Alg (Saarai et al., 2013), in  $941\text{ cm}^{-1}$ ,  $946\text{ cm}^{-1}$ , to (C-O stretching) in  $887\text{ cm}^{-1}$  and  $878\text{ cm}^{-1}$  to (C-C), in  $817\text{ cm}^{-1}$  and  $815\text{ cm}^{-1}$  to (C-C-O), in  $680\text{ cm}^{-1}$ ,  $668\text{ cm}^{-1}$ ,  $662\text{ cm}^{-1}$  and  $660\text{ cm}^{-1}$  to (C - C).

The two carboxylic groups of alginates interact with the divalent calcium ions. Alginates that have already interacted with calcium do not interact ionically afterwards. An ionically crosslinked hydrogel matrix can be created by crosslinking sodium alginate with calcium chloride. During this process, polyvalent calcium ions ( $\text{Ca}^{2+}$ ) and the negatively charged poly(guluronic) acid units of alginate ( $-\text{COO}^-$ ) interact to form bonds. Furthermore, the incorporation of lecithin also affects the ultimate characteristics of hydrogel. Lecithin can potentially interact with alginate either through quaternary ammonium or with calcium ions via negatively charged phosphate residues (Heger et al., 2022). The bioplatfroms reveal that upon the addition of  $\text{CaCl}_2$  proportions, the resulting chemical structure shifts from  $\text{COO-Na}^+$  to  $\text{COO-Ca}^{2+}$ , accompanied by a decrease in intensity in these regions. These observations align with the findings reported by Mndlovu et al. (Mndlovu et al. 2019). The degree of alginate crosslinking did not cause substantial alterations to the chemical structure.

### 3.3.4 X-ray powder diffraction analysis of the bioplatfroms

X-ray diffraction was conducted to evaluate the physical state of the bioplatfroms, determining whether they were amorphous or crystalline. The XRD was applied to this study to confirm the hydrogel composition after crosslinking the polymer solution with the  $\text{CaCl}_2$ . As depicted in Figure 3.3b, the P-Alg diffraction pattern exhibited distinct amorphous peaks at 21 and 43 degrees. Conversely, the diffraction pattern of the crosslinked alginate revealed two additional amorphous peaks at 22 and 43 degrees. Moreover, crystalline peaks were observed at 31, 45, 56, 66, 75, and 84 degrees. Notably, the 7-degree peak observed in the P-Alg was absent in the crosslinked alginate bioplatfroms, likely due to the cross-linking of the carboxylic part of alginate as confirmed by the calculated degree of crosslinking of 84.32%.

When comparing Alg- $\text{CaCl}_2$  with Alg-soy lecithin- $\text{CaCl}_2$  hydrogels, the latter displayed larger crystalline peaks at 31 and 45 degrees. This can be attributed to the inclusion of soy lecithin in the formulation, which exposed non-crosslinked amorphous alginate particles. The greater degree of crosslinking in the Alg hydrogel caused this effect. FTIR analysis verified that these crystalline peaks were attributed to the calcium content from the  $\text{CaCl}_2$ , indicating successful crosslinking as per the calculated degree of crosslinking of 84.32% (Figure 3.3a). As reported by Laia et al., the crosslinking effect of  $\text{Ca}^{2+}$  in  $\text{CaCl}_2$  led to heightened crystallinity in the alginate bioplatfroms (Laia et al., 2014).

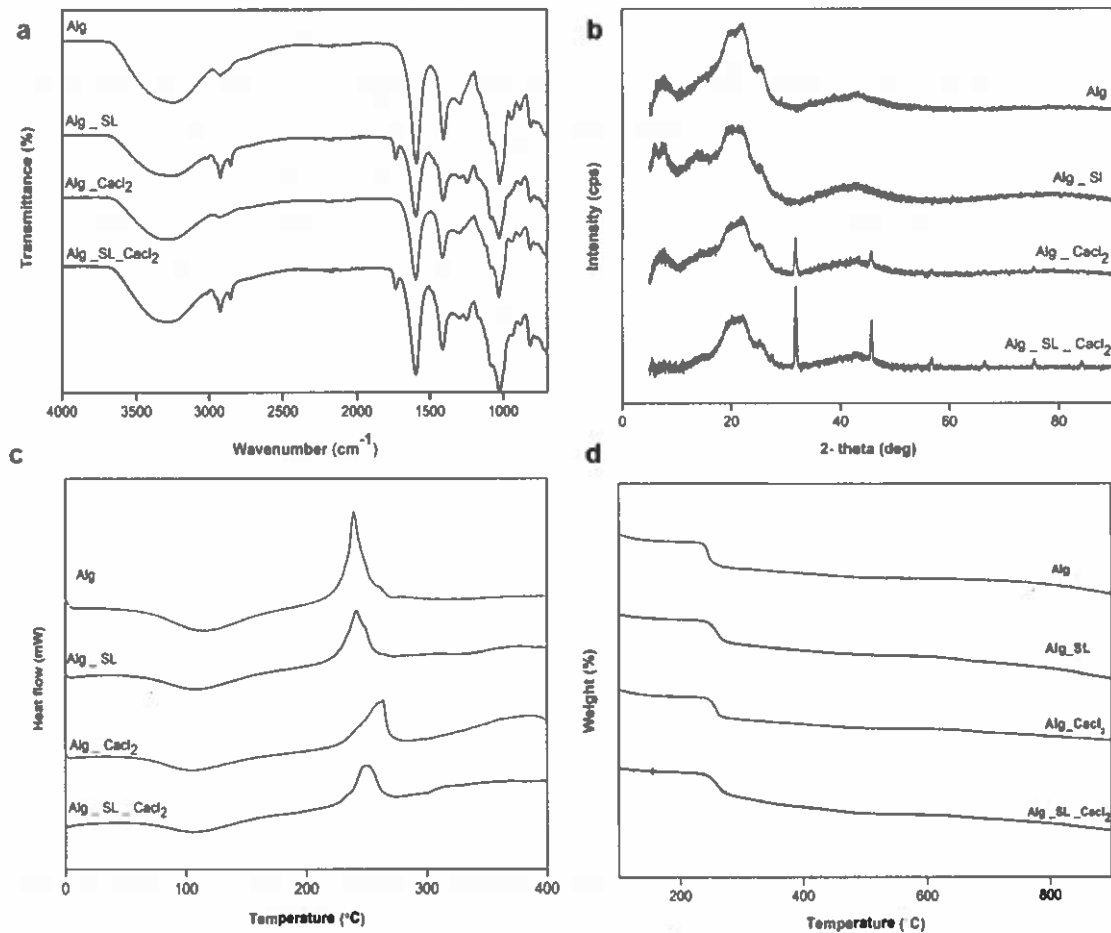


**Figure 3.3** The analytical techniques (a) FTIR spectra, (b) X-ray diffractograms, (c) DSC and (d) TGA thermograms of the bioplateforms used to evaluate chemical composition, functional groups, and phase changes of the bioplateforms induced by cross-linking.

### 3.3.5 Assessing thermophysical properties of the bioplateforms using DSC and TGA

The thermograms presented in (Figure 3c) for the bioplateforms revealed a consistent dehydration process occurring at 115 °C for P-Alg, Alg-SL, Alg-CaCl<sub>2</sub>, and the crosslinked counterpart. Notably, the exothermic peak temperatures of crosslinked alginate and alginate displayed a noticeable upward shift, rising from 239 °C to 248 °C (Figure 3.3c). A similar trend was observed when comparing P-Alg to Alg - CaCl<sub>2</sub>, with a temperature shift from 239 °C to 263 °C, and from 239 °C to 241 °C when comparing with Alg - SL. This temperature

shift is attributed to the alteration in the polymer's thermal properties induced by crosslinking, thereby elevating the polymer's degradation temperature (Figure 3.3c).

The P- Alg demonstrated significant weight loss (29.56%) between 238 and 275 °C. In contrast, Alg - SL exhibited a notable weight loss (28.61%) within the temperature range of 238 to 277 °C and Alg - CaCl<sub>2</sub> displayed a substantial weight loss (25.56%) between 234 and 275 °C. A notable weight loss (26.58%) was observed for the crosslinked alginate hydrogel between 234 and 280°C, suggesting a potentially lower degradation temperature influenced by the crosslinking process. Notably, the crosslinked alginate hydrogel demonstrated the least weight loss at 26.58% (Figure 3.3d).

These findings align with those obtained from Differential Scanning Calorimetry (DSC), indicating that the crosslinked platforms demonstrate a shift in exothermic behaviour towards lower temperatures in comparison to the polymers. The main chains of alginate undergo thermal degradation, as evidenced by the exothermic behaviour observed in DSC analysis between 239 and 268°C, along with the significant weight loss observed in Thermogravimetric Analysis (TGA) between 234 and 272°C. As a consequence of crosslinking, the degradation temperature range was reduced. However, despite this, the crosslinked polymers exhibited a lower percentage of weight loss compared to the polymers alone, suggesting that crosslinking facilitated controlled thermal degradation. The chemical and physical characteristics of the bioplayers above are summarized in Table 3.1.

Table 3.1: Summary of the chemical and physical characteristics of bioplatforms using FTIR, XRD, DSC, and TGA.

| Chemical and physical characteristics of biomaterials |                                     |  |                           |             |                      |                                |  |                            |  |
|---|-------------------------------------|--|---------------------------|-------------|----------------------|--------------------------------|--|----------------------------|--|
| Biomaterials  | FTIR wavenumber (cm <sup>-1</sup> ) | FTIR characteristic bonds/functional groups                                  | XRD peak 2theta (Degrees) | XRD phase   | DSC temperature (°C) | DSC profile description        | TGA degradation temperature range (°C) | TGA percentage weight loss |  |
| Alg   | 3261                                | O-H stretch  | 21                        | Amorphous   | 98                   | Dehydration (endothermic peak) | 238 - 275                              | 29.56                      |  |
|   | 2925                                | CH stretch   | 43                        | Amorphous   |                      |                                |  |                            |  |
|   | 1594                                | Asymmetric stretching of carboxylate in the salt form (COO-Na <sup>+</sup> ) |                           |             | 239                  | Degradation (exothermic peak)  |  |                            |  |
|   | 1406                                | symmetric -CO <sub>2</sub> - stretching                                      |                           |             |                      |                                |  |                            |  |
|   | 1297                                | to C-O stretching  |                           |             |                      |                                |  |                            |  |
|   | 1024                                | C-O-C stretching   |                           |             |                      |                                |  |                            |  |
| Alg-SL  | 3262                                | O-H stretch  | 21                        | Amorphous   | 110                  | Dehydration (endothermic peak) | 234 - 277                              | 28.61                      |  |
|   | 2924                                | CH stretch   | 43                        | Amorphous   |                      |                                |  |                            |  |
|   | 1736                                | -co stretch of carbonyl group  |                           |             | 248                  |                                |  |                            |  |
|   | 1407                                | c-h blending vibration   |                           |             |                      | Degradation (exothermic peak)  |  |                            |  |
| Alg-CaCl <sub>2</sub>                                 | 3262                                | O-H stretch  | 22                        | Amorphous   | 110                  | Dehydration (endothermic peak) | 234 - 275                              | 25.56                      |  |
|   | 1597                                | CH stretch   | 31                        | Crystalline |                      |                                |  |                            |  |
|   | 1412                                | CO <sub>2</sub> symmetric stretching vibration                               | 43                        | Amorphous   |                      |                                |  |                            |  |
|   |                                     |  |                           | 56          | Crystalline          |                                |  |                            |  |
|   |                                     |  |                           | 66          | Crystalline          | 263                            |  |                            |  |
|   |                                     | 75   | Crystalline               |             |                      |                                |  |                            |  |

|                   |      |   |    |             |     |  |                                |                 |
|-------------------|------|---|----|-------------|-----|--|--------------------------------|-----------------|
|                   | 1028 | -C-O-C- stretching vibration              | 84 | Crystalline |     |  | Degradation (exothermic peak)  |                 |
| Alg-              | 3282 | O-H stretch                               | 31 | Crystalline | 108 |  | Dehydration (endothermic peak) | 234 - 280 26.58 |
| SL-               | 2924 | -CH stretching vibration                  | 45 | Crystalline |     |  |                                |                 |
| CaCl <sub>2</sub> | 2854 | -CH stretching                            | 66 | Crystalline |     |  |                                |                 |
|                   | 1735 | -co stretch of carbonyl group in lecithin | 75 | Crystalline | 248 |  |                                |                 |
|                   | 1597 | a symmetric -CO <sub>2</sub> - stretching | 84 | Crystalline |     |  | Degradation (exothermic peak)  |                 |
|                   | 1412 | symmetric -CO <sub>2</sub> - stretching   |    |             |     |  |                                |                 |
|                   | 1296 | -C-O-C- stretching vibration              |    |             |     |  |                                |                 |
|                   | 1025 | -C-O-C- stretching vibration              |    |             |     |  |                                |                 |

### 3.3.6 Zeta potential of the bioplatfoms

Surface charge analysis is crucial as it offers insights into particle stability, particularly regarding ionic interactions between polymers and ionic salts (Mndlovu et al., 2019). The average zeta potentials of P-Alg, Alg-SL, and crosslinked Alg-SL were  $-10.14 \pm 3.38$  (mV),  $-42 \pm 3.38$ , and  $-36.8 \pm 3.38$  (mV) for pristine Alginate and the corresponding bioplatfoms, respectively. The pristine polymer exhibited its highest surface charge but underwent a decrease following the crosslinking procedure. This reduction in surface charge indicates successful polymer crosslinking. Moreover, the reduced surface charge of the crosslinked polymers suggests a high level of crosslinking, as the decrease in surface charge brought it to below 10 mV. Zeta potential offers insights into electrostatic repulsion; however, the technique does not convey information about attractive van der Waals forces. Instances have been documented where colloids with low zeta potential exhibit stability, and conversely, those with highly positive or negative zeta potential may not (Nqoro et al., 2023). The zeta potential of the alginate hydrogel was measured at 10 mV, suggesting the possibility of stabilization through electrostatic interactions.

### 3.3.7 Determining the extent of crosslinking of the bioplatfoms

The crosslinking extent of the alginate hydrogel was determined using FTIR and zetasizer. The crosslinking degree in the crosslinked alginate (Alg-SL-CaCl<sub>2</sub>) was found to be 84.32% through FTIR and 75.85% through zeta potential analysis. The substantial alteration in zeta potential from pristine alginate to crosslinked alginate further supports the evidence of polymer crosslinking. Despite a minor variance in the crosslinking degrees obtained through these two methods, both indicate the significant crosslinking present in Alg-SL-CaCl<sub>2</sub> hydrogel. The controlled absorption of fluids is a vital characteristic of bioplatfoms used in wound dressings. The cross-linking process enhanced the hydrophilic properties of the polymer, enabling it to effectively hold a substantial amount of fluids within the wound cavity.

### 3.3.8 Assessing the viscoelastic properties and gelation kinetics of the bioplatfoms

Hydrogels are expected to emulate the mechanical characteristics of the skin, encompassing gel strength ( $G'$ ) and viscoelastic properties denoted by the loss tangent ( $G'/G''$ ). They should possess the ability to absorb wound exudate, uphold a moist environment, and demonstrate high viscosity to adhere to the wound while retaining

flexibility (Norahan et al., 2022). This was achieved by assessing the gelling kinetics of the Alg-SL-CaCl<sub>2</sub> hydrogel using the ElastoSens™ Bio<sup>2</sup>. The alginate with soy lecithin solution was subjected to CaCl<sub>2</sub> and permitted to undergo gelation over some time. This gel formation process led to the development of a crosslinked hydrogel. This hydrogel occurs through crosslinking between the carboxylic group of alginate and Ca<sup>+2</sup> of the CaCl<sub>2</sub>. Figure 3.4 demonstrates the formation of a crosslinked hydrogel between Alg-SL-CaCl<sub>2</sub>.

This was evident from the initial rise in shear storage modulus, loss modulus, and complex modulus upon the reaction of the hydrogel components. As a result, the sample height decreased, indicating the hydrogel's ability to absorb fluid over time. Enhanced viscosity during the gelation process is reflected in the loss modulus (G''), which is associated with the increase in storage modulus and robust interactions between the Ca<sup>2+</sup> and carboxylic groups. The optimal gelling point was observed at 37°C, with the highest average storage modulus measured at 2890 ± 100 Pa. Under these specific experimental conditions, the sample height notably decreased as the viscosity (loss modulus) increased in proportion to the elasticity (storage modulus). The hydrogel's rigidity and viscoelastic properties were indicative of its flexibility and the sol-gel transition.

The reduction in sample height and the formation of the complex confirmed the sol-gel transition of the hydrogel. The presence of both viscoelastic properties and a stable sol-gel state in the hydrogel is further confirmed by the constant value of the loss tangent over time (Figure 3.4(a)). For hydrogels to stay in the wound cavity and maintain a moist environment, they must have viscous qualities. Additionally, hydrogels should not be excessively rigid, as this would hinder their interactions with the (ECM) (Mndlovu et al., 2019). It is optimal for the mechanical properties of the gel to closely mimic those found in the skin environment. These findings indicated that the hydrogel obtained exhibited desirable gel strength (G') and viscosity (G'').





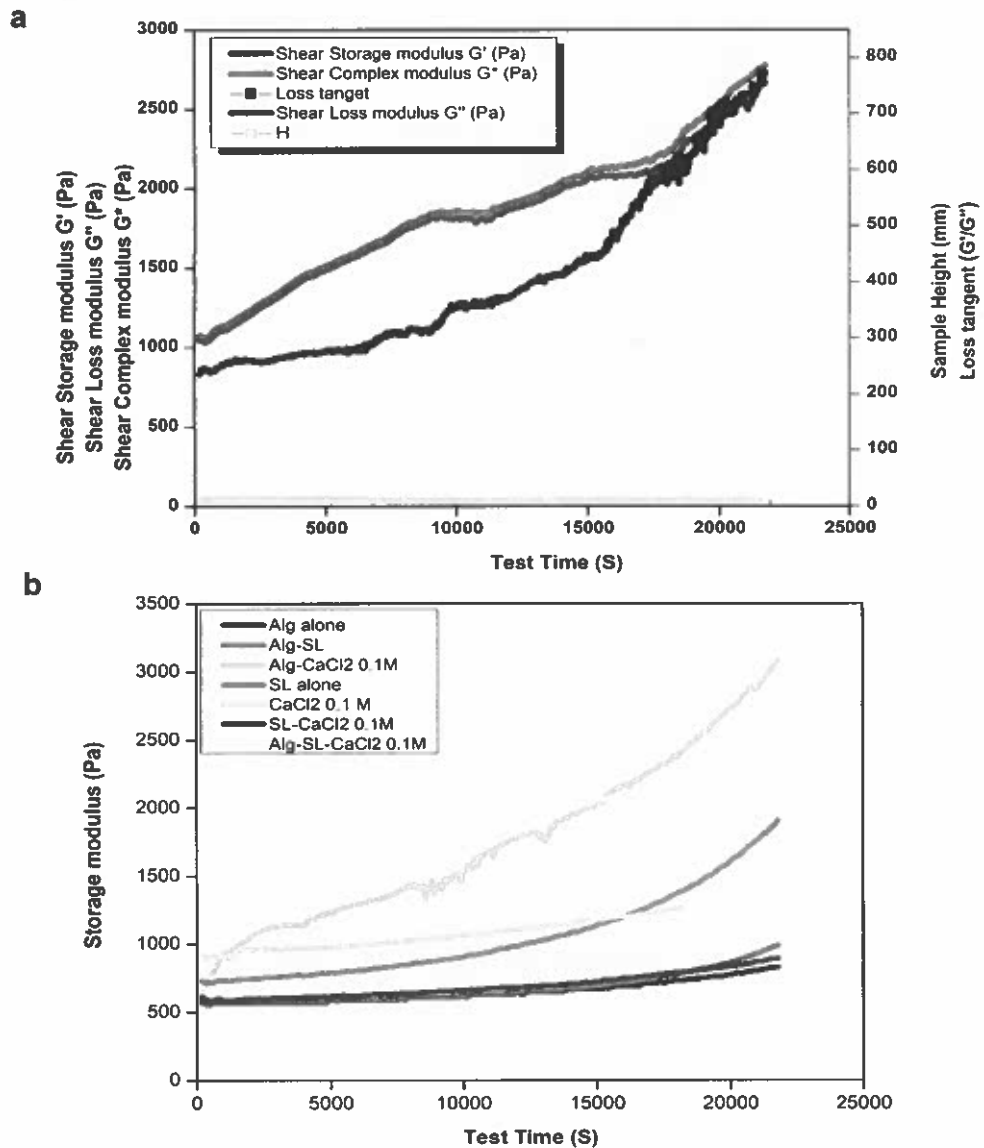


**Figure 3.4** The kinetics of Alg-SL hydrogel formation in 37°C water. (a) Alg-SL solution was mixed with a CaCl<sub>2</sub> crosslinker to initiate hydrogel formation. Real-time measurements were taken of sample height (swelling and absorption functions), shear complex modulus, loss tangent (viscoelastic properties), shear storage modulus (gelling and elasticity measurements), and shear loss modulus (viscosity). (b) The shear storage modulus of each component alone and mixed one.

### **3.3.9 Hydrogel mechanical evaluation and stability studies**

#### **3.3.9.1 Physical stability of the hydrogel**

The homogeneity, organoleptic characteristics, and rheological properties of the Alginate–Soy lecithin hydrogels were assessed and there were no significant changes in those properties as presented in pictures in (Figure 3.5 (a)). Over 3 months, the hydrogels were stored at two distinct temperatures: a low temperature ( $8\pm 2$  °C) in the fridge and a room temperature ( $27\pm 2$  °C). The findings revealed that the hydrogel maintained its physical stability throughout the storage period. Weekly evaluations of the hydrogel did not show any alterations in organoleptic properties, encompassing appearance, odour, and colour.

Rheological evaluations were conducted on different days, namely D0, D3, D7, D15, D21, D28, D60, and D90. Viscosity measurements using a Rheometer revealed consistency in the viscosity of all formulations at the two storage conditions, and this provided reliable insights into the hydrogel's usability for wound application. The findings revealed consistent viscosity levels at different time points, indicating robust stability, as illustrated in (Figure 3.5 (b)). Maintaining a high viscosity is crucial for ensuring the hydrogel effectively stays within the wound cavity (Hoseinpour Najari et al., 2018).

#### **3.3.9.2 Stability of secretome proteins after loaded into the hydrogel**

Assays based on immunology are employed to test a diverse array of recognized proteins. These assays are typically user-friendly, requiring minimal sample preparation and employing analysis methods that yield quantitative results. ELISA was utilized to provide elevated levels of specificity, sensitivity, and reproducibility, achieving consistent results in detecting VEGF levels within the hydrogel formulated at different time intervals following the preparation, as mentioned earlier.

The stability of the hydrogel formulations was assessed over 29 days at  $-20^{\circ}\text{C}$  storage temperature. The targeted protein secreted by the secretome was VEGF which is present at low levels in picograms. Figure 3.5 (c) gives insight into the results obtained. Four formulations were tested, which include secretome collected after 72 hrs incubation (F9), secretome powder (F7), lyophilized secretome hydrogel (F8), and secretome hydrogels that were tested on D0 (F1), D4 (F2), D7 (F3), D10 (F4), D21 (F5), and D29 (F6). The findings from the secretome hydrogels indicate a statistically significant difference ( $P < 0.05$ ) in

VEGF concentration over time, possibly attributed to protein degradation with time. The other samples tested included secretome collected after 72 hours and tested immediately to compare protein levels before and after mixing with biomaterials. The variation of the result ( $P < 0.05$ ) can be interpreted as inter-batch differences in the bioactive components when compared to secretome hydrogel formulated at D0. The lyophilized secretome hydrogel and secretome powder showed statistical differences of  $P < 0.05$  in the VEGF level suggesting variation of protein content in different cell passages and density.

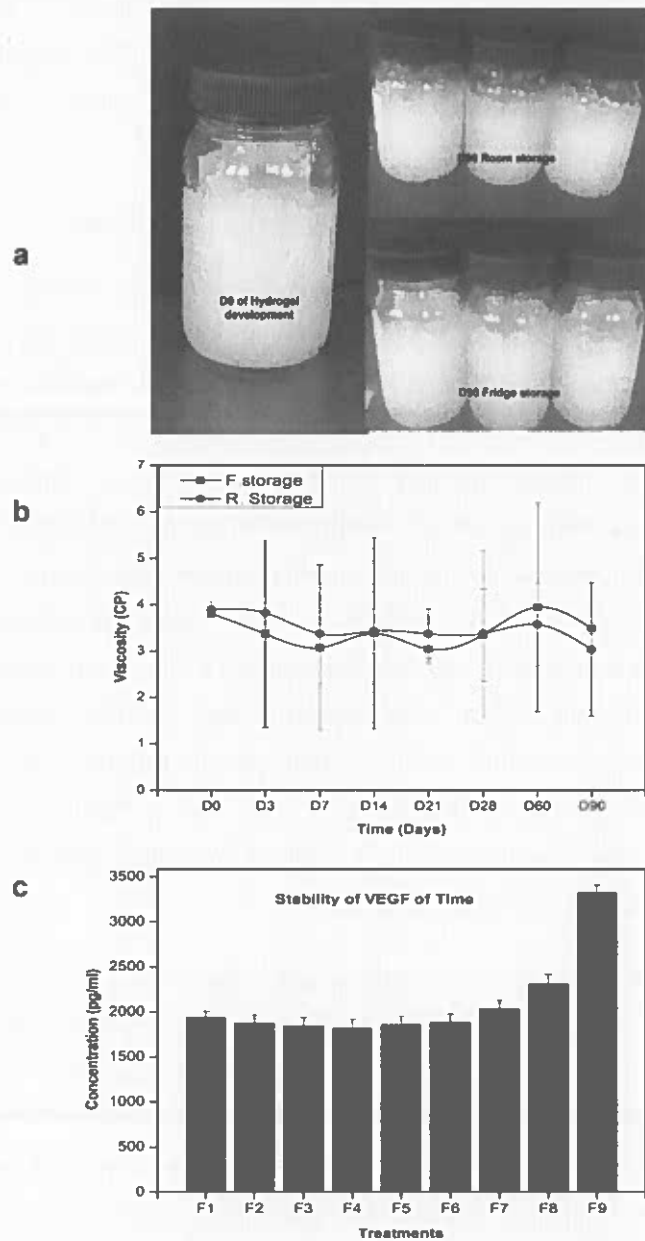


**Figure 3.5** The stability of the hydrogel (a) The appearance of the hydrogel over 3 months (b) Mechanical stability of the hydrogel observed over three months, with "F" denoting storage in a refrigerator and "R" indicating room storage temperature. (c) Employing an ELISA kit for the quantitative assessment of VEGF to illustrate the stability characteristics of different formulations, specifically the secretome collected after 72 hours of incubation (S72), secretome powder (S powder), lyophilized secretome hydrogel (LS gel), and secretome hydrogels (S gel) at various time intervals. F1, F2, F3, F4, F5, and F6

represented Secretome loaded hydrogel which stored at  $-20^{\circ}\text{C}$  after been prepared in different time intervals D0, D4, D7, D10, D21, and D29 respectively. F7 represents secretome powder. F8 represents secretome collected after 72 hrs, and F9 represents lyophilized secretome hydrogel.

### **3.3.10 Swelling and degradation studies of the bioplatfroms**

Wound bed pH varies depending on the stage of wound healing, typically ranging from neutral to alkaline (pH 6.5 to 8.5) (Bennison et al., 2017). Given the reason for selecting the PH 6.5 for this study. The swelling index of hydrogel-based biomaterials is crucial and varies based on the type of wound (dry or heavily exudating), as well as the hydrogel's structure and constituents. Proper swelling is important for tissue compression and controlled bioactives release through diffusion and material porosity (Mohite et al., 2018). Exceeding the swelling parameter can lead to biomaterial rupture, releasing its contents into the wound bed prematurely (Laurano et al., 2022). One key aspect of hydrogels is their capacity to expand in water and retain a significant amount of it. This is primarily due to the hydrophilic nature of the polymer chains, which absorb water, and the cross-linking between these chains, which traps the water within the hydrogel and protects the polymer from dissolving in the surrounding media (Nazarnezhada et al., 2020). Additionally, biocompatibility and biodegradation are essential criteria for wound dressings, as they influence drug release and compatibility with biological systems.

The bioplatfroms exhibited rapid swelling within the initial 6 hours and reached a stabilized state after 24 hours. The swelling ratio was approximately 702.08% within one hour under  $37^{\circ}\text{C}$  conditions for S.gel, whereas for LS.gel, it reached 4959.22%, surpassing that of S.gel. After 8 hours, the swelling reached 897.89% for S.gel and 4959.22% for LS.gel with the significance difference of  $P < 0.05$  (Figure 3.6b). The findings align with a previous investigation that utilized alginate hydrogel incorporating hydrogen sulfide for wound healing. This earlier study noted that hydrogel holds high water content, which is advantageous for promoting moist wound healing (Nazarnezhada et al., 2020). Based on the findings, LS.gel demonstrates a notable capacity for absorbing significant volumes of fluid, presenting a considerable advantage for applications in skin tissue engineering. They effectively absorb wound exudate, maintain a moist wound area, and release their bioactive components, promoting the proliferation of fibroblasts and the migration of keratinocytes. These functions are essential for the thorough epithelialization of the wound.

Controlled biodegradation of hydrogels used in wound dressings is crucial for wound healing, as they gradually degrade alongside the healing process, minimizing the need for frequent dressing changes (Mndlovu et al., 2019). A slow degradation rate can impede the replacement of the wound dressing with new tissue formation. Conversely, if the degradation rate is excessively high, the wound site may become vacant, potentially halting the healing process (Bagher et al., 2020). Based on the degradation results in PBS (Fig. 3.6a), the LS. gel sample experienced a weight loss of approximately 24% within 3 days, whereas S. gel lost 84% within the same timeframe. The degradation rates escalated over the subsequent 3 days, with LS. gel at 43% and S. gel at 94.57%. The increased weight loss observed after the seventh day of testing suggests recurring degradation after 7 days which necessitates dose repetition after 7 days for *in vivo* studies.

The solubility of alginate in the water had a notable effect on the behaviour of the Secretome hydrogel. Unlike P-Alg, crosslinking resulted in decreased solubility and an accelerated degradation rate. Weight loss was observed after three days, and approximately 90% degradation was achieved within seven days, indicating a gradual degradation process over time. This underscores the achievement of controlled degradation through polymer crosslinking. When compared to other alginate-based hydrogels documented in the literature, one study involving an alginate/chitosan hydrogel containing hesperidin demonstrated a swelling percentage of  $344 \pm 12\%$  at 240 minutes after incubation, with 58% degradation after 14 days (Ishfaq et al., 2023). Another study utilizing Gelatin methacrylate MSC-secretome-laden hydrogel showed slow degradation behaviour over 10 days (Sears et al., 2021).

As a result, it is hypothesized that the water absorption and degradation properties of the secretome hydrogel may expedite wound healing compared to other known alginate-based hydrogels. Initially, the secretome hydrogel swiftly absorbs wound exudate, leading to rapid swelling and filling of the wound cavity. This process promotes essential hemostasis and establishes a controlled moisture environment conducive to wound healing. Secondly, it is proposed that the hydrogel's consistently regulated yet relatively constant rate of degradation will assist in various phases of wound healing, including the initiation of hemostasis and cellular infiltration, without hindering subsequent stages of tissue remodeling, which may span from four to twenty-four days (Fan et al., 2021). Additionally, this rapid swelling response followed by controlled degradation could potentially decrease the necessity for hydrogel application, alleviating concerns regarding the cost and frequency

of dressing changes. Furthermore, the high water uptake of the secretome hydrogel confirms its bioresorbability and biodegradability properties. Moreover, bioactive agents can be incorporated into the hydrogel networks and delivered to the wound site through sustained release, offering advantages over the topical administration of biomolecules.

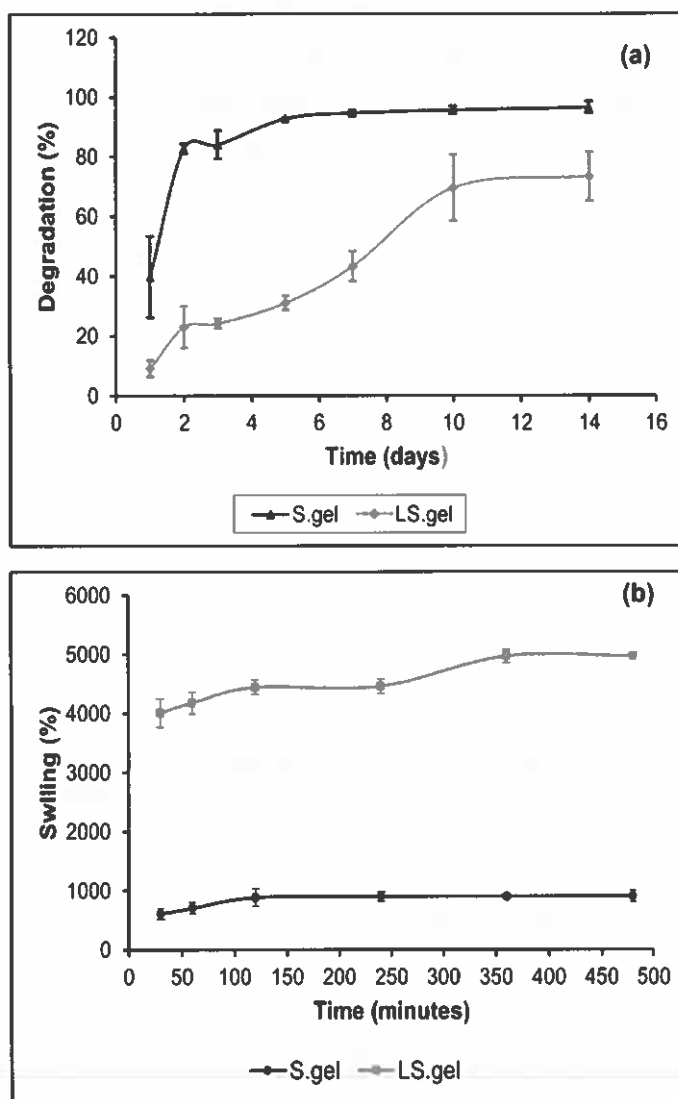


**Figure 3.6** (a) Biodegradation (weight loss) and (b) swelling behaviour of the S. gel and LS. gel in PBS (pH 6.5) solution at 37°C at 50 rpm.

### 3.3.11 Release profile of total secretome proteins

The administration of secretome continues to pose challenges due to its rapid clearance during wound healing, leading to a shorter half-life and diminished tissue retention. This could potentially decrease the bioactivity of secretome molecules at the wound site (Ajit and Ambika Gopalankutty, 2021). To address these challenges, incorporating secretome into alginate soy lecithin hydrogels offers a valuable solution. These hydrogels can be readily applied to the lesion site, effectively binding, protecting, and providing sustained delivery of the secretome components. The primary aim is to reduce the frequency of dressing changes while enhancing the therapeutic benefits. Additionally, the controlled release of bioactives, with minimal toxicity, offers a viable solution. Therefore, the objective of this study was to harness the gelling capacity of alginate to create a system capable of controlled release of bioactives. *In vitro* studies were conducted to assess the release profiles of the secretome proteins.

Quantitative evaluation of secretome release rates within LS. gel and S. gel was conducted based on total protein levels. In the early stages, both hydrogels exhibited a consistent release pattern. However, LS gel exhibited a notably higher release of proteins compared to S.gel with LS.gel releasing up to 90% within seven days whereas, the S.gel released less than 45% within seven days (Figure 3.7). The LS. gel specifically, showed burst release of 73% within 24 hrs followed by steady release up to 90% in seven days. The S. gel didn't show the burst release as that of LS.gel, S.gel displayed slow release for the first two days followed by an increase in release from 26 % to 42% from day 2 to day 3 respectively (Figure 3.7). S.gel showed a total release of 45% in seven days. The difference between the release profile of S.gel and LS.gel can be attributed to the point that the proteins in the LS.gel were stable due to solid form, whereas S.gel in a semi solid form which decreases stability of proteins compared to LS.gel. The difference at this time frame was statistically significant  $P < 0.05$ . The release profile is more linear in the first 3 days for both samples indicating a controlled release of secretome. The *in vitro* release results demonstrated that secretome hydrogels were effective in controlling the release of total protein over 7 days. The findings of the study are consistent with the secretome release profile for another study, which further quantified total and specific proteins known to accelerate wound healing (Kwon et al., 2023).

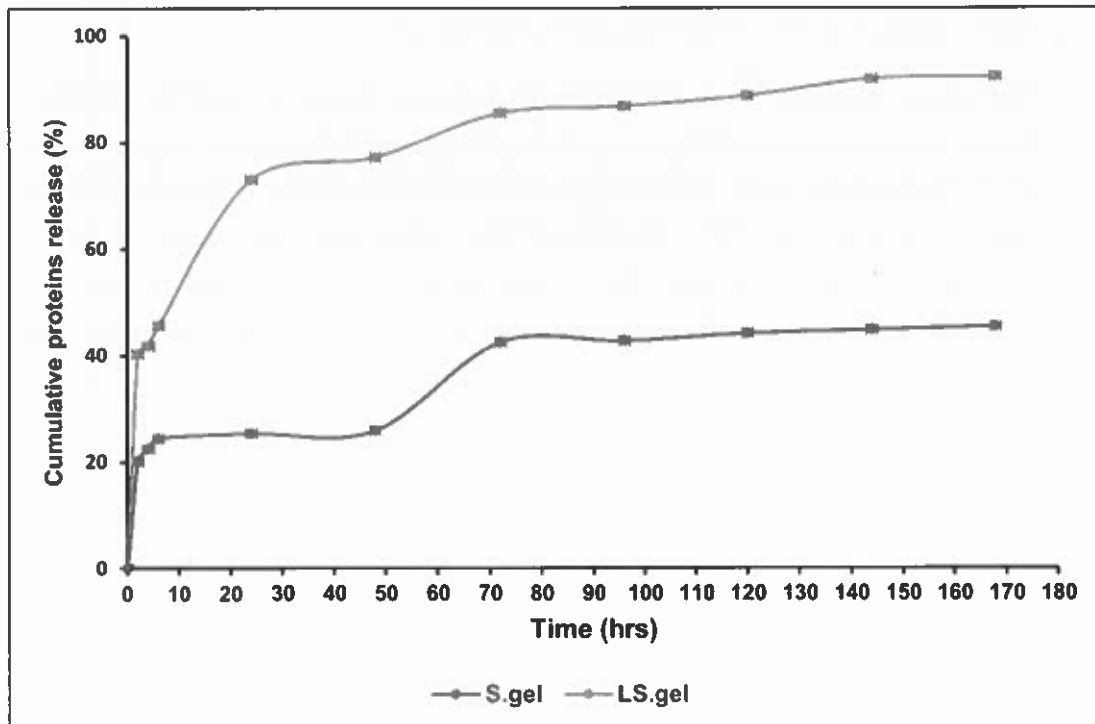


**Figure 3.7** Protein release profiles. Protein content released from LS. gel and S. gel into the supernatant was estimated using a BCA protein assay kit.

The literature reveals studies of secretome protein release, in one research, a nanocomposite hydrogel (NP-H) was developed, incorporating poly-L-lactide nanoparticles (NPs) within a gelatin/hyaluronic acid (Gel/HA) hydrogel, serving as a carrier for MSC-CM. Hydrogels facilitate protein delivery through a diffusion-controlled mechanism, triggered by the swelling of the polymer matrix. The release rate of proteins in ScCM-NP-H is notably higher until day 6 (Shoma Suresh et al., 2020). Another study demonstrates an initial burst release of the secretome from a hydrogel designed for spinal cord injury within the first day, followed by a sustained release profile, with cumulative release reaching up to 70% by day 10 (Silva et al., 2023).

Hydrogels are widely recognized for their capability to protect the secretome from degradation by regulating both its dosage and diffusion. A key attribute of hydrogels is to minimize the exposure of the secretome to external factors that may compromise its integrity and stability. Consequently, the release profile demonstrates a controlled release of the secretome, which is highly advantageous for clinical applications.

procedure of cells [49]. ADSC secretome produced by the maturation process could be helpful in the mass-production of secreted factors and account for a readily available supply of bioactive factors [40]. Secretome therapy's cost-effectiveness can overcome the high cost of cellular therapy. The reduction of cell culture and immediate secretome therapies can be applied to manage acute pathological conditions such as military trauma, cerebral ischemia, and myocardial infarction, and modification of the biological product can take place to achieve a cell-specific effect [19,50].

Based on the advantages listed above, secretome has the potential to overcome the ethical problems associated with cellular transplantation. In addition to that, complications related to the survival and inaccurate differentiation of cells in the host tissue are reduced. The overall capability of cell therapy can be maintained by paracrine activity. Secretome-based therapies provide advantages such as availability, scalability, and longer shelf life [51]. In general, both cell-based therapy and secretome have advantages and disadvantages. However, the prolongation of the survival of transplanted cells and knowing how to predict decreased cell viability and biological functions during *in vitro* culture are the current challenges of cell-based therapies [40]. Accordingly, several strategies have been developed to improve the therapeutic efficacy of stem cells and secretome, such as genetic modification, preconditioning, and tissue engineering [40].

### 2.3. The Role of the Secretome in Different Stages of Wound Healing

Skin wound healing is a choreographed and closely regulated process comprised of inflammation, proliferation, matrix formation, and remodeling phases [52]. After skin injury, wound healing can be coordinated normally by keratinocytes, dermal fibroblasts, and immune cells [26,44]. However, secretome-based therapy has the potential to contribute to the acceleration of the wound-healing process. This is due to its components that promote anti-inflammatory factors, cell mitogenesis, re-epithelization, proliferation, and tissue remodeling, and induce neovascularization, leading to overall wound healing, particularly wound closure [42].

The secretome components relevant to various wound-healing stages include growth factors (PDGF, IGF-1, bFGF, FGF, granulocyte-colony stimulating factor (G-CSF), GM-CSF, HGF, PGE2, TGF- $\beta$ , VEGF, and KGF), inflammatory proteins (IL-1, IL-8, IL-10, IL-6, tumor necrosis factor- $\alpha$  (TNF), leukemia inhibitory factor (LIF), IL-11, MCP-1, PGE2, IL-9, and IL-13), ECM proteins (MMP-1, MMP-2, MMP-3, MMP-7, TIMP-1, TIMP-2, ICAM, elastin, collagens, decorin, and laminin), and angiogenic factors (VEGF, ANG-1, ANG-2, PDGF, MCP-1, TGF- $\beta$ 1, FGF, EGF, CXCL5, MMPs, and TGF- $\alpha$ ). The secretome effect on the inflammatory phase has been assessed by Lotfinia et al.; the report indicated the use of mesenchymal stem-cell-secretome to treat peripheral blood mononuclear cells *in vitro* [53]. The study found that pro-inflammatory cytokine production was reduced, while anti-inflammatory cytokine production increased [53]. Another study on mice excisional wounds injected with bone-marrow-derived stem cell secretome resulted in the promotion of wound healing by reduced inflammation mediated by macrophage polymerization [22].

A study by Park et al. indicated that secretome includes bioactive factors such as EGF, bFGF, and HGF, which are known to activate the PI3K/ Akt and/or FAK/ ERK1/2 signaling pathway [42]. This pathway is involved in the migration and proliferation of dermal cellular components during tissue repair. The bioactive and the activated pathway are believed to improve the proliferative and migratory capabilities of dermal fibroblasts, keratinocytes, and endothelial cells, among other biological components of the dermis [42].

In the proliferation phase of wound healing, soluble substances of the secretome can enhance fibroblast migration and the secretion of ECM components, particularly collagens I and III, resulting in wound-healing acceleration within the wound bed [42]. During the remodeling phase, the total collagen content increases, leading to wound contraction. This effect has been confirmed in a study that applied a human gingival fibroblast condition medium to treat wounds [43]. Endothelial cells treated with human multipotent adult pro-

genitor cell-conditioned medium MAPC-CM also formed more vessel-like tubes [54]. The secretome accelerates wound healing by promoting angiogenesis. This has been demonstrated by a study carried out on wounds treated with MAPC-CM. The outcome of the study was an increasing number of endothelial cells and blood vessels in the wound bed due to increased VEGF in the CM, which accounts for a proangiogenic factor stimulating the vessel formation of endothelial cells [54]. Secretome components can accelerate wound healing by promoting target cell proliferation, differentiation, vascularization, and wound remodeling.

### 3. Secretome Applications in Wound Healing

Stem cell secretome or condition medium shows good outcomes in accelerating wound closure and promoting skin regeneration in wound healing. This evidence has been outlined in many studies due to secreted growth factors and cytokines and their potential for wound healing [22]. Many physiological processes relevant to wound healing are mediated by stem-cell-mediated paracrine and autocrine cell signaling pathways. Furthermore, the secretome is composed of several constituents with extensive regenerative potential for wound tissue.

An analysis of the human adipose-derived stem cell secretome revealed a high level of various growth factors, as mentioned in Table 1. These biological factors play a crucial role in wound healing and tissue repair as they can promote skin tissue regeneration and modulate the immune response [55]. These secreted factors can act directly on normal wound-healing stages to promote re-epithelialization and angiogenesis and indirectly by immunomodulatory capacities. These factors can stimulate existing skin cells' proliferative and migratory abilities through PI3K/Akt or FAK-ERK1/2, signaling an acceleration of wound healing [42]. The mechanisms of mesenchymal stem cell secretome in wound healing are illustrated in Figure 2. Therefore, extensive studies take place in this area to evaluate the different mechanisms for wound repair. Consequently, the focus is on the secretome of stem cells as a novel tool for treating various types of wounds. Current applications of the secretome from the various MSC sources, and their involvement in wound closure acceleration, are summarized in Table 1.

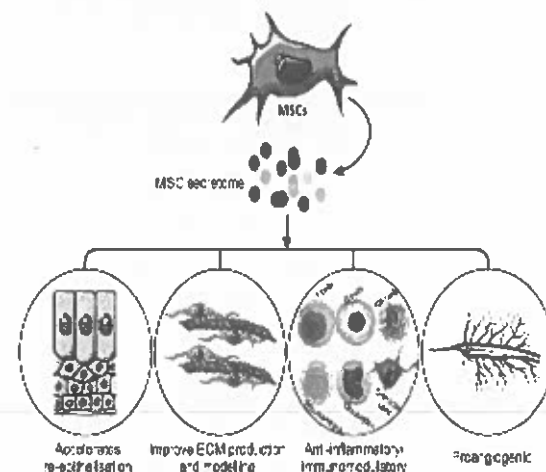


Figure 2. Mechanisms of mesenchymal stem cells secretome on wound healing. Image reproduced under an open access license from Ahangar et al. [22], Copyright 2020, © authors.

Table 1. The therapeutic outcomes of MSC secretome (MSC-S) in wound healing.

| Stem Cell Type                 | Type of Wound and Model   | Secretome Component                            | In Vitro Outcome  | In Vivo Outcome   | Ref. |
|--------------------------------|---|--|---|---|------|
| Human (hMSC) from SCD patients | Murine excisional wound/endothelial cells in a mouse model                              | VEGF, IL8, MCP-1, and ANG                      | Using HUVECs in a 3-dimensional in vitro model demonstrates proliferation and migration in the presence of hypoxic CM that supports angiogenesis.<br>Rat dermal fibroblast cell line was treated with secretome as revealed viability, proliferation ability, and higher migration capability, which represent better-wound healing. Macrophages were treated with secretome and it reduction of pro-inflammatory cytokines, including IL-6, TNF- $\alpha$ , and MCP-1. | hMSC condition media exerts high trophic factors that promote angiogenesis and skin regeneration with accelerated wound healing.  | [56] |
| ADMSC                          | Full-thickness skin excision on SD rats   | VEGF   |   | Rapid wound closure enhanced fibroblast proliferation and migration. Moreover, the higher expression of VEGF promotes angiogenesis, which accelerates wound healing potential.  | [9]  |
| MUCSCs                         | Corneal epithelial cells/corneal ulcer on SD rats                                       | TIMP-1, TIMP-2, FGF, and HGF                   | Enhanced epithelial wound healing, rapid regeneration, and the contribution of the corneal surface.<br>The secretome itself promotes proliferation, migration, and tube formation of endothelial cells, reflected in enhanced proangiogenic properties. Additionally, the secretome miR-146a has immunomodulation effect that can potentially promote wound healing.  | Bactericidal effect on corneal contact lenses (CLs) infected with <i>Escherichia coli</i> and <i>Staphylococcus epidermidis</i> .   | [43] |
| hASC transfected with miR-146a | In vitro model using HUVECs   | miR-146a, UPA, (DPP IV), HGF, RGF-1, and FGF 2 |   | In vivo outcome was not studied.  | [57] |
| ADSCs                          | 6-mm diameter biopsy punch piercing in mice dorsal skin of male BALB/c-male mice        | TGF- $\beta$ 1 and VEGF                        | Increased transdermal delivery of secretome proteins was expressed in an ex vivo porcine skin using iontophoresis as a permeation enhancer.   | Acceleration of wound closure with reduced scars, accompanied by rapid re-epithelialization, proliferation, increased tissue remodeling rate, and high vascularization.<br>Speeding up of wound closure due to a decrease in myofibroblasts' positive expression of $\alpha$ -SMA—rather than contraction enhanced re-epithelialization after 14 days of treatment, and overall fetal-like wound healing without scarring as a result of high expression of type III collagen accomplished by transformation of dermal fibroblasts into fetal-like fibroblasts rather than myelo fibroblasts. | [67] |
| HA FS                          | The full-thickness cutaneous excisional wound created on the dorsal skin of BALB/c mice | VEGF   | In vitro effect was not tested in this study.   |   | [58] |

Table 1. Cont.

| Stem Cell Type                              | Type of Wound and Model   | Secretome Component   | In Vitro Outcome  | In Vivo Outcome   | Ref. |
|---|---|---|---|---|------|
| HGFs  | Dorsal excisional wounds of female BALB/c mice  | IL-6, arginase, MCP-1, and IL-8 are examples of cytokines. Growth factors and ECM proteins such as HGF, FGF-2, VEGF, Arg-1, Arg-2, MMP-2, MMP-9, and TIMP-1 are also present. | Human keratinocytes and foreskin fibroblasts cells were used in vitro to evaluate a higher proliferation and migration rate. There was also an increase in capillary density, indicating enhanced angiogenesis. Additionally, increased collagen deposition is reflected in higher wound contraction without reducing fibrosis. | Wound closure acceleration with reduced inflammation, promotion of angiogenesis, and higher collagen deposition. Higher re-epithelization.  | [63] |
| Human bone marrow MSC                       | Full-skin thickness incision wound on the dorsal part of diabetic Wistar male rats (chronic diabetic wound) | bFGF and BGF expression   | Human dermal fibroblasts cultured in a high glucose concentration medium resulted in an in vitro advanced wound closure due to rapid fibroblast migration, higher proliferation, and increased bFGF gene expression.  | Acceleration of wound healing in terms of reduction of inflammation, increased vascularization, granulation tissue formation and enhanced, collagen deposition, and some trophic factor genes expression. | [59] |
| (W)-MSCs                                    | Radiation-induced skin injury on Female Sprague-Dawley (SD) rats  | ————  | (HUVECs) growth rate and proliferation rate are increased. Enhanced number of blood vessels due to increased $\alpha$ -SMA expression.  | Acceleration of wound closure enhances the quality of wound healing by promoting cell proliferation, sebaceous gland cell-like regeneration, and angiogenesis.  | [60] |
| Gamma irradiation to induce apoptosis PBMCs | Burn wounds of 40 cm <sup>2</sup> were created on the dorsum of the female Dan Bred pigs                    | IL-8 and VEGF   | Histology studies carried out by using wound biopsies.  | Improved epidermal regeneration and differentiation, a better wound quality without scarring, and increased numbers of CD31+ and $\alpha$ SMA+ cells as markers for angiogenesis.                         | [61] |
| MSC from fetal umbilical cord               | Burn wound on the dorsal area of the White rat (Rattus Norvegicus)  | bFGF  | Histological analysis of skin tissues using M and H stains  | Acceleration of wound closure, a most significant number of fibroblasts, high density of collagen fibers, and significant number of blood vessels.  | [62] |
| Warton Jelly MSC                            | Burns on a 67-year-old woman's left hand due to hot water exposure.   | ————  | ————  | Three weeks of treatment with 10% secretome gel acceleration wound healing without scarring.  | [63] |
| UMSC-Exos                                   | Full-thickness skin wound on ICR mice and nude mice.  | Exosome enriched microRNA represented as (miR-21, -23a, -125b and -145)   | Fibroblasts cells treated with recombinant YGF-6 protein upon exposure to CM, leading to $\alpha$ -SMA suppression.   | Wound healing promotion due to suppression of myofibroblast and scar formation through inhibition of transforming growth factor- $\beta$ 2/SMAD2 pathway.   | [64] |

#### 4. Secretome Delivery in Wound Healing

Biomaterials play an important role in tissue regeneration, which comprises delivering bioactives and provides structural support for endogenous cell invasion. For biomaterials to be applied, they must fulfill the following criteria involving biocompatibility, degradability, and suitable mechanical properties. Biomaterials are classified into three categories: naturally derived, synthetic, and chemically modified polymers. Natural biomaterials shown in this field comprise alginate, collagen, hyaluronan, and decellularized extracellular matrix (ECM). Biomaterial scaffolds made of synthetic polymers or ceramics such as polylactide-co-glycolide (PLGA) or beta-tricalcium phosphate ( $\beta$ -TCP) are extensively employed, with gelatin methacrylate (GelMA) being the natural material with chemical modifications [65].

Synthetic materials offer multiple advantages, such as cost, supply, and batch-to-batch homogeneity. However, they lack native tissue shape and structure. Hybrid hydrogels combining natural and synthetic materials have also been employed to attain the biological benefits of natural materials while attaining the benefits of tunable synthetic materials [66]. Biomaterials may be able to overcome the inadequate tissue retention of bolus EV and MSC-CM injections by offering a controlled release platform for healing tissues.

Biomaterials, which include scaffolds, meshes, matrices, hydrogels, and substrates, have completely transformed the way drugs are delivered and used. Some of the most frequently employed scaffolds are collagen-derived matrices, silk-based meshes/matrices, dextran hydrogels, and electrospun nanofiber matrices such as poly-L-lactic acid (PLLA) [67,68]. However, electrospun nanofiber matrices are recommended in biological applications. These scaffolds provide a three-dimensional (3D) structure that is similar to that of the extracellular matrix (ECM)-like nano-architecture [69]. These matrices have a similar tensile strength to skin, making them a suitable candidate for skin wound healing.

Biomedical hydrogels, which have a comparable structure to the natural ECM, have been highlighted as promising biomaterials for delivering therapeutics and cell components to wounds. The following characteristics should be present in an ideal wound-healing hydrogel scaffold: suitable mechanical qualities, good water retention, anti-infection capacity, injectable capacity, and excellent cell biocompatibility. Exosome-based administration via hydrogel, on the other hand, is likely to improve angiogenesis and tissue regeneration during wound healing [70]. Table 2 mentions some examples of biomaterials and their application in wound healing.

Table 2. Biomaterials and their application in wound healing.

| Polymer  | Secretome Source  | Bioactive Molecules           | Type of Hydrogel                 | Biomedical Apps   | References |
|--|---|-------------------------------|----------------------------------|---|------------|
| Polyisocyanate (PIC)   | Human adipose-derived stem cells (hASCs)                              | IL-10                         | Gel                              | Fibroblast wound healing assay or artificial wound                        | [71]       |
| Carrageenan/ poly(vinyl alcohol)   | SD-MSCs   | VEGF                          | Hydrogel                         | full-thickness excisional wounds  | [31]       |
| Polycaprolactone /gelatin  | Bone marrow-derived mononuclear cells                                 | ————                          | Electrospun scaffold             | Diabetic wounds   | [69]       |
| Hyaluronic acid (HA) and chondroitin sulfate (CS) Methacrylate anhydride.                        | Bone-marrow-derived human mesenchymal stem cells (hMSC)               | ————                          | Viacrielastic gel                | Corneal wound   | [72]       |
| Hyaluronic acid, N-(2-aminoethyl)-4-(4-(hydroxymethyl)-2-methoxy-5-nitrophenoxy)-butanamide (NH) | Amnon-derived conditioned medium (AM-CM)                              | VEGF and TGF- $\beta$ 1       | In situ gel                      | In vivo diabetic wound  | [50]       |
| chitosan/collagen/ $\beta$ -glycerophosphate   | Human umbilical cord mesenchymal stem cell                            | ————                          | Thermosensitive hydrogel         | In vivo burn wound  | [51,73]    |
| Pluronic F-127   | human umbilical cord-derived MSC(hUCMSC)-derived exosomes             | VEGF/(TGF- $\beta$ -1)        | A thermosensitive hydrogel       | In vivo diabetic wound  | [74]       |
| Pluronic F127 /oxidative hyaluronic acid/( $\epsilon$ -poly-L-lysine, EPL)                       | Adipose mesenchymal stem cells (AMSCs)-derived exosomes               | ————                          | Hydrogel                         | Diabetic full-thickness cutaneous wounds                                  | [70]       |
| Polycaprolactone /gelatin  | Bone-marrow-derived human mesenchymal stem cells                      | ————                          | Electrospun fiber                | In vitro corneal fibroblast cells and rabbit corneal organ culture system | [75]       |
| Chitosan   | Human endometrial stem cell (hESC)-derived exosome                    | ————                          | Hydrogel                         | full-thickness cutaneous wounds   | [76]       |
| Carboxymethyl chitosan/polyoxamer 407  | Human umbilical cord-mesenchymal stem cells (hUCSCs)-derived exosomes | ————                          | Thermo and pH-sensitive hydrogel | Rat cutaneous wound   | [77]       |
| Sodium Alginate/Sodium hyaluronate/PBC   | Human BM-MSCs   | VEGF and FGF                  | Hybrid gel                       | Tissue regeneration after surgery   | [78]       |
| Sodium alginate  | Periphral blood mononuclear cells (PBMCs)                             | CD31+ cells                   | NU-GEL™ Hydrogel                 | Burn wound  | [61]       |
| Chitosan/ silk fibroin   | Cingival mesenchymal stem cells (CtMSCs) derived exosomes             | Exosomal markers CD9 and CD81 | Sponge                           | Diabetic rat cutaneous wound  | [79]       |

### 5. Structural Formulation Using Biomaterials with Secretome for Wound-Healing Applications

Polymer-based biomaterials are widely used in tissue engineering. They can mediate tissue engineering through their *in vitro* structural support to help cell–cell interaction and growth factors. They can aid in *in vivo* transplantation of the regenerated tissue to integrate structurally and functionally with the system [80]. Hydrogels, which are three-dimensional hydrophilic polymers, have been used as a bioactive scaffold material for drug delivery and cell encapsulation [80]. However, recent studies have identified that biocompatible hydrogels as carriers of MSC CM and MSC exosomes can maintain the bioactive molecules of the CM at the wound site [81]. This is an attempt to overcome cell-based therapy-associated risks in terms of lowering processing time and local storage conditions.

MSC-secreted factors, which include extracellular vesicles and soluble factors, contribute mainly to their therapeutic benefit. However, the biomaterials can be combined with those factors, offering a delivery system to enhance the secretome retention rate and accelerate healing efficacy. This review highlights the use of biomaterials with secretomes in wound healing, providing insight into different examples applied *in vitro* and *in vivo*. Figure 3 below shows how secretome can be extracted from MSC and the CM and exosome mixed with polymers to develop a biomedical system that can be applied to treat *in vivo* wounds.

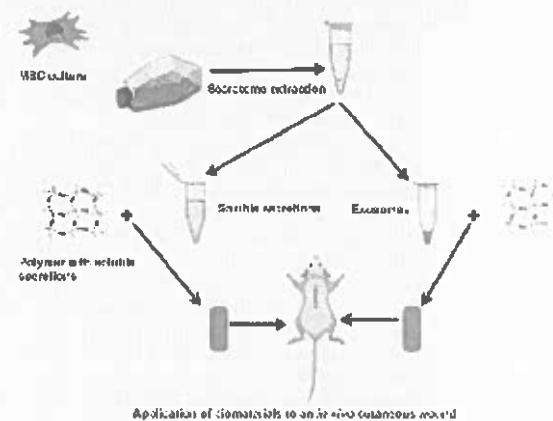


Figure 3. Schematic representation of MSC secretome extraction and exosome separation and combination with polymers for *in vivo* wound application.

#### 5.1. MSC Soluble Secretions and Their Combination with Biomaterials for Application in Different Wounds

Secretomes collected from *in vitro* culturing of MSC is also known as MSC-conditioned media (MSC-CM). The analysis showed the composition of the soluble factors, which are made up of cytokines, chemokines, growth factors, and hormones, with immunomodulatory, angiogenic, and anti-apoptotic functions [82]. The second part of secretion is termed extracellular vesicle secretions loaded with specific miRNA involved in both diagnosis and treatment [83]. The advantages of the *in vitro* applications of MSC-CM include cell proliferation and migration enhancement [84,85], the promotion of angiogenesis [85,86], and revealing anti-apoptotic and anti-inflammatory effects [84,87,88]. Furthermore, *in vivo* MSC-CM has demonstrated healing potentials in different wound types, which involve cutaneous wounds [89], burn wounds [73], and diabetic chronic wounds [59].

MSC CM can be administered by botus injection, resulting in a shorter half-life and poor tissue retention. A combination of MSC CM with biomaterials presented a controlled

release platform for healing tissues to overcome these adverse problems [65]. A recent study by Vasily et al. demonstrated the use of placental multipotent mesenchymal stromal cell (MMSC) secretome-loaded in chitosan hydrogel (MSC-Ch-gel) for infected burn wounds [90]. The method used in developing the MSC-CH gel involved the addition of chitosan solution to CM. The study revealed that MSC-CH-gel had antimicrobial activity along with high anti-inflammatory abilities [90]. The high level of anti-inflammatory mediators was released upon the proteomic analysis of secretome besides proteins crucial for the different stages of wound healing. Furthermore, MSC-CH gel promoted skin tissue repair, which was observed after histological examination regarding higher vascularization and angiogenesis [90].

Another study conducted by HonorataK et al. evaluated the effect of human adipose tissue mesenchymal stem cell (HATMSC2) secretome-loaded hydrogel on chronic wounds [90]. The collagen hydrogel was prepared by adding the concentrated PBS to the type I collagen solution and then gently mixed. HATMSC supernatant was added to the collagen mixture before adding the crosslinker. The last step was adding 10K 4-arm Succinimidyl Glutarate PEG crosslinker followed by gentle mixing; then, the formed hydrogel was pipetted into Petri dishes and incubated at 37 °C for 1 h to allow for complete crosslinking [90]. The developed hydrogel was tested in an in vitro wound model using different cells, including endothelial, keratinocytes, and fibroblasts, during a 3-days culture. The results showed highly released interleukin-8 and macrophage chemoattractant protein-1 proteins from endothelial cells [91]. Additionally, pro-angiogenic activity was assessed using in vitro tube formation assay on human skin endothelial cells and confirmed by the expression of pro-angiogenic miRNAs, especially miR126, which shows the highest expression and antimicrobial activity against *Staphylococcus aureus* MRSA, and *Pseudomonas aeruginosa* was also confirmed [91].

A recent study developed by Victoria et al. focused on developing mesenchymal stem cell (MSC)-conditioned media (CM) loaded in hydrogel and its application in an in vitro hyperglycemic human dermal fibroblast to investigate the wound healing potential [92]. The components of the hydrogel were GelMA-PEGDA, loaded with MSC-CM, which demonstrated higher proliferation of the hyperglycemic fibroblast due to the combined effects of matrix properties together with the prolonged release of MSC-secreted bioactive molecules. Hence, it was potentially beneficial in diabetic chronic wounds [92].

A study by Anny et al. investigated the use of biocompatible polymers as transporters to preserve the bioactive molecules of CM at the wound site by combining MSC secretome with carrageenan and polyvinyl alcohol [31]. After preparing each hydrogel, the conditioned media embedded in each of it was polymerized, then it was derided and tested in in vitro human umbilical vein endothelial cells for angiogenic activity. Additionally, in in vivo application in mice, the cutaneous wound was carried, which showed the healing potential of both hydrogels' impeded CM based on the proangiogenic properties of the secretome [31].

Another study applied BM-MSC secretome in vitro to primary cultured human corneal epithelial cells and an in vivo mouse model after both mechanical and alkaline corneal burn, hyaluronic acid (HA), and chondroitin sulfate (CS) gel were used as carriers (they were compared with secretome alone). The secretome was used in a lyophilized form to impart long stability and consistency to the different products. The study revealed secretome HA/CS gel accelerates epithelial wound closure after both injuries and can reduce neovascularization, scar formation, and hemorrhage after chemical injury [93]. Yiqing et al. developed a photo-crosslinking adhesive in situ-formed hyaluronic acid hydrogel grafted with the methacrylic anhydride and N-(2-aminoethyl)-4-[4-(hydroxymethyl)-2-methoxy-5-nitrophenoxy]-butanamide (NB) groups to encapsulate a lyophilized amnion-derived conditioned medium (AM-CM) [50]. The hydrogel displayed strong tissue adhesion, excellent mechanical properties, high elasticity, favorable biocompatibility, and prolonged AM-CM release. This was reflected in in vitro and in vivo accelerated diabetic wound healing resulting from the regulation of macrophage polarization and the promotion of angiogenesis [50]. Another study by Gabriella et al. developed a viscoelastic gel composed of hyaluronic

acid (HA) and chondroitin sulfate (CS) to deliver lyophilized secretome from human bone-marrow-derived mesenchymal stem cells for the treatment of mechanical and chemical corneal injuries [93]. The *in vitro* and *in vivo* results accelerated epithelial wound closure and reduced corneal neovascularization, scar formation, and hemorrhage [93]. Vasily et al. developed placental multipotent mesenchymal stromal cell (MIMSC) secretome-based chitosan hydrogel (MSC-Ch-gel) to treat infected burn wounds in rat [90]. Accelerated wound healing, tissue regeneration, reduced inflammation, improved re-epithelialization, and the encouragement of the development of well-vascularized granulation tissue were the outcomes [90]. The secretome produced by human fetal mesenchymal stem cells (hMSC) in diabetic wounds was investigated by Bin Wang et al. [94]. The poly lactic-co-glycolic acid (PLGA)-encapsulating lyophilized hMSC exhibited improved wound healing by encouraging vascularization and reducing inflammation in the cutaneous wound bed [94]. Chen et al. developed adipose-derived stem-cells-conditioned medium loaded in electrospun micro-nano fibers using poly lactic acid (PLA), which imparted protection and controlled release properties [95]. The *in vitro* and *in vivo* outcomes of the study were wound-healing acceleration and tissue regeneration [95].

#### 5.2. MSC EVs and Their Combination with Biomaterials for Application in Different Wounds

Extracellular vesicles (EV) are nano or micro-sized vesicles that constitute the insoluble part of the secretome. They play a key role in cell-to-cell communication by transporting cargo directly into the cell or activating specified cell surface receptors. They are important in tissue repair and regeneration, disease detection, and oncology because they can transport membrane and cytosolic proteins, lipids, and RNAs [16,96]. Exosomes, the nano-sized vesicles, have become popular for application in cellular regenerative medicine, especially in wound healing. They organize cell-to-cell communication by carrying mRNA, miRNA, and proteins to target cells [70,97]. The following studies are examples demonstrating the combination of EV with biomaterials for wound healing. A study carried out by SHI-CONG TAO et al. describes the use of exosomes from microRNA-126-3p overexpressing synovium MSC mixed with chitosan hydrogel for cutaneous wound healing [96]. After the isolation and characterization of SMSC, the miRNA-126-3p lentiviral vector transfected them, then the exosomes were isolated and identified by specific procedures. After that, chitosan hydrogel-loaded exosome was prepared and tested *in vitro* and *in vivo*, which resulted in an *in vitro* promotion of proliferation and migration in human dermal microvascular endothelial cells (HMVEC-1 cells) and human fibroblasts (FBs) [96]. However, a faster healing rate was reflected in diabetic wounded rats treated with CS-SMSC-126-Exos, which was reflected by epithelialization, granulation tissue formation, collagen deposition, and vascularization [96].

Another study demonstrated the preparation of chitosan/silk hydrogel sponge loaded with exosome derived from human gingival MSC and application to diabetic rat wounds. After the polymers dissolved, they stirred mechanically for 30 min. The hydrogel was prepared by the freeze-drying method and lyophilized to produce a sponge to which the collected exosomes were added [96]. Then, the hydrogel was applied to the wound area of the diabetic rats and accelerated wound healing. This is a noninvasive delivery system compared to the direct injection of exosomes, which can cause infection. The histological results showed enhanced re-epithelialization, collagen depositing, neovascularization, and neuronal ingrowth [96].

An adipose-derived MSCs exosome loaded in alginate-based hydrogel has been applied to a full-thickness wound in a rat model. The study was performed by the isolation of ADSCs first, followed by exosome isolation and characterization; after that, the alginate hydrogel was prepared from alginates solution. The exosome was added and finally crosslinked with calcium chloride. The hydrogel was applied to assess its healing potential in a rat model. The exo-loaded hydrogel provided a novel delivery platform that accelerated wound closure by the enhancement of fibroblast migration, collagen synthesis, and vascularization [98]. A study done by Qijun Li et al. illustrated the dual-sensitive

hydrogel comprised of poloxamer 407, and carboxymethyl chitosan encapsulates exosomes derived from human umbilical cord mesenchymal stem cells (hUCMSCs). The polymers were crosslinked with genipin, and the exosome suspension was mixed into the solution to form the hydrogel that exhibited sustained release behavior upon application to the cutaneous wound in a rat model, resulting in an enhancement of wound closure and tissue regeneration.

In addition to that, the formation of skin appendages and the inhibition of inflammatory reactions [77] occurred. Wang et al. fabricated self-healing hydrogel from methylcellulose and chitosan via Schiff base reactions [99]. The hydrogel was loaded with exosomes extracted from placental mesenchymal stem cells. The hydrogel-loaded exosome exhibited accelerated wound healing, which was reflected in rapid wound contraction, new tissue formation, vascularization, and hair follicle and gland appearance when applied to the full-thickness wound in diabetic mice (*Lepr<sup>db</sup>*). Thus, wound healing promotion took advantage of an injectable hydrogel and the biocompatibility of the polymers [99]. Liu et al. explored the enhanced retention of adipose stem cell-derived exosome when combined with HA in the acute cutaneous wounds of nude mice [100]. The outcomes demonstrated that ASC-Exo+HA could significantly enhanced fibroblast activity, re-epithelialization, and vascularization in wound healing [100]. Figure 4 represents the hydrogel formation method using exosome-loaded polymers as one of the examples of the fabrication approach.

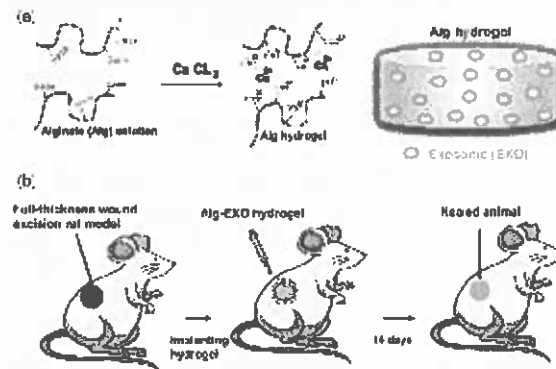


**Figure 4.** Schematic illustration of the hydrogel crosslinking and full-thickness wound excision mouse model used to evaluate the wound healing properties of alginate hydrogel-incorporated exosome (Alg-EXO). (a) Alginate solution loaded with adipose-derived stem cells (ADSCs)-derived EXOs cross-linked via ionic crosslinking. (b) Creation of a full-thickness wound excision rat model, and the transplantation of hydrogel into the injury area. Image reproduced with permission from Shafei et al. [98]. Copyright 2019, John Wiley and Sons.

### 5.3. Secretome in 3D Bioprinting

Three-dimensional printing technology can be used for wound healing and skin engineering through the application of bioprintable materials known as bioinks. These bioinks must have good printability, mechanical stability, biocompatibility, biodegradability, non-toxicity, high availability, and high shape fidelity [101]. The 3D printing technology, rather than conventional approaches, can generate scaffolds that can resemble the complex ECM structures and provide a microenvironment for cell attachment, proliferation, distribution, and differentiation, with the capability to create functional tissue [102]. 3D technology can be used to carefully distribute cells, biological components, and growth factors into complex 3D bioscaffolds to construct tissue engineering structures that mimic biological ones. Leila et al. developed a collagen/alginate 3D bioprinted gel scaffold loaded with adipose-derived stem cells (ADSCs) for burn-wound healing, which resulted

in complete epithelization and accelerated healing [103]. A study in bone regeneration used a 3D scaffold constructed from PCL and alginate hydrogel that contains hyaluronate (freeze-dried MSC secretome) for the controlled release of secretome to promote *in vitro* osteogenic differentiation [104]. Another study on 3D electrospun fiber scaffold, fabricated with polycaprolactone (PCL) and gelatin, was used as a cell culture medium with harvest (cell-free) MSC secretome, as well as continuous delivery from MSCs. The secretome was harvested and used to evaluate *in vitro* wound healing on corneal fibroblasts and subsequently explored a chemical burn on rabbit corneas employing an organ culture model. The outcome was epithelial layer recovery [105]. The effectiveness of 3D scaffold-based exosome treatment for skin regeneration has been examined in several research. Wang et al. verified that a biocompatible 3D porous self-healing methylcellulose-chitosan hydrogel, supplied with placental MSC-derived exosomes, promoted wound healing by cooperatively promoting angiogenesis and inhibiting apoptosis [106]. Therefore, using secretome 3D printing technology for wound healing is a promising area for further research.

## 6. Conclusions

Comprehensive studies have been done on the wound healing capability of MSC. They emphasized that their therapeutic benefit was mediated by paracrine secretions, including soluble factors and extracellular vesicle components collectively named secretome. They explore healing potential through the inhibition of apoptosis and inflammation, fibrosis, and angiogenesis. The secretome components can be delivered to the wound site when combined with biomaterials, which show better retention. Their effects proven *in vitro* and *in vivo* demonstrate valuable results in accelerating wound healing and promoting skin regeneration due to their tissue retention. To translate the experience of secretome to clinical situations, it is necessary to further understand its production procedures, which will reveal the way to enhance the production, advancement of isolation, and standardization methods for purification and characterization.

## 7. Future Prospective

Secretome-based therapeutics have become a potentially effective replacement for cell-based therapies. The secretome is at the vanguard of next-generation tissue and organ regenerative engineering applications due to its capacity to be produced, stored, and used as an off-the-shelf, ready-to-use product with minimal safety issues while maintaining the therapeutic benefits of stem cells. Advancing secretome-based therapeutics and determining their safety and efficacy will require the creation and evolution of methodologies and technology in MSC secretome culture, as well as a comprehensive grasp of secretome's components. Biomaterials have also been investigated as a supplement to control secretome production and as delivery systems. To accomplish clinical translation, the expansion of MSCs should be carried out under defined GMP culture conditions that are reproducible, scalable, and well-controlled, with the intention of limiting heterogeneity and enhancing the predictability of secretome-derived products in terms of composition and function.

**Author Contributions:** Conceptualization, H.M., P.K. and Y.E.C.; investigation, R.I., S.A.A., H.M. and P.K.; resources, Y.E.C.; writing—original draft preparation, R.I.; writing—review and editing, H.M., S.A.A., P.K. and Y.E.C.; supervision, H.M., P.K. and Y.E.C.; project administration, Y.E.C.; and funding acquisition, Y.E.C. All authors have read and agreed to the published version of the manuscript.

**Funding:** This work was supported by the National Research Foundation of South Africa.

**Institutional Review Board Statement:** Not applicable.

**Informed Consent Statement:** Not applicable.

**Data Availability Statement:** Not applicable.

**Conflicts of Interest:** The authors declare no conflict of interest.

### Abbreviations

|   |                  |
|---|------------------|
| Activated phosphatidylinositol 3 kinase/Protein kinase    | PI3K/Akt         |
| Adipose tissue-derived stem cells                         | ADSCs            |
| Alginate hydrogel-incorporated exosome                    | Alg-EXO          |
| Angiopoietin  | Ang              |
| Basic fibroblast growth factor                            | bFGF             |
| Beta-tricalcium phosphate                                 | $\beta$ -TCP     |
| Bone marrow mesenchymal stem cells                        | BM-MSCs          |
| Chemokine   | CXCL5            |
| Conditioned medium from human uterine cervical stem cells | CM-hUCESCs       |
| Endothelial growth factor                                 | EGF              |
| Extracellular matrix                                      | ECM              |
| Extracellular signal regulated kinase 1                   | ERK1             |
| Extracellular vesicles                                    | EV               |
| Focal adhesion kinase                                     | FAK              |
| Gelatin methacrylate                                      | GelMA            |
| Good manufacturing practice                               | GMP              |
| Granulocyte-colony stimulating factor                     | G-CSF            |
| Hepatocyte growth factor                                  | HGF              |
| Human adipose tissue mesenchymal stem cell                |                  |
| HATMSC  |                  |
| Human bone marrow mesenchymal stem cell                   | BMSC             |
| Human microvascular endothelial cells                     | HMEC             |
| Human umbilical cord perivascular cells                   | HUCPVCs          |
| Human umbilical vascular endothelial cells                | HUVECs           |
| Human uterine cervical stem cells                         | hUCESCs          |
| Hyaluronic acid   | HA               |
| Hyperbaric oxygen therapy                                 | HBO <sub>2</sub> |
| Interleukins  | IL               |
| Keratinocyte growth factor                                | KGF              |
| Leukemia inhibitory factor                                | LIF              |
| Matrix metalloproteinase                                  | MMP              |
| Mesenchymal stem-cell-conditioned media                   | MSC-CM           |
| Mesenchymal stem cells                                    | MSC              |
| Mesenchymal stromal cell acetone-chitosan hydrogel        | MSC-Ch           |
| Monocyte chemoattractant protein                          | MCP              |
| Multipotent adult progenitor cell-conditioned medium      | MAPC-CM          |
| Multipotent mesenchymal stromal cell                      | MMSC             |
| Platelet-derived growth factor                            | PDGF             |
| Poly(lactide)   | PLA              |
| Poly(lactide-co-glycolide)                                | PLGA             |
| Poly-L-lactic acid  | PLLA             |
| Sickle cell disease                                       | SCD              |
| Smooth muscle actin                                       | SMA              |
| Synovium mesenchymal stromal cell                         | SMSC             |
| Tissue inhibitors of metalloproteinases                   | TIMP             |
| Transforming growth factor                                | TGF              |
| Tumor necrosis factor-alpha                               | TNF              |
| Umbilical cord mesenchymal stem cells C-derived exosomes  | UMSC-Exos        |
| Vascular endothelial growth factor                        | VEGF             |
| Wharton's jelly mesenchymal stem cells                    | WJ-MSCs          |
| Polyethylene glycol                                       | PBG              |

## Development of a Biocompatible Hydrogel Platform for Wound Healing and Skin Regeneration.docx

### ORIGINALITY REPORT

14%

SIMILARITY INDEX

8%

INTERNET SOURCES

13%

PUBLICATIONS

2%

STUDENT PAPERS

### PRIMARY SOURCES

|   |   |     |
|---|---|-----|
| 1 | <a href="http://link.springer.com">link.springer.com</a><br>Internet Source   | 1%  |
| 2 | Hillary Mndlovu, Lisa C. du Toit, Pradeep Kumar, Thashree Marimuthu, Pierre P.D. Kondiah, Yahya E. Choonara, Viness Pillay. "Development of a fluid-absorptive alginate-chitosan bioplatfrom for potential application as a wound dressing", Carbohydrate Polymers, 2019<br>Publication | 1%  |
| 3 | <a href="http://www.mdpi.com">www.mdpi.com</a><br>Internet Source   | 1%  |
| 4 | <a href="http://www.ncbi.nlm.nih.gov">www.ncbi.nlm.nih.gov</a><br>Internet Source   | 1%  |
| 5 | Samson A. Adeyemi, Yahya E. Choonara, Pradeep Kumar, Lisa C. du Toit, Thashree Marimuthu, Pierre P.D. Kondiah, Viness Pillay. "Folate-decorated, endostatin-loaded, nanoparticles for anti-proliferative chemotherapy in esophageal squamous cell                                       | <1% |

